INFLUENCE OF CREEP ON THE STABILITY OF PULTRUDED E-GLASS / POLYESTER COMPOSITE COLUMNS AT ELEVATED SERVICE TEMPERATURES

A Thesis
Presented to
The Academic Faculty

By

Evan A. Bennett

In Partial Fulfillment
Of the Requirements for the Degree
Master of Science in Civil Engineering

Georgia Institute of Technology

August 2005

INFLUENCE OF CREEP ON THE STABILITY OF PULTRUDED E-GLASS / POLYESTER COMPOSITE COLUMNS AT ELEVATED SERVICE TEMPERATURES

Approved by:

Dr. David W. Scott, Chair
School of Civil and Environmental Engineering
Georgia Institute of Technology

Dr. Rami Haj-Ali
School of Civil and Environmental Engineering
Georgia Institute of Technology

Dr. Stanley Lindsey
School of Civil and Environmental Engineering
Georgia Institute of Technology

Date Approved: July 15, 2005

ACKNOWLEDGMENTS

The author wishes to acknowledge the assistance provided by many throughout the completion of this research. Firstly, he would like to thank his advisor, Dr. David Scott, for his endless patience, for his guidance, and for his encouragement. The helpful comments of the thesis committee members, Dr. Rami Haj-Ali and Dr. Stanley Lindsey, are also greatly appreciated.

The author would also like to thank his friends and colleagues, Kevin Smith and Melanie Parker for their aid in the experimental process and for their company and support. Thanks go to Don Fayler at Strongwell Corporation for much needed information, as well as to Dr. Douglas Yoder, Clint Jones, and Quality Machine Company for the use of essential equipment. The author also wishes to thank Charlie Williams for his help in procuring many of the materials and equipment used throughout the experimental process.

Finally, the author would like to express his deepest gratitude for the patience, encouragement, and support of his fiancée, Karen Boyett.

TABLE OF CONTENTS

LIST OF TABLES

LIST OF FIGURES

NOMENCLATURE

A_g	gross cross-sectional area
A_i	maximum amplitude of the initial imperfection of a component
b	nominal width of a specimen
COV	coefficient of variation
d	nominal depth of a specimen
e	eccentricity of an axial load
E_L, E_L^c, E_L^t	longitudinal, compressive, and tensile moduli in the longitudinal direction
E_0, E(t)	instantaneous and time-dependent moduli
F_L^c, F_L^t	compressive and tensile ultimate stress in the longitudinal direction
G_{LT}	in-plane shear modulus
I	section moment of inertia
k	spring constant
l	coupon overall length
l_g	coupon gage length
L_0, L_{eff}	initial and effective length of a specimen
m	power law creep parameter
m’	power law creep parameter
n	power law creep parameter
n_s	form factor for shear

P	applied load
P_{cr}, P_{exp}, P_E, P_e	critical, experimental, Euler, and elastic buckling loads
P_{pred}	predicted bucking load
r_x,r_y	section radius of gyration about the x and y axis
SG	specific gravity
STD	standard deviation
t	coupon thickness, elapsed time
T, T_R	test and room temperature
$w_i(x)$	initial imperfection of a specimen along the x axis
β	power law creep parameter
δ_0	maximum out-of-straightness of a specimen, initial midheight lateral deflection
$\delta(t)$	time-dependent midheight lateral deflection
Δ	axial displacement
λ	ratio of applied load to critical buckling load (P/P_{cr})
λ_m	power law creep parameter
τ	ratio of test temperature to room temperature (ºF)
ν_{csm}, ν_{fil}, ν_{re}, ν_{rov}, ν_v	volume fraction of continuous strand mat fibers, fillers, resin, roving fibers, and voids
$\psi(t)$	creep function

SUMMARY

This thesis presents results from an experimental investigation pertaining to the creep behavior of slender pultruded fiber-reinforced polymeric (FRP) columns subjected to sustained concentric axial loading at elevated service temperatures. Six creep tests were performed on columns having a slenderness ratio of 49 at different combinations of axial load and temperature for a duration of at least 1,000 hours. The axial loads used represented 33%, 67%, and 90% of the critical buckling load for the column selected. For each load level, one test was performed at 22.8ºC (73ºF), and one test was performed at 65.5ºC (150ºF). Knife-edge end supports were utilized to simulate pinned-pinned boundary conditions. Midheight lateral deflection and axial shortening were recorded incrementally for the duration of the testing. Following termination of the creep tests, the columns were allowed to recover and tested for buckling strength. A semi-empirical model for long-term behavior of concentrically loaded FRP columns at elevated service temperatures is proposed based on experimental results.

CHAPTER I

INTRODUCTION

1.1 INTRODUCTION

Fiber-reinforced polymeric (FRP) materials have been widely utilized in the aerospace industry for more than 60 years (Galli and Pollock, 1965). Since the mid 1950's, these composites have also been increasingly used for civil and structural engineering applications such as strengthening concrete structures (ACI 440R-96); however, their use as full structural shapes has had limited acceptance. Depending on the type of fiber and resin, FRP sections can have unique physical and mechanical properties making them attractive for use as load-bearing members. Many possess high strength-to-weight ratios, resistance to corrosion, lack of magnetism, transparency to electromagnetic waves, and low thermal and electrical conductivity. Also, because of the pultrusion process and other means of mass production, the cost of FRP components is becoming increasingly competitive (Liskey, 1989).

Pultrusion is a means of manufacturing continuous lengths of fiber-reinforced structural sections. Continuous lengths of fiber and continuous strand fiberglass mat material are pulled through a guide and impregnated in a bath consisting of resin, fillers, pigment, and catalysts. Surfacing material is added, and the flat sheet is pulled into a preformer and then a heated die, where it is formed into the desired shape and cured. The newly hardened section is then pulled to a cutoff saw and cut to the desired length.

Pulling is performed by either reciprocating or caterpillar-type pullers.

Despite their potential advantages, the use of FRP members in civil engineering has been hindered in part due to a limited understanding of FRP structural behavior. In particular, the effects of time and elevated temperatures have not been sufficiently investigated and accounted for. The ASCE Structural Plastics Design Manual (1984) states that many types of FRP materials exhibit accelerated brittle failure and drastic reductions in strength and stiffness at elevated temperatures. FRP materials also display viscoelastic behavior. Sustained loads over time will reduce the stiffness of FRP members, which results in a continuous increase in deflection. Creep behavior is more evident at high stress levels; the rate of creep increases as the applied stress approaches the material's ultimate strength. Combining the effects of elevated temperatures and sustained loads further reduces the structural capacity of FRP members, as elevated temperatures have been shown to accelerate the creep rate of FRP composites (Yeow, Morris, and Brinson, 1979). FRP materials also tend to possess a relatively low glass transition temperature T_g, the temperature at which a material transitions from a glassy solid state to a rubbery state. Thus, creep buckling becomes a crucial limit state for FRP structural components exposed to elevated temperatures in service. Rational criteria that incorporate such effects are necessary for competent structural design utilizing FRP members. This study specifically investigates the problem of slender pultruded FRP columns exposed to elevated service temperatures under concentric axial loads. The goal of this research effort is to develop an accurate means of incorporating the effects of elevated temperature over time into the currently available design criteria for pultruded composite columns.

1.2 SCOPE AND OBJECTIVES

This thesis presents results from an experimental investigation pertaining to the creep behavior of slender pultruded fiber-reinforced polymeric (FRP) columns subjected to sustained concentric axial loading at elevated service temperatures. Six creep tests were performed on columns having a slenderness ratio of 49 at different combinations of axial load and temperature for a duration of at least 1,000 hours. The axial loads used represented 33%, 67%, and 90% of the critical buckling load for the column selected. For each load level, one test was performed at 22.8ºC (73ºF), and one test was performed at 65.5ºC (150ºF). Knife-edge end supports were utilized to simulate pinned-pinned boundary conditions. Midheight lateral deflection and axial shortening were recorded incrementally for the duration of the testing. Following termination of the creep tests, the columns were allowed to recover and tested for buckling strength. A semi-empirical model for long-term behavior of concentrically loaded FRP columns at elevated service temperatures is proposed based on experimental results.

CHAPTER II

PREVIOUS WORK

Numerous studies have been performed investigating the viscoelastic behavior of fiber reinforced polymeric materials. An expansive survey of existing technical literature pertaining to the creep behavior of FRP composites has previously been performed by Scott, Lai, and Zureick (1995). Reviewed in the current study are a number of investigations pertaining to the stability of FRP members, the influence of creep on the stability of FRP members, and the influence of temperature on the stability and/or creep behavior of FRP members. Some historical studies concerning creep of polymeric materials are also included, along with any similar studies published since the above mentioned survey.

2.1 STABILITY OF FRP COMPONENTS

Goodman and Gilksman (1969) evaluated the structural behavior of long boron composite columns. Boron-epoxy thin-walled circular tubes were tested as possible weight-saving substitutes for aluminum members in spacecraft. Two slender columns consisting of three plies of longitudinal boron filament and one consisting of four plies were tested in axial compression with pinned-end restraints. The columns had a length of 2438 mm (96 in), a diameter of 81 mm (3.2 in), and thicknesses of 0.53 mm (0.021 in) and 0.79 mm (0.031 in), respectively. The stiffness of each section was determined

through short column tests and flexure tests, allowing for calculation of Euler buckling loads. The failure loads of the three long columns were 81, 97, and 106% of the respective Euler approximations. Due to excessive lateral deflection during the test, the column that failed at 81% of the Euler buckling load was assumed to have been loaded eccentrically. The columns tested in the study were considered by the authors to be a satisfactory replacement for the aluminum members, as they were able to support the required loads and were approximately 30% lighter.

Hewson (1978) examined the buckling strength and modes of failure of pultruded unidirectional glass fiber/epoxy resin channel sections under axial compression. Local/flange buckling, bending, and torsion-bending were the possible modes of failure for the members tested. Buckling loads were predicted using solutions for axially loaded singly symmetric isotropic sections. In the solutions, values for the isotropic Young's and shear moduli, E and G, were replaced with experimentally determined longitudinal and in-plane shear moduli, E_L and G_{LT}, respectively. The solutions for each mode of failure were combined to derive a non-dimensional graph that could be used to predict the failure mode of any channel of this type, given the section dimensions, the applied stress, and the modulus of elasticity. Several different channel sections were tested in axial compression with ends restrained from rotation. Southwell's method (1932) was used to approximate the buckling loads, and the results were compared to the predicted buckling loads. Southwell's method is a plot of the ratio of experimentally measured midheight lateral deflection to applied load vs. midheight lateral deflection, δ/P vs. δ. The slope of this plot gives a close approximation of the critical buckling load, taking into consideration any initial geometric imperfections that may exist. According to the

author, a poor correlation existed between the predicted and experimental results. The discrepancy was attributed to the possibility of end rotation and load misalignment.

Scott, Yoon, and Zureick (1992) reported the results of an experimental investigation pertaining to the short-term behavior of vinylester/polyester E-glass reinforced pultruded structural members under concentric axial loading. Two cross-sections were considered: I-shaped stub (non-slender) columns and square tube slender columns. The stub columns were 304.8 x 12.7 mm (12 x 1/2 in) I-shaped sections having a length of 3.05 m (10 ft), slenderness ratio of 41.8, half-flange width to thickness ratio ($b_f/2t_f$) of 12, and web depth to web thickness ratio (h_w/t_w) of 23. The slender columns were 76.2 x 6.4 mm (3 x 1/4 in) box sections having an effective length of 2.57 m (8.42 ft), slenderness ratio of 89.4, and wall width to thickness ratio of 12. The dimensions of the slender members ensured that local buckling would not occur prior to global buckling. A screw-type testing machine was used to apply the load with a uniform crosshead speed of 0.635 mm/min (0.025 in/min). Computerized data acquisition recorded load, lateral displacement, axial shortening, and strain data throughout testing. The stub columns were loaded with large steel plates at both ends, providing a fixed-fixed boundary condition. The slender columns were loaded with a single knife edge at both ends, simulating a pinned-pinned boundary condition and controlling the plane of lateral deflection.

The experimental buckling loads of the stub columns were calculated using load-strain difference, load-strain, and load-deflection curves. Each method provided approximately the same result. The experimental buckling loads of the slender columns were calculated using the Southwell method. In both the stub and slender column

experiments, elastic behavior was observed for the duration of the tests, and the specimens exhibited linear behavior for a large portion of the tests.

Barbero and Tomblin (1992) performed buckling tests on pultruded columns of various size and length. The appropriateness of the classical Euler buckling theory and Southwell's method for the prediction and analysis of the load carrying capacity of composite columns was considered. The authors asserted that buckling was the governing failure mode of the type of columns under consideration, due to the material's capacity for large elongation prior to failure. As such, the Euler buckling theory was found to be useful for the prediction of critical loads, although the theory did not account for imperfections in the members, which can be significant in composite columns made by the pultrusion process. Therefore, the authors recommended using Southwell's method in the analysis of experimental buckling measurements.

A complete description of the stacking sequence for all layers in all sections tested had been previously given (Tomblin, 1991). An approximate torsional analysis was performed, and the torsional buckling load was found to be at least twice the Euler buckling load for each section tested. Therefore, the possibility of twisting during testing was considered minimal.

Two I-shaped sections were tested under simulated pinned-end conditions: 102 x 102 x 6.35 mm (4 x 4 x 1/4 in) and 152 x 152 x 6.35 mm (6 x 6 x 1/4 in). The former section was tested with lengths of 2.98 and 4.48 m (9.78 and 14.70 ft), and the latter was tested with lengths of 3.58, 3.89, and 6.03 m (11.75, 12.76, and 19.78 ft). The authors determined that loading until a lateral deflection of approximately L/100 was achieved

would provide a sufficient number of data points to use a Southwell plot. At least two experiments were performed for each column length.

The test results indicated that all experimental buckling loads were less than predicted, and all were within 6% of the predicted loads. These results led the authors to conclude that the Euler estimation could be considered the upper bound for the true buckling load. With such small variation between predicted and true buckling loads, the authors asserted that the Euler load could be considered an accurate prediction of the load-carrying capacity of pultruded composite columns.

Barbero and Raftoyiannis (1993) proposed an analytical model for Euler buckling of pultruded composite columns. Local buckling was specified as the governing failure mode for short columns, and overall buckling was specified as the governing failure mode for long composite columns due to their ability to remain linearly elastic for large deflections and strains. Euler's classical buckling theory was combined with basic concepts of classical lamination theory (CLT) for the analysis of an I-shaped section.

Through a stiffness component analysis, modeling the flanges and webs as anisotropic laminated plates, the cross-section was transformed to an equivalent laminate. The resulting beam stiffness was similar to that presented in previous studies. Due to the complications of plate theory, the authors developed another analytical approach for calculating the stiffness of thin-walled beams with unsymmetrical material and/or geometry. Here, the stiffness was formulated with respect to the neutral axis using constitutive equations based on the assumption of plane stress through the thickness and width of the beam. Laminate constitutive equations were derived individually for both the flange and the web based on the stress resultants. The contributions of the flanges

and the web were then combined to obtain the bending stiffness with respect to the neutral axis using the parallel axis theorem.

Next, the Euler buckling behavior of a pinned-pinned perfect column was examined. The stiffness equation derived from CLT in conjunction with the Euler equation for critical buckling load was used to produce long-column failure envelopes for five specific structural shapes.

Butz (1997) performed short-term buckling tests on pultruded E-glass/polyester composite square tubes with eccentricity. Three columns were tested having slenderness ratios of 35, 50, and 65. Six axial loadings were applied to each column with eccentricities ranging from 0 to 0.875 times the width of the tube, 0 to 88.9 mm (3.5 in). For each test, two of the specimens were compressed until a midheight lateral deflection of 18 mm (0.71 in) was achieved, and the third specimen was compressed until a midheight lateral deflection of 13 mm (0.51) in was achieved. For each of the concentric load tests, the buckling load was determined using Southwell's method. Lateral and axial deformations from each test were compared to values predicted using elastic stability theory. It was found that Euler's buckling equation closely predicted the buckling loads determined in the concentric tests. The predicted lateral deflections for the eccentric tests were within 8% of the measured values for the two most slender columns with eccentricities less than 1/2 of the width of the tubes. For the least slender specimen, the predictions were not accurate. The author suggested that the inaccuracy was due to the presence of other limit states such as local buckling. Some success was seen in predicting axial displacements for the concentric tests and for the least slender column with eccentricities less than 1/2 the width of the tube. Thus, the observed trend was that

with a higher degree of bending exhibited by a specimen, more accuracy was seen in the predicted midheight lateral deflections, and less accuracy was seen in the predicted axial displacements.

Zureick and Scott (1997) investigated the short-term behavior of concentrically loaded FRP composite slender columns. Two types of pultruded cross-sections were tested: wide flanges sections (I-shapes) and box sections. All specimens were made from a vinylester matrix containing flame retardant additives, reinforced with E-glass roving and nonwoven mats. A total of 108 uniaxial tension and 108 compression tests (10 coupons for each I-shape section, 8 for each box section) were performed in order to estimate short-term longitudinal material properties. The material properties were used in the Euler equation to predict the critical buckling load for the test specimens. The effect of transverse shear was also incorporated into the predictive formulation (Engesser, 1889). Coupons were cut from the flanges and webs of the I-shaped sections and from each wall of the box sections. In-plane shear properties were determined using an asymmetric four-point bending test setup.

A total of 12 box and 12 I-shaped members with slenderness ratios ranging from 36 to 103 were tested. The effective lengths of the sections ranged from 1.22 to 2.44 m (4 to 8 ft). Knife-edge supports were used at each end in order to simulate pinned-end conditions. Failure was taken as the point where deflections increased dramatically with little or no increase in load. The buckling load of each tested specimen was estimated using the Southwell method. Most of the axial deflection curves showed a linear elastic response for 75-95% of the buckling load.

A nondimensional slenderness parameter was found for each section based on the material properties found in the coupon tests and the slenderness ratio of the full section. A normalized plot of this slenderness parameter showed little variation between the two types of cross-sections. Axial displacement behavior during testing was compared with a classical predictor equation for isotropic materials. The experimental axial displacement consistently exceeded the predicted deflection. This was attributed to the fact that the predictor equation does not account for material inhomogeneity, initial curvature, or experimental error.

Using Euler's buckling equation or the modified form of Euler's buckling equation to predict the critical load was reasonable for the slender members that were tested in the investigation. Inclusion of transverse shear effects in predicting behavior of slender members may not be necessary in all materials; however, the authors recommended that these effects be included in the case of FRP composites because shear properties of FRP composite are highly reliant on the matrix material, which is more susceptible to degradation over time. Finally, based on the results of the study, limited design guidelines for slender FRP composite columns were given.

Hashem and Yuan (2001) conducted a study in order to establish a distinguishing criterion between short and long column behavior for FRP composite columns. Twenty-four full-scale glass fiber-reinforced polymeric (GFRP) composite columns were tested to failure, and the modes of failure were used to distinguish each column as short or long. Of the 24 specimens, 15 were "universal" sections and 9 were box sections, all manufactured by the pultrusion process. The matrix materials of the "universal" and box

specimens were vinylester and polyester, respectively. Mechanical properties were determined experimentally using coupons cut from the specimens.

For the full-scale tests, effective slenderness ratios (L/r) ranged from 3.79 to 78.9, and specimen lengths varied from 0.46 to 5.87 m (1.5 to 19.25 ft). Steel cylindrical rollers were utilized in the experimental setup in order to simulate pinned-end conditions. The results of the coupon tests were used with the Euler equation to predict the ultimate load for each section. For short columns, classical plate theory was used to predict failure loads. The authors constructed a plot of slenderness ratio vs. the ratio of critical and ultimate loads (L/r vs. P_{cr}/P_{ult}). The approximate point at which the plot converged on the Euler curve was taken as the experimentally determined point of transition from short to long column behavior. The value of L/r at this point was taken as 50. The plate buckling expression was equated with the Euler buckling equation, and the result was a slenderness ratio of $L/r = 46.6$. This difference was attributed to incomplete fixity of the flange plate to the rest of the "universal" section, which added error to the plate buckling analysis. The authors concluded that GFRP columns with slenderness ratios greater than 50 will fail due to global buckling and columns with slenderness ratios less than 50 will fail due to either local buckling or crippling.

2.2 CREEP AND CREEP BUCKLING OF POLYMERS AND FRP

Findley (1944) introduced a mathematical expression for the prediction of time-dependent behavior of plastics in the form of a power function. Several different plastics were tested for at least 1000 hours, and the experimental data were fit to the equation with excellent agreement. Based on the results, the author asserted that this method of

analysis may permit reliable extrapolation of creep data for plastics. The power function of time presented in the study was as follows:

$$\varepsilon = \varepsilon_0 + mt^n \tag{2.1}$$

in which ε represents total strain, *t* represents time, and ε_0, *m*, and *n* represent creep parameters. The author rewrote the equation in the form:

$$\log(\varepsilon - \varepsilon_0) = n\log(t) + \log(m) \tag{2.2}$$

which when plotted on a log-log scale forms a straight line, where *n* is the slope and *m* is the y-intercept at one hour. It was observed that the value of *n* was independent of stress for all materials tested and that the value of *m* could be related to stress by an exponential function.

Kempner (1954) carried out an analytical investigation of the creep bending and buckling behavior of linearly viscoelastic materials. Based on a combination of a Maxwell element and a Kelvin element and the assumption of small deflections, a general dynamic equation was derived. This equation allowed for modeling the behavior of a linearly viscoelastic material that displays instantaneous and retarded elasticity and pure flow, and whose mechanical properties can be characterized by four parameters. The author used the general equation to derive a representation of the creep deflection of a beam in pure bending and of a column with initial sinusoidal deviation from straightness. The ratio of creep deflections of the beam in pure bending to deflections of an identical purely elastic beam proved to be the same as the ratio of creep strain and the corresponding elastic strain of a bar under tension or compression. The creep deflection of the column was shown to increase continuously with time, becoming infinitely large. The amount of time required to obtain boundless deflection was found to decrease as the

applied load approached the Euler buckling load of the column. The author asserted that this type of analysis could be applied to similar column problems with initial shapes other than sinusoidal based on the linear nature of the general differential equation of bending. Deflection-time curves obtained from a numerical example showed similar characteristics to those of aluminum columns determined experimentally by Jackson, et al. (1949) and Rosenthal and Baer (1952).

Distefano (1965) performed an analytical investigation concerning the problem of creep buckling of slender columns. The problems addressed in this study were evaluation of critical loads for axially loaded bars displaying linear and nonlinear bounded creep. Through the use of a time-dependent elastic modulus $E(t)$, Boltzmann's superposition principle (1876), and Volterra's theory of hereditary elasticity (1913), expressions were derived for deflections and critical loads for invariable creep and for aging materials. It was determined that the critical load could be directly related to a reduced elastic modulus independent of end conditions, cross-sectional variations, initial eccentricities and lateral forces, and the form of the creep function of the material, i.e. Maxwell, Kelvin, or Standard bodies. Subsequently, an expression for the critical load of nonhomogeneous materials was obtained. Then, based on elastoplastic behavior as seen in reinforced concrete beams, an expression that accounted for load-moment interaction was derived. A modification of the reduced modulus expression found previously was found to closely approximate the elastoplastic behavior.

Schapery (1965) proposed a method of approximating solutions of viscoelastic problems using elastic solutions, called the quasielastic method. The proposed approximation was the solution of an elastic body geometrically identical to the

viscoelastic body, under identical thermal and mechanical loading conditions. The corresponding elastic body had elastic properties equal to the instantaneous relaxation modulus or creep compliance of the viscoelastic body. Expressions for the difference between the quasielastic solutions and the exact solutions to viscoelastic problems were derived. The author asserted that a graphical comparison of the proposed method to the exact solutions of two numerical examples showed satisfactory agreement. The differences between the solutions were shown to be virtually negligible. It was concluded that the proposed quasielastic method could successfully be used to closely approximate the viscoelastic response of a body under many conditions.

Schapery (1967) also performed a viscoelastic stress analysis of anisotropic composite materials. The similarity between the behaviors of elastic media and linear viscoelastic homogeneous material, known as the correspondence principle, was used to derive effective viscoelastic moduli and thermal expansion properties for composites in terms of constituent properties. The correspondence principle was incomplete in the case of anisotropic media, so thermodynamic theory was required for the analysis. Three example problems were solved with the effective viscoelastic moduli and thermal expansion properties through three previously established approximate methods of analysis: the collocation method of Laplace transform inversion, the direct method of Laplace transform inversion, and the quasielastic method. Each method was shown to yield very similar results. The correspondence principle used in this analysis was not applicable to bodies with moving boundaries or transient, nonuniform temperatures.

Booker, Frankham, and Trahair (1974) presented a method of analyzing the buckling behavior of viscoelastic structural members. Several specific problems were

solved using the correspondence principle. The problems addressed in the study included three problems concerning lateral buckling of columns under various conditions and three problems concerning flexural-torsional buckling of beams under various conditions. Each problem was solved under the assumption that the material could be modeled as a three-element model. Through taking the Laplace Transform of the stress-strain relationships of the three-element model, the viscoelastic differential equations were transformed into elastic algebraic equations. In order to solve the individual problems, the moment-curvature relationships and the torque-twist relationships were transformed according to the same methods. For each problem it was found that a long-term buckling load less than the short-term elastic buckling load existed. If the applied load exceeded the long-term buckling load, the member would fail after some finite time; if the applied load was less than the long-term buckling load, the member would achieve some final position and remain stable indefinitely.

Holmes and Rahman (1980) tested 150 x 300 mm (6 x 12 in) box beams made of glass-reinforced plastic for long-term creep in flexure. Three 6 m (20 ft) long beams with diaphragms placed every 500 mm (20 in) were simply supported at each end and subjected to various loading patterns for a duration of 20 months (15,000 hours). Loads were applied in the form of concentrated loads at 1/3 span points. One beam supported a constant static load of 500 kg (1100 lb) at each point for the duration of the experiment. This equated to approximately 1/3 of the ultimate strength of the beam. A second beam was loaded similarly; however, it was loaded and unloaded with decreasing frequency for the first 90 days of the experiment, after which the load was applied permanently. The final beam supported its self-weight only. Throughout the tests midspan deflection,

tensile strain, compressive strain, and shear strain were recorded. More than 65% of the creep deflection in the two beams supporting loads occurred in the first 500 hours. After the tests were terminated, the two loaded beams had deflected 109% and 113% of their initial deflections, and the unloaded beam had deflected 35%. The tensile and shear strains showed similar trends, with a large percentage of the creep occurring in the first 500 hours, but at a slightly lesser rate. The compression strain data was scattered and was not useful for reliable prediction of long-term creep. The beam that was not loaded displayed a steadier rate of creep with much smaller magnitudes. Predictive power law equations were derived for each type of strain and for deflection. A comparison of the measured data to the predictions showed fair similarity except in the case of compressive strain.

Vinogradov (1987) performed an analysis of the creep buckling behavior of viscoelastic columns and beam columns. Two simple problems were analyzed based on creep properties of the materials being defined by the constitutive equations of linear viscoelasticity theory. The two specific problems addressed were an initially imperfect column loaded under concentric axial compression and a beam column simultaneously subjected to axial compression, end moments, and lateral pressure. Creep behavior that was either limited or unlimited in time was assumed in each problem for comparison. The constitutive equations of linear viscoelasticity theory were solved through use of the quasielastic method proposed by Schapery (1965). This allowed for the derivation of an equation that characterized the creep buckling behavior based on two parameters in the form of:

$$A(t) = A_i \frac{\lambda[1+\psi(t)]}{1-\lambda[1+\psi(t)]} \tag{2.3}$$

where $A(t)$ is the amplitude of the time-dependent lateral deflection, A_i is the amplitude of the initial imperfection, λ is the ratio of the applied load to the Euler buckling load, and $\psi(t)$ is an experimentally determined creep function of the material. It was shown that a safe load limit existed such that columns with limited creep characteristics would remain stable indefinitely if the safe load was not exceeded. The magnitude of the safe load was dependent on the creep function of the material. For columns with unlimited creep, the magnitude was found to be zero. Quasielastic solutions were compared with the exact solution, given by Kempner (1954), in order to evaluate the effectiveness of the quasielastic approximation. It was concluded that the quasielastic method is a sufficient approximation when the applied load is less than the safe load limit.

Bank and Mosallam (1990) reported on the results of an experimental study of the short-term failure and long-term creep of a plane portal frame consisting solely of pultruded FRP components. Two identical frames were constructed using standard "off-the-shelf" glass/vinylester pultruded beams, nuts, and threaded rods. Each frame was made up of two columns and one girder in the form of 203 x 203 x 9.5 mm (8 x 8 x 3/8 in) wide flange sections, and connections consisted of 152 x 152 x 12.7 mm (6 x 6 x 1/2 in) angle sections and 19 and 25.4 mm (3/4 and 1 in) threaded rods and nuts. For each test, the frame was loaded symmetrically with concentrated forces at each 1/3 point of the girder length. Deflections, axial strains, and shear strains were recorded during both the long-term and short-term tests.

The short-term test was conducted in several cycles of loading and unloading, increasing the peak load with each cycle. Load and deflection data supported the conclusion that the frame was linearly elastic until some critical point after which

irreversible damage to the frame led to nonlinear behavior. Once this critical point was established, the frame was loaded until ultimate failure was achieved. The first portions of the frame to fail were the connections between the columns and the girder, followed by failure in the compression flange of the girder.

For the long-term creep test, dead weights were hung from the same points as in the short-term test, providing a static load equal to approximately 23% of the initial failure load. The frame was tested for a duration of 10,000 hours. The majority of creep occurred during the first 2,000 hours, after which the rate became nearly constant. After testing for 3,500 hours, the midspan deflection of the girder had increased by 12.8%. At that time, Findley's power law (1944) was employed to formulate semi-empirical expressions for a viscoelastic longitudinal modulus and for a viscoelastic shear modulus. These expressions were then used to predict the behavior of the frame over a ten year span. The viscoelastic longitudinal modulus and shear modulus were predicted to decrease by 35 and 46%, respectively, in that time span.

Chen and Lottman (1991) proposed theoretical buckling loads of viscoelastic columns under various loading conditions. All assumptions made were the same as in Euler buckling theory with the exception of linear viscoelasticity. Global buckling failure and pinned-end boundary conditions were also assumed. A Maxwell solid, a Kelvin solid, and a standard anelastic solid (Kelvin model in series with a spring) were each considered under four loading conditions. The axial loading conditions were a constant load, a ramp load, a wave load, and a combination of constant and wave loads. For each loading condition, a critical buckling load was determined for the three material

types at which the column would eventually fail. In all cases, the time to failure was dependent on the elastic and viscoelastic constants of the material.

Vinogradov (1992) examined nonlinear creep buckling associated with elastic bifurcation of equilibrium. A simple structural model with linear viscoelastic material properties was analyzed by means of the quasielastic method. It was shown that the problem was governed by two parameters: applied load and time. The solution was compared for various load levels and eccentricities (or imperfections), and it was found that in general the creep buckling of the viscoelastic model could be regarded as stable. The author also observed that after a certain "critical point", the viscoelastic system behaved similarly to the buckling response of the corresponding elastic model. The closed-form solution for a Maxwell material was found in order to verify the accuracy of the results. A comparison of the two solutions revealed that the quasielastic approximation is generally conservative and that it is most accurate when creep buckling is characterized by low deformation rates.

Vinogradov (1993) also performed a study of the nonlinear buckling and post-buckling behavior of laminated composite columns and beam-columns with elastic and viscoelastic material properties. Material properties of the laminates were defined by the constitutive equations of the linear hereditary viscoelasticity. The problem was addressed in general terms according to geometrically nonlinear theory; then the special case of laminated columns loaded eccentrically was examined. Both symmetric and asymmetric laminated composite columns with initial imperfections were considered in the analysis. First, the elastic response was established assuming small deformations. Analysis of the creep buckling response followed. Creep buckling was represented according to the

quasielastic method. For both elastic and viscoelastic buckling, numerical results were found over a range of loads and imperfections and compared to the respective predicted buckling responses of identical homogeneous columns. The comparison showed that the time-dependent behavior of laminated composite columns depends on the sequence and creep characteristics of its constituent layers. The laminated sections that included elastic and viscoelastic layers were predicted to exhibit lower deformation rates than their homogeneous counterparts. Laminated sections that included only viscoelastic layers were predicted to exhibit similar deformation rates to those of the homogeneous sections.

Minahen and Knauss (1993) investigated the creep buckling of polymethylmethacrylate (PMMA) column specimens subjected to axial compressive loads. The main purpose of the study was to determine an exact analytical formula for creep buckling within the limits of linear viscoelasticity. The authors asserted that the instability problem should be viewed as the time dependent response of an initially imperfect structure, not that of a perfectly straight, slender column. The growth of the initial imperfections was calculated using the hereditary integral formulation. After adopting a relaxation modulus in terms of a Prony-Dirichlet series, the authors were able to extract explicitly the non-dimensional amplitude of the deformation at a given time in terms of the deformation mode.

The authors conducted experiments in an effort to verify their analytical results. The verification of the viscoelastic model was performed under simulated pinned-end conditions at an elevated temperature of 75ºC (167ºF) in order to accelerate the creep rate of the specimens. Test specimens were coupons cut from a sheet of commercially obtained PMMA. The coupons had a length of 152.4 mm (6 in), a width of 25.4 mm (1

in), and a thickness of 6.35 mm (1/4 in). Each test was carried out until a midspan lateral displacement of 2 cm (0.78 in) was achieved.

The experimental results and predictive models were compared on a time scale; the authors asserted that the comparison yielded "excellent agreement" during the slow growth phase and a "reasonable" prediction in the subsequent accelerated growth phase. The difference in the latter phase was attributed to non-uniform residual stresses in the materials tested and slight temperature fluctuations. Based on the results of predictive models with various initial imperfections, the authors concluded that while it is necessary to include initial imperfections in the analysis of viscoelastic columns, the time to buckling is only marginally affected. The authors asserted that the short-term and slow growth phases of the viscoelastic response can be well modeled using a linear model and a parameter characterizing geometric imperfection, despite some inconsistency in the final growth phase.

McClure and Mohammadi (1995) examined the compression creep behavior of pultruded angle sections composed of isophthalic polyester resin reinforced with E-glass fibers in the forms of mats and longitudinal rovings. Short-term compression testing was performed on 11 full stub sections and 20 coupons cut from the legs of the angles in order to determine the short-term properties. The stub sections were 50.8 x 50.8 x 6.35 mm (2 x 2 x 1/4 in) angle sections cut to a length of 152.4 mm (6 in). Coupons were cut from the middle of each leg of the angle with a cross-section of 12.7 x 6.35 mm (1/2 x 1/4 in) and a length of 31.75 mm (1.15 in). These dimensions gave the stub sections a slenderness ratio of 15.4 and the coupons a slenderness ratio of 12.5. The coupons all failed at an average stress much larger than the stub sections, meaning that the failure of

the stub sections was caused by geometric instability. The coupon tests revealed that, due to the pultrusion process, one leg of the angle was systematically stronger and stiffer than the other. Thus, some eccentricity existed between the applied loads and the center of rigidity of the stub sections; however, this was not accounted for in the analysis of the long-term test results.

Long-term compression tests were carried out on stub sections and coupons of the same dimensions as in the short-term testing for a duration of 2500 hours, and then the recovery of each specimen was monitored for an additional 250 hours. The coupons that were tested for creep were all taken from the stronger of the two angle legs. Each specimen was stressed to approximately 45% of its respective failure stress determined in the short-term tests. After 2500 hours the strain in the stub sections had increased by an average of 14.4% over the initial strain, and the strain in the coupons had increased by an average of 13.8%. Once the stress was removed, an average of 67% of the creep strain in the stub sections was recovered after 250 hours, and an average of 54% was recovered in the coupons. Finley's power law was used to model the creep behavior of both specimen types, and Boltzmann's superposition principle was used to predict the relaxation behavior of the specimens, both with good agreement. For each specimen type, there was little variation in the creep parameter *n* in Findley's power law. However, there was a substantial difference between the average value obtained from the stub tests and the average value obtained from the coupon tests (0.170 and 0.254, respectively). No explanation of this difference was provided by the authors. Findley's power law was used to predict the creep strain in the stub sections based on the data from the coupon tests with good results. Based on this outcome, the authors concluded that this type of

variation of *n* does not affect the accuracy of creep predictions utilizing Findley's power law, and that creep tests on full sections offer no benefits over coupon tests.

Scott and Zureick (1998) investigated the creep behavior of pultruded FRP materials subjected to long-term compressive loading. Coupons cut from a pultruded vinylester/E-glass I-shaped section were tested at various compressive stress levels for up to 10,000 hours. The section consisted of a vinylester matrix reinforced with unidirectional E-glass roving and continuous filament mat. Using the modified ignition loss method, the glass fiber volume fraction was found to be 0.3, with filler content about 5% by volume. Coupons were cut from each flange and the web (five total locations) of a 102 x 102 x 6.35 mm (4 x 4 x 1/4 in) pultruded FRP wide flange section.

Long-term creep testing was performed using dead-weight lever-arm creep fixtures that were able to load three coupons simultaneously in compression. Three stress levels were investigated in the study: 65, 129, and 194 MPa (9.43, 18.71, and 28.14 ksi), which represented 20%, 40%, and 60% of the short-term ultimate stress of the coupons, respectively. Three coupons were tested at each stress level. The coupons stressed to 40% of ultimate were tested for approximately 10,000 hours, and the rest of the coupons were tested for approximately 5,000 hours.

The results were then compared to a practical power law formulation with good agreement. An equation for time dependent longitudinal modulus, $E_L(t)$, was formulated based on hyperbolic functions of stress and empirical constants. A plot of normalized viscoelastic modulus vs. time proved the equation to be conservative compared with an extrapolation of the measured creep data.

Kang (2001) examined creep behavior of pultruded FRP members subjected to sustained eccentric compression and separately to sustained flexure. The compression testing portion of the study relates most directly to the current study. For this portion of the investigation, six samples at different axial load/eccentricity combinations were investigated. The experiments were each carried out for 2,000 hours, during which the midheight lateral deflections were recorded regularly. The samples were 1.83 m (6 ft) long square tube sections, the eccentricities varied from 0 to 88.9 mm (3.5 in), and the sustained loads varied from 13 to 28% of the critical buckling load.

Analytical formulae for prediction of creep lateral deflection were based on two models: the quasielastic solution proposed by Schapery (1965) and the power law model proposed by Findley (1944). The quasielastic solution was examined for two cases of eccentric loading. The first was eccentric axial loads at both ends of the component. The governing differential equation for lateral deformation was established and manipulated so that it could be expressed as two components: short-term and time dependent bending stiffness. Further manipulation yielded an equation that was a linear combination of the lateral deflection due to eccentric loading of a perfect section and lateral deflection due to concentric loading of an imperfect section. The second case of loading examined under the quasielastic equation was eccentric loading at one end of the component. A similar analysis was done for this case, and the equation for lateral deflection at midheight was derived. Another equation, which could be plotted on a logarithmic scale, was derived according to Findley's power law.

The experimental program included six combinations of load/eccentricity, with each specimen loaded eccentrically at both ends. The assumed short-term behavior of the

specimens was based on results of the experimental analysis done by Butz (1997) on identical sections. All load/eccentricity combinations were chosen such that short-term lateral deflections at midheight were within L/120, as follows in Table 2.1:

Table 2.1: Load/Eccentricity Combinations Used by Kang (2001)

Sample	P/P_{cr}	Eccentricity mm (in)
1	0.19	12.7 (0.5)
2	0.19	25.4 (1.0)
3	0.19	50.8 (2.0)
4	0.13	25.4 (1.0)
5	0.13	50.8 (2.0)
6	0.28	25.4 (1.0)

Test specimens were all 102 x 102 x 6.35 mm (4 x 4 x 1/4 in) square tubes cut to a length of 1.83 m (6 ft). The out-of-straightness of each specimen was measured according to ASTM D3917-94, and all specimens fell within the standard limit of L/240. The test samples rested on knife-edge supports in a test frame consisting of four threaded rods, four steel plates, springs, and hexagonal nuts. The load was initially applied to the specimens using a hydraulic jack, and the nuts were used to lock the plates in place in order to maintain the load. The springs were used to minimize any load lost due to creep shortening. Dial gages were used to measure lateral deflection at midheight and to measure axial shortening at the base of the specimens. Data were recorded immediately

after load application, at increasing time intervals from 30 minutes to 6 hours over the first day, every day for the following 20 days, and twice per week thereafter.

The measured creep deflections at midheight of the specimens resulting from the experiments were all less than 10% of the initial elastic deflection. The formulae that were derived were used along with the time-dependent longitudinal modulus and the time-dependent bending stiffness, which were based on the study by Scott and Zureick (1998), to predict the time-dependent midheight lateral deflection. The measured results were slightly lower than the predicted results.

2.3 TEMPERATURE EFFECTS ON FRP BEHAVIOR

Daniali (1990) performed a study in which E-glass-reinforced polyester and vinylester T-shaped lintels were tested for short- and long-term behavior under flexure. Two types of T-shaped lintels were tested under uniformly distributed loads at room temperature and at 54°C (130°F): lintels having solid webs and lintels having a cavity in their webs to provide improved lateral stability. Short-term destructive tests were performed on a number of two-span continuous beams at both temperatures. Results showed that the solid web lintels all failed due to lateral torsional buckling, while the cavity web lintels failed from buckling and cracking of the web. The elevated temperature reduced the average ultimate load for the solid web and cavity web polyester lintels by 38 and 28%, respectively. Reductions of 18 and 20% were shown for the solid web and cavity web vinylester lintels, respectively.

Two sets of creep tests were performed: one at room temperature and one at the elevated temperature. In the first, one of each type of lintel (four total) was loaded to

50% of its respective average ultimate load. The solid web specimens were loaded for 5,000 hours, and the cavity web specimens were loaded for 10,000 hours. Additionally, four cavity web vinylester specimens were loaded to values ranging from 75 to 85% of their ultimate load. In the case of the solid web specimens, after 5,000 hours the creep deflection exhibited by the polyester lintels was more than twice that of the vinylester lintels. Alternately, the creep deflections of the polyester and vinylester cavity web specimens remained very close through 10,000 hours of testing, deflecting 20 and 15% of their initial deflections, respectively. The additional vinylester specimens were loaded until either unbounded deflection or a stabilized state was reached. The latter was the case for all but the specimen tested at 85% of ultimate.

In the second set of creep tests, both types of cavity web specimens were tested at 54°C (130°F). A total of 12 lintels were loaded with 50, 60, and 80% of their respective ultimate load. The vinylester specimens performed much better than the polyester specimens under the elevated temperature. At 80% capacity, the polyester specimens failed in less than 10 hours, while the vinylester specimens lasted for more than 50 hours. However, in both cases, the creep deflections observed were far greater than those in the room temperature tests. It was noted that all specimens fully recovered after termination of the tests. The author concluded that vinylester performs better and more predictably than polyester under sustained loading conditions, especially at elevated temperatures.

Bradley et al. (1998) investigated the long-term creep characteristics of polyesters and vinylesters as a function of curing conditions. The creep behavior of post-cured neat and glass-reinforced polyesters and vinylester were compared. In addition, several samples of vinylester were cast and allowed to cure under various combinations of time

and temperature. Flexural creep of the samples was measured for 10,000 hours at room temperature, and the results were fit to models based on Findley's power law. It was observed that as the time and/or temperature of curing were increased, the value of *n* decreased. This trend was attributed to the amount of cross-linking that was able to take place during the curing process. Higher temperatures and longer cure times produced more complete cross-linking of the polymers, which in turn increased the samples' resistance to creep. In the case of room temperature curing for a short duration, the value of *n* decreased over time as the sample continued to cure during testing. The polyester samples were shown to possess higher values of *n* and creep more than the vinylester samples. It was also shown that the addition of reinforcement had little effect on value of *n*, but decreased the magnitude of creep.

Petrie, Sorathia, and Warren (1999) reported on a collaborative study involving three institutions in which a series of composite beams was designed, tested, and analyzed for their response to elevated temperatures. The beams were 1.8 m (6 ft) long, 150 mm (6 in) wide, and made up of a vinylester resin matrix reinforced with E-glass, with a fiber volume fraction of 0.5. Four-point bending tests were performed both isothermally and non-isothermally on the specimens. The beams tested under isothermal conditions were 31.75 mm (1.25 in) thick, and those tested under non-isothermal conditions were 25.4 mm (1 in) thick.

In the isothermal tests, the beams were placed in an oven, quickly brought up to the target temperature, and allowed to fully acclimate to the ambient heat. Incremental loads were then applied manually by placing steel weights in a frame resting on the beam. Test temperatures were 95 and 150ºC (203 and 302ºF). Room temperature tests were

performed on each beam before and after the elevated temperature test to verify that no degradation had occurred. At room temperature, the beams consistently displayed linearity between load and deflection, and no degradation between tests was evident. Some specimens actually showed an increase in modulus following the elevated temperature tests, which the authors attributed to post-curing. In the elevated temperature tests, the beams initially sagged under their own weight with the temperature increase, and there were creep deflections over time at each incremental load. The creep deflections were greater in magnitude at higher temperatures.

In the non-isothermal tests, the beams were placed in the oven with an initial constant load. The oven was then brought up to the target temperature as the increase in deflection due to creep and degradation of elastic modulus was monitored. The target temperature and load were then maintained for four to six hours. Maximum test temperatures were 95, 120, and 150ºC (203, 248, and 302ºF).

The structural performance and creep properties of a similar composite were examined separately on a material level. The material was a glass/vinylester composite panel, 70% fiber by weight. A Dynamic Mechanical Thermal Analysis (DMTA) technique, a technique often used in polymer laboratories, was used to determine the flexural modulus as a function of temperature. At 65ºC (150ºF) the material showed a 15% reduction in modulus, and at 150ºC (302ºF) a reduction of 91% was observed. The trends observed in the DMTA tests were used to predict the loss of elastic modulus for a solid laminate beam under load at elevated temperatures so that the deflection could be predicted. A quasi-isotropic panel of unidirectional tape was tested using DMTA in order to measure the percent reduction in apparent modulus, the ratio of constant stress to total

strain, as a function of temperature. This would provide insight into the creep behavior of the material. A power law was developed through fitting curves to the results for each temperature. The finite element modeling program ABAQUS was then used to model the full-size beams in an effort to obtain another prediction of structural behavior under the various conditions.

The predicted deflections based on the DMTA testing were significantly larger than those measured in the isothermal tests, especially near the glass transition temperature of the material. Based on the size of the coupons relative to the full size beams, the authors concluded that there was a scale effect that influenced the loss of modulus. Similar results were obtained from the predictive creep model. A good correlation existed between the predicted creep deflections and those measured in the non-isothermal tests for the first 90 minutes, after which the predicted values greatly exceeded the measured data. Again, the conclusion was that a scale effect existed in the transition from the coupon-level tests to the full-scale tests. The deflections predicted through ABAQUS showed what the authors considered good correlation for the isothermal tests. For the non-isothermal tests, because the creep parameters of the finite element model were based on the power law derived from the DMTA tests, the prediction was again close for the first 90 minutes and deviated thereafter. The authors concluded that for similar laminates, the derived form of the power law in conjunction with ABAQUS finite element code may be suitable for modeling short-term creep at elevated temperatures. The authors also asserted that ABAQUS could be useful for the design of structures built with similar composite members.

Dutta and Hui (2000) completed a study of tension and compression behavior of glass-fiber reinforced polyester composite material under sustained loads and elevated temperature. The goal of the study was to develop constants to be used as material parameters in a model that could allow engineers to assess the heat durability of composites.

A series of coupon level tension and compression tests were performed in order to determine short-term mechanical properties. The coupons were cut from glass/polyester FRP plates with a thickness of 6.35 mm (1/4 in). Identical coupons were then tested under sustained loads ranging from 60 to 80% of ultimate in order to determine the time to failure. Sustained-load tests were carried out at 25, 50, and 80ºC (77, 122, and 176ºF). Tests were performed in a testing machine with a well-insulated chamber around the loading fixtures. The applied load was sustained by adjusting the controller of the testing machine. Temperature, applied load, and strain were all recorded during testing. The sustained-load tests performed at room temperature were generally terminated after 30 minutes of testing. Tests at the elevated temperatures were carried out until failure of the specimens, which typically occurred within an hour of applying the load. In some tests the applied load was increased to a higher level and then held constant until the specimen failed.

A curve-fitting equation was developed based on the test data. The equation was similar to Findley's power law except that the two creep constants of Findley's equation were replaced with functions of time ratios and temperature ratios. This yielded an equation with only two constants instead of four. According to the authors, the semi-empirical model matched very well to many published creep curves. The equation

required that some initial parameters such as initial strain be arbitrarily fixed. The authors stated that by running systematic tests for each material, the required material constants could be determined, the strain-time-temperature curve could be predicted, and the time to failure at various temperatures could be estimated.

Violette and Schapery (2001) investigated the time and temperature dependence of a unidirectional carbon/epoxy composite material under compression. Experimental results were compared with analytical predictions based on fiber micro-buckling models and finite element models. The material used was E719LT/AS4C, a carbon-fiber composite with a rubber-toughened epoxy matrix. The glass transition temperature of the material was approximately 125°C (257ºF), and the fiber volume fraction was 0.57. Testing temperatures were 24, 50, and 60°C (75.2, 122, and 140ºF). Test specimens were cut to a width of 12.7 mm (1/2 in), a thickness of 3.2 mm (1/8 in), and an overall length of 91.4 mm (3.6 in); 38.1 mm (1.5 in) tapered tabs were secured to each end, leaving a gage length of 15.2 mm (0.6 in). Prior to testing, each specimen was notched at the centerline of the gage length in order to ensure failure within the gage length and away from stress concentrations caused by the tabs. A notch depth of 0.38 mm (0.015 in) was determined to be sufficient to warrant proper failure.

The composite behavior of the material was characterized using two constitutive models. One was a homogenized model, in which the fibers and matrix were combined to form an orthotropic continuum in plane stress. The other was a two-dimensional model, in which the fibers and matrix were represented as alternating layers, also in plane stress. In the latter model, the fiber and matrix layer thickness were different so that the 0.57 fiber volume fraction could be maintained. In each case the behavior was predicted

by a nonlinear quasielastic constitutive model. The properties in the fiber direction were represented by a combination of linear elastic, linear viscoelastic, and non-linear viscoelastic behavior. The contribution of each type of behavior varied with the temperatures at which the specimens were tested. The authors determined that the material behavior could be modeled as a sum of several power laws. Near the notch, the homogenized material model was inadequate due to variations in the strains of the fibers and the matrix.

A plane stress analysis was performed using a commercially available finite element analysis program. A global model was constructed representing the full, tabbed specimen. In addition, a more detailed sub-model was constructed in order to more accurately characterize the stress and strain distribution near the notch.

Specimens were tested at three loading rates at each temperature: 104, 17, and 5.8 MPa/min (15.1, 2.5, and 0.8 ksi/min). The loading rate had little impact on the strength of specimens tested at room temperature; however, the average strength was 26% lower at 50°C (122º F) and 33% lower at 60°C (140ºF). A micro-buckling theory was employed such that failure initiated at some region of fiber misalignment. The predictions for failure were based on three assumed angles of misalignment. As the test temperatures varied, the results corresponded to different assumed angles of misalignment. This showed that there was fault in the theory on which the global finite element model predictions were based, as the angle of misalignment should be the same for all specimens cut from the same sheet. This error was attributed to a stress gradient at the notch, which was not accounted for in the predictions. A comparison of experimental

strength and the predictions provided by the finite element sub-model showed far better agreement, particularly at elevated temperatures.

Seven specimens were creep tested at a constant stress of 634 MPa (92 ksi) at 50°C (122ºF). Four failed prematurely at the tab, and three failed at the notch. Failure times spanned several decades of minutes, and the constant load rate tests showed a roughly linear trend between stress and time. The authors concluded that the relationship between failure stress and time followed a power law. The creep test results were found to be consistent with a linear extrapolation of the constant load rate results.

The authors concluded that a finite element model based on a non-linear quasielastic constitutive equation and a locally discrete representation of the fibers and matrix successfully predicted the compressive strength of a notched unidirectional composite material over a range of time and temperature.

Wong, Davies, and Wang (2003) investigated the compressive strength of 100 x 30 x 4 mm (3.94 x 1.18 x 0.16 in) glass reinforced plastic (GRP) C-shaped channels at several temperatures. The specimens used were off-the-shelf products made by the pultrusion process in which E-glass fibers were embedded with isophthalic polyester resin cured at elevated temperatures. One study was done using 30 mm (1.18 in) long specimens to determine the longitudinal compressive strength of the material. A second study was done using 400 mm (15.75 in) specimens to determine column behavior. The test temperatures used were 20, 60, 90, 120, 150, 200, and 250˚C (68, 140, 194, 248, 302, 392, and 482ºF). Testing methods for the studies were not carried out according to standard testing procedures. The testing of the short specimens was done using the entire channel section instead of coupons. The restraints were solid steel plates with C-shaped

grooves, simulating a fixed-end condition. The tests were performed using a test rig consisting of a hydraulic jack with an electric kiln built around it. The specimens were heated at a rate of 2˚C (3.6ºF) per minute until the target temperature was achieved, at which point the compressive load was applied until failure.

For the compressive strength analysis, four or five tests were performed at each temperature. Failures at the lowest three temperatures were characterized by crushing near midheight accompanied by a "loud bang". The failure mode was a combination of fiber micro-buckling and kinking under uniaxial compression. At temperatures exceeding 90˚C (194ºF), the failure mode was crushing due to softening of the resin. For the column analysis, two tests were performed at each temperature. The temperature variation inside the kiln during the tests was approximately 10% of the target temperature. The values in Tables 2.2 and 2.3 are the average results for the compressive strength tests and the column tests.

Table 2.2: Compression Test Results from Wong, Davies, and Wang (2003)

Temperature ˚C (ºF)	20 (68)	60 (148)	90 (194)	120 (248)	150 (302)	200 (392)	250 (482)
Average Load kN (kip)	171.58 (38.57)	108.05 (24.29)	53.20 (11.96)	27.73 (6.23)	19.26 (4.33)	18.48 (4.15)	13.73 (3.09)
Average Stress N/mm^2 (ksi)	282.20 (40.93)	177.72 (25.78)	87.50 (12.69)	45.61 (6.62)	31.68 (4.59)	30.39 (4.41)	22.58 (3.27)

Table 2.3: Column Test Results from Wong, Davies, and Wang (2003)

Temperature °C (°F)	20 (68)	60 (148)	90 (194)	120 (248)	150 (302)	200 (392)	250 (482)
Average Load kN (kip)	62.8 (14.1)	38.4 (8.6)	36.4 (8.2)	16.3 (3.7)	13.8 (3.1)	5.8 (1.3)	5.3 (1.2)

A numerical modeling study was also done based on the results of the experimental studies. This was an investigation of the commercial finite element package called ABAQUS and its performance in the prediction of the behavior of GRP at elevated temperatures. The numerical simulation gave slightly conservative results for low temperatures and substantially nonconservative results for the two highest temperatures. The discrepancy at high temperatures is attributed to great uncertainty in the mechanical properties of the composite when the resin has lost the majority of its stiffness.

The authors concluded that GRP structures have a rapid reduction in strength above the heat distortional temperature of the resin, and that at elevated temperatures, GRP mechanical properties are highly dependent on the softening resin. They also asserted that ABAQUS could be used to give accurate numerical simulations of GRP behavior at elevated temperatures given reliable mechanical properties.

CHAPTER III

SHORT-TERM PROPERTIES

In separate studies, Butz (1997) and Kang (2001) performed an exhaustive investigation of the short-term mechanical properties of a polyester/E-glass material identical to that used in the present study. A description of methods used by Butz and Kang follows along with resulting short-term properties. Further testing of the specimens was performed as part of the current work in order to verify the results found in the earlier studies.

3.1 MATERIAL DESCRIPTION

The specimens examined in this study were slender square tube columns made up of isophthalic polyester resin mixed with Kaolin clay fillers and reinforced with E-glass fibers, depicted in Figure 3.1. The E-glass fiber reinforcements were in the forms of roving and continuous strand mats (CSM). Kang (2001) determined the specific gravity *SG* of the polyester/E-glass composite and the volume fraction of all constituents. The specific gravity was determined in accordance with ASTM D792; the weight of the material in air was compared to the weight of the material in distilled water. The specific gravity was found to be 1.84, with a coefficient of variation (COV) of 0.9%. The volume fractions of the constituents of the section were determined according to methods proposed by Ye, et al. (1995). The material was burned in a furnace to eliminate the

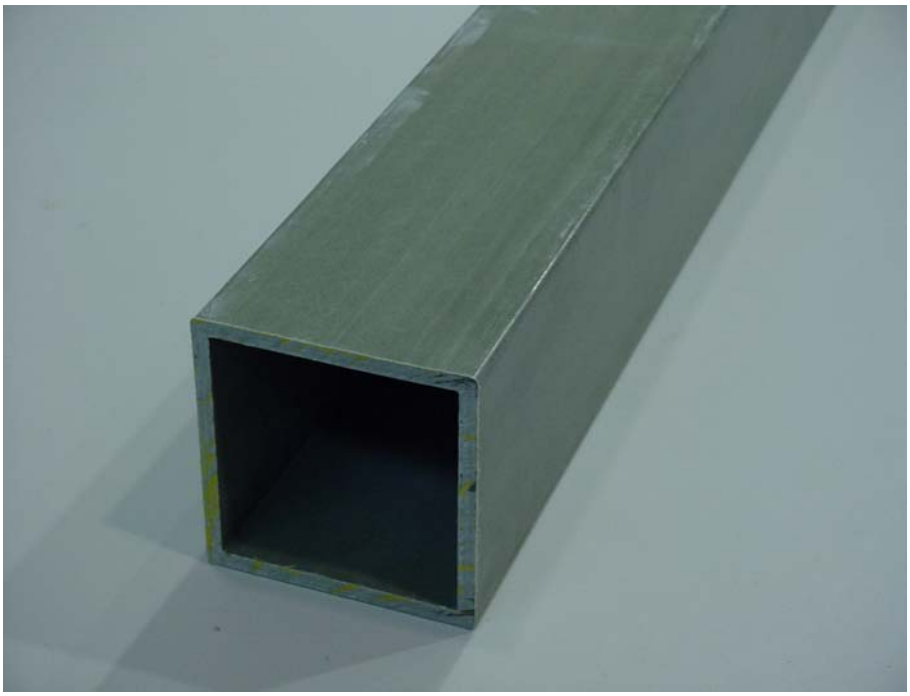

Figure 3.1: Pultruded Square Tube Section Tested

resin, and the weight lost was assumed to be the resin weight. The remaining rovings and CSM's were then separated, and the fillers were removed from each using sulfuric and nitric acids. The weight of the remaining material was assumed to be the roving and CSM weights. The resulting weights were then used to calculate the volume fraction of each constituent. Summing the individual volume fractions and subtracting from 1.0 gave the volume fraction of voids in the samples. The results follow in Table 3.1:

Table 3.1: Volume Fractions of Polyester/E-glass Constituents (from Kang, 2001)

	Roving υ_{rov} (%)	CSM υ_{csm} (%)	Resin υ_{re} (%)	Filler υ_{fil} (%)	Void υ_{v} (%)
Average	23.1	12.2	53.7	9.3	1.7
STD	1.4	0.8	1.2	1.1	0.2
COV	6.2	6.7	2.3	12.0	12.9

3.2 MECHANICAL PROPERTIES

Thirty compression and eighteen in-plane shear tests were performed by Butz (1997), and thirty uniaxial tension tests were performed by Kang (2001), all on coupons cut from identical sections. The compression tests and in-plane shear tests were carried out following the procedures described in ASTM D3410 and ASTM D5379, respectively. Coupons larger than standard were tested for mechanical properties in shear in order to account for inhomogeneity of the sections (Zureick, et al., 1999). The uniaxial tension tests were performed according to ASTM D3039. The coupon specimen dimensions for all tests are shown in Figure 3.2. The resulting values for mechanical properties are provided in Tables 3.2 and 3.3. Figures 3.3 and 3.4 are typical stress vs. strain curves from tension, compression, and shear tests, respectively.

Table 3.2: Modulus Values from Coupon Tests (from Kang, 2001)

	Compression	Tension	Shear
	E_L^c GPa (ksi)	E_L^t GPa (ksi)	G_{LT} GPa (ksi)
Average	23.83 (3456)	23.75 (3445)	2.73 (396)
STD	0.96 (139)	1.50 (218)	0.28 (41)
COV	4.0%	6.3%	10.4%

Table 3.3: Strength Values from Coupon Tests (from Kang, 2001)

	Compression	Tension	Shear
	F_L^c MPa (ksi)	F_L^t MPa (ksi)	F_V MPa (ksi)
Average	380.0 (55.1)	372.8 (54.1)	73.0 (10.6)
STD	45.4 (6.6)	25.6 (3.7)	7.1 (1.0)
COV	12.0%	6.9%	9.7%

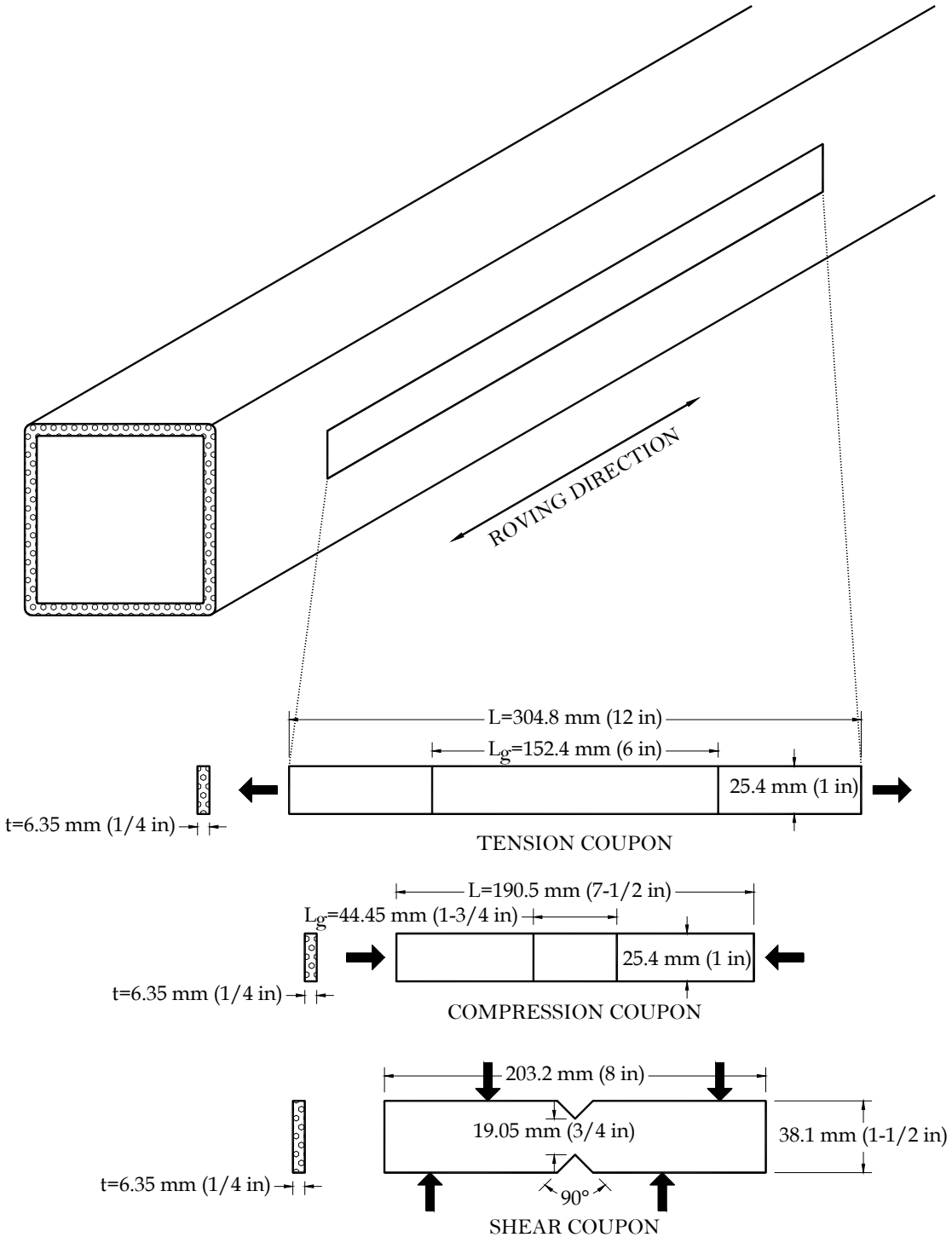

Figure 3.2: Coupon Dimensions (from Kang, 2001)

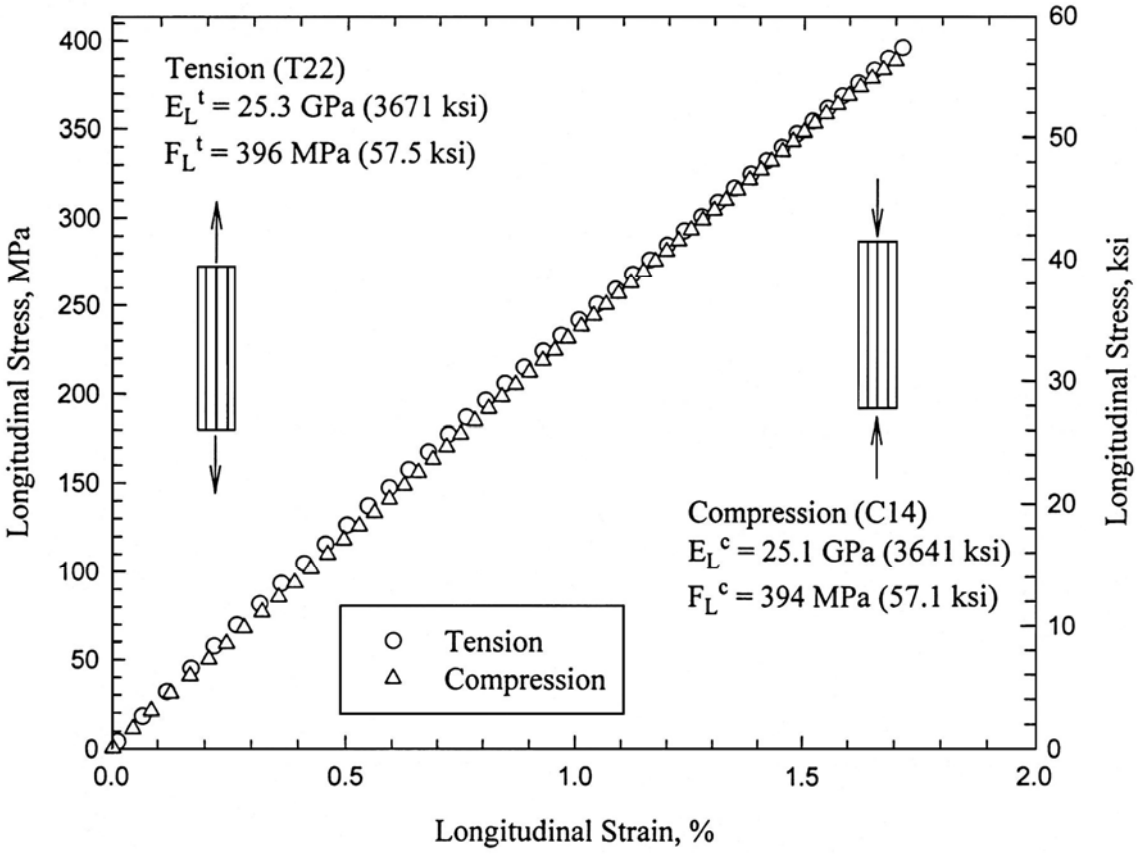

Figure 3.3: Typical Tension and Compression Stress vs. Strain (from Kang, 2001)

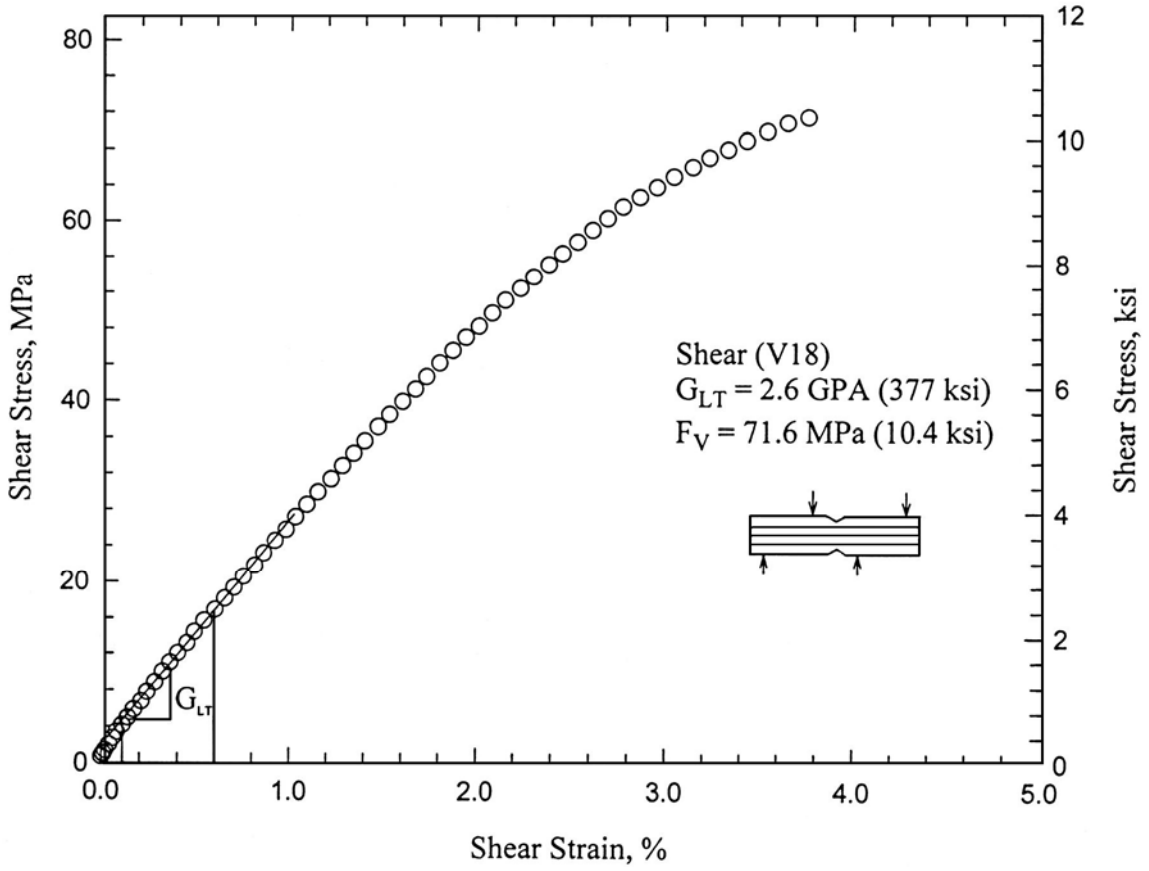

Figure 3.4: Typical Stress vs. Strain from Shear Tests (from Kang, 2001)

Fifteen compression and fifteen uniaxial tension tests were performed as part of the present work to validate the mechanical properties established by Butz and Kang. The tests were carried out according to ASTM D3410 and D3039, respectively; however, the coupon lengths were somewhat varied from the previous tests. The compression coupons had an overall length of 170 mm (6.7 in) with a gage length of 43 mm (1.7 in). The tension coupons had an overall length of 330 mm (13 in) with a gage length of 203 mm (8 in). All other dimensions were the same. The resulting average values of modulus and strength are summarized in Tables 3.4 and 3.5, and typical stress vs. strain curves for each test type are provided in Figures 3.5 and 3.6. Individual test results appear in Appendix A.

Table 3.4: Modulus Values from Current Coupon Tests

	Compression	Tension
	E_L^c GPa (ksi)	E_L^t GPa (ksi)
Average	23.97 (3476)	22.75 (3300)
STD	2.46 (357)	1.62 (235)
COV	10.3%	7.1%
Difference from Values Found by Butz and Kang	0.6%	4.2%

Table 3.5: Strength Values from Current Coupon Tests

	Compression	Tension
	F_L^c MPa (ksi)	F_L^t MPa (ksi)
Average	367.3 (53.28)	376.8 (54.65)
STD	32.1 (4.65)	33.2 (4.82)
COV	8.7%	8.8%
Difference from Values Found by Butz and Kang	3.3%	1.1%

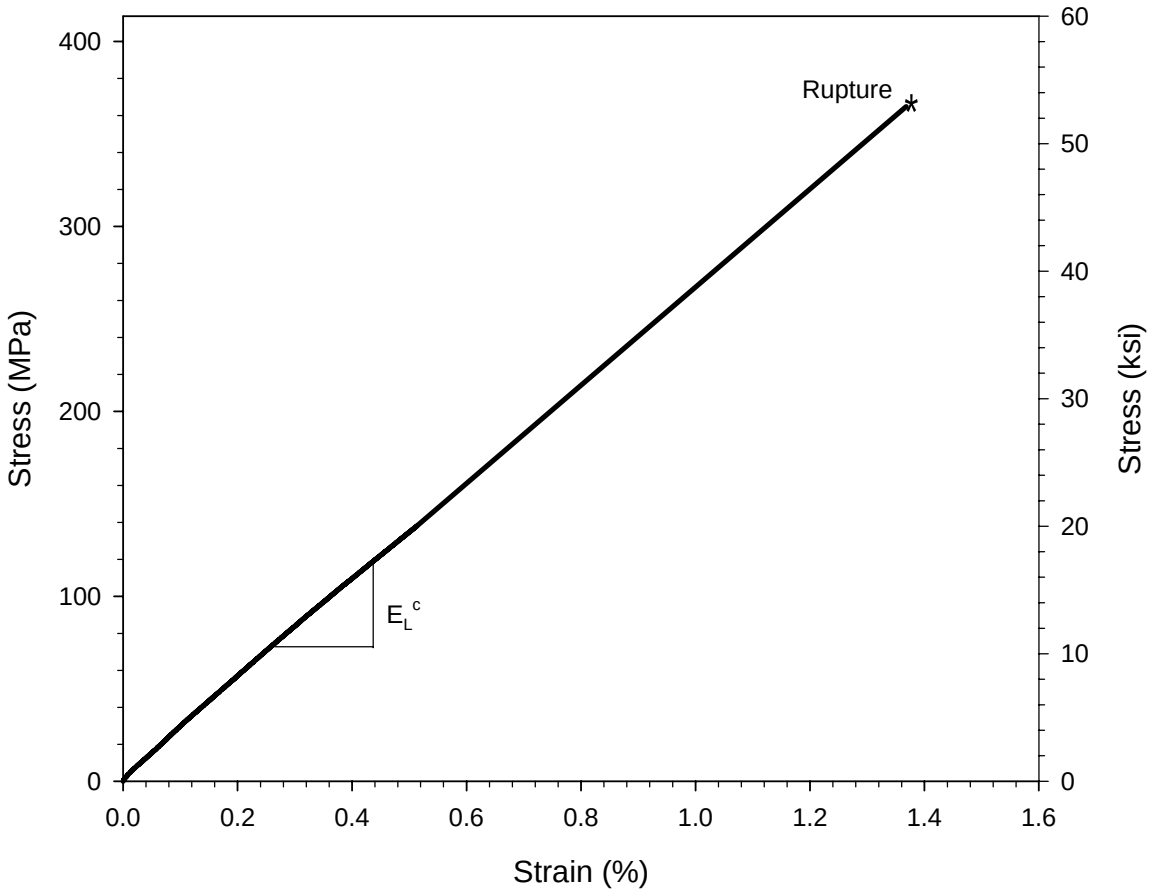

Figure 3.5: Typical Stress vs. Strain from Compression Tests in the Present Study

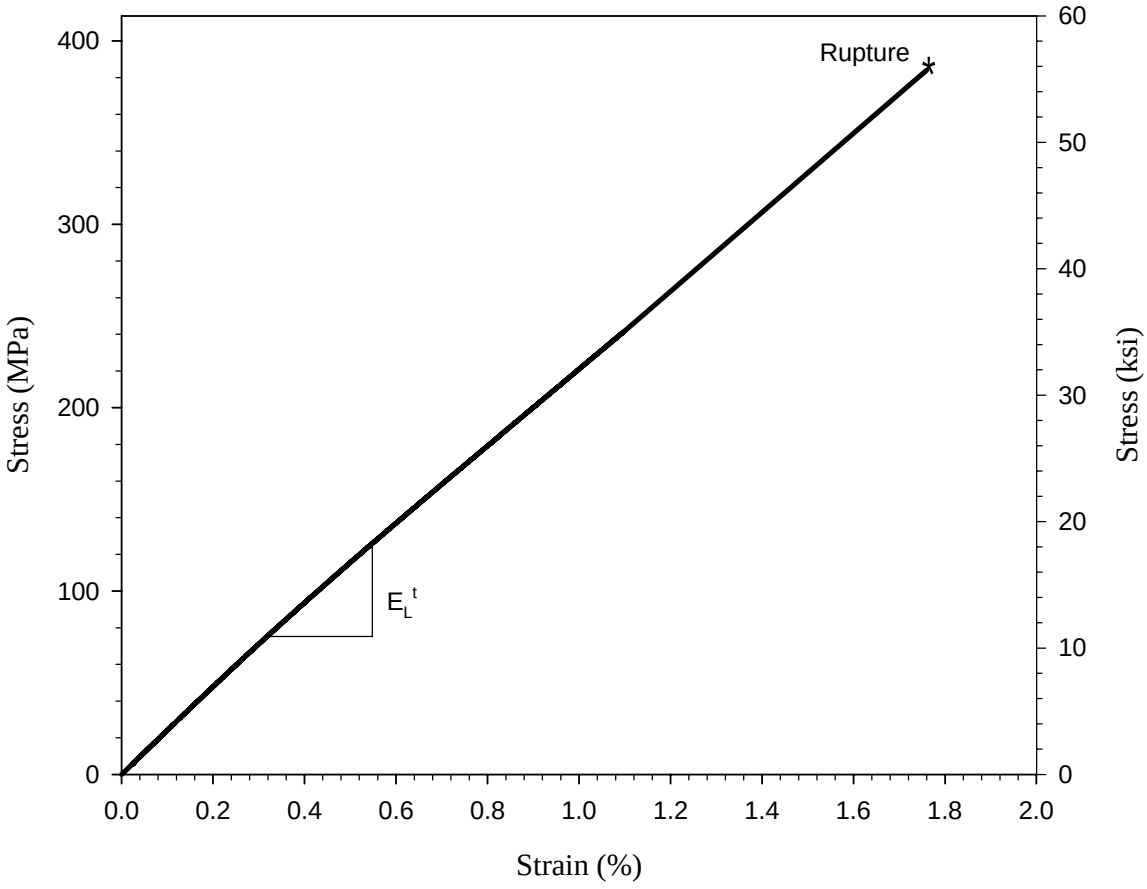

Figure 3.6: Typical Stress vs. Strain from Tension Tests in the Present Study

Based on the high degree of consistency between the mechanical properties found in the present work and those already established by Butz and Kang, and taking into account the statistical analysis that was performed in Kang's study, the values from the previous studies will be used in this work.

3.3 SHORT-TERM BUCKLING

Butz (1997) performed short-term buckling tests on several square tube specimens with the same dimensions as those in the current study. While specimens were tested under both concentric and eccentric axial loads, only the concentric buckling tests are relevant to the current investigation. Prior to testing, the out-of-straightness of each specimen was measured, and all measurements were well below the maximum value specified by ASTM D3917-94 of

$$\delta_i \leq \frac{L_0}{240} \tag{3.1}$$

Buckling tests were performed in a three-screw testing machine with knife-edge supports, simulating pinned-end boundary conditions. As the compressive load was applied at a constant rate of 0.64 mm/min (0.025 in/min), load, longitudinal strain, midheight lateral deflection, axial shortening, and end rotation were measured. The load vs. displacement during loading and unloading proved the specimens to be elastic. Southwell's method (1932) was used to approximate the critical buckling load of the specimen. Figure 3.7 shows a typical load vs. midheight lateral deflection curve from the buckling tests performed by Butz. The Southwell approximation of the critical buckling load is also shown.

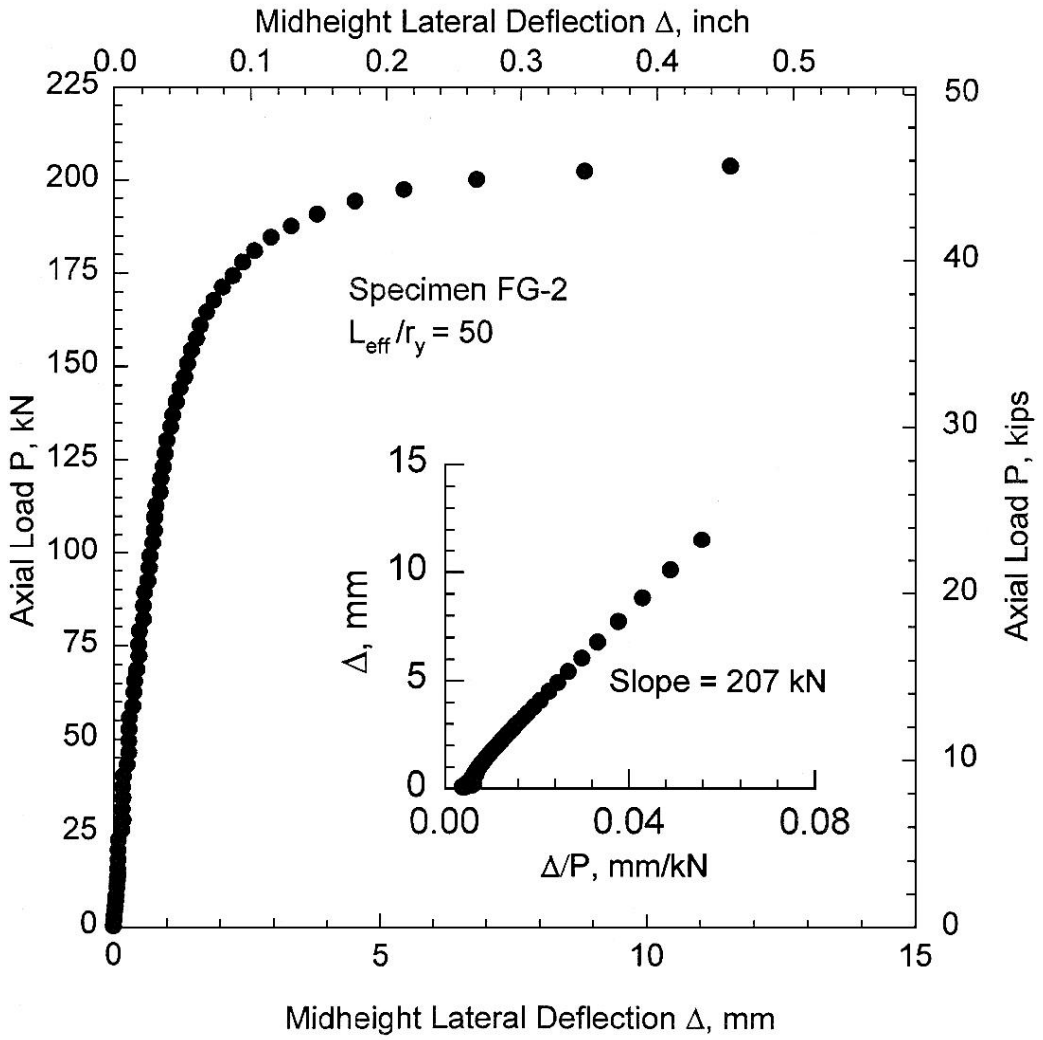

Figure 3.7: Load vs. Deflection of Buckling Test and Southwell Plot (from Butz, 1997)

A short-term concentric load test was performed as part of the current investigation in order to verify the previously obtained results. The deviation from straightness of each specimen was measured prior to testing in accordance with ASTM D3917-94. A dial gage stand was fixed at an arbitrary height and placed on a flat reference table at one end of the specimen. The dial gage and stand were then moved down the length of the specimen, taking readings at 50.8 mm (2 in) intervals along the centerline. The procedure was repeated for each side of the specimen in order to determine the maximum out-of-straightness, δ_i. The maximum out-of-straightness of the specimen was found to be 0.2 mm (0.008 in), well within the limits of Equation 3.1. The test setup was similar to that of the creep tests, described in Chapter 4; however, in this case the specimen was loaded until buckling occurred. Buckling was defined as the point at which the column began to rapidly deflect laterally with minimal increase in load. During testing, applied load, midheight lateral deflection, and axial shortening were measured. The data were used to construct a Southwell plot so that an approximation of the critical buckling load could be made. A plot of load vs. midheight lateral deflection and the Southwell approximation are shown in Figure 3.8, and a photograph of the buckled column is provided in Figure 3.9. The resulting short-term buckling load of the specimen P_{ST} was 225 kN (50.54 kips).

Euler's equation was employed to provide an approximation of the critical buckling load of the specimens tested in the current study. A modification to Euler's equation first proposed by Engesser (1889) was also used. The modified form includes the effects of transverse shear on the column. The form of Euler's equation used was:

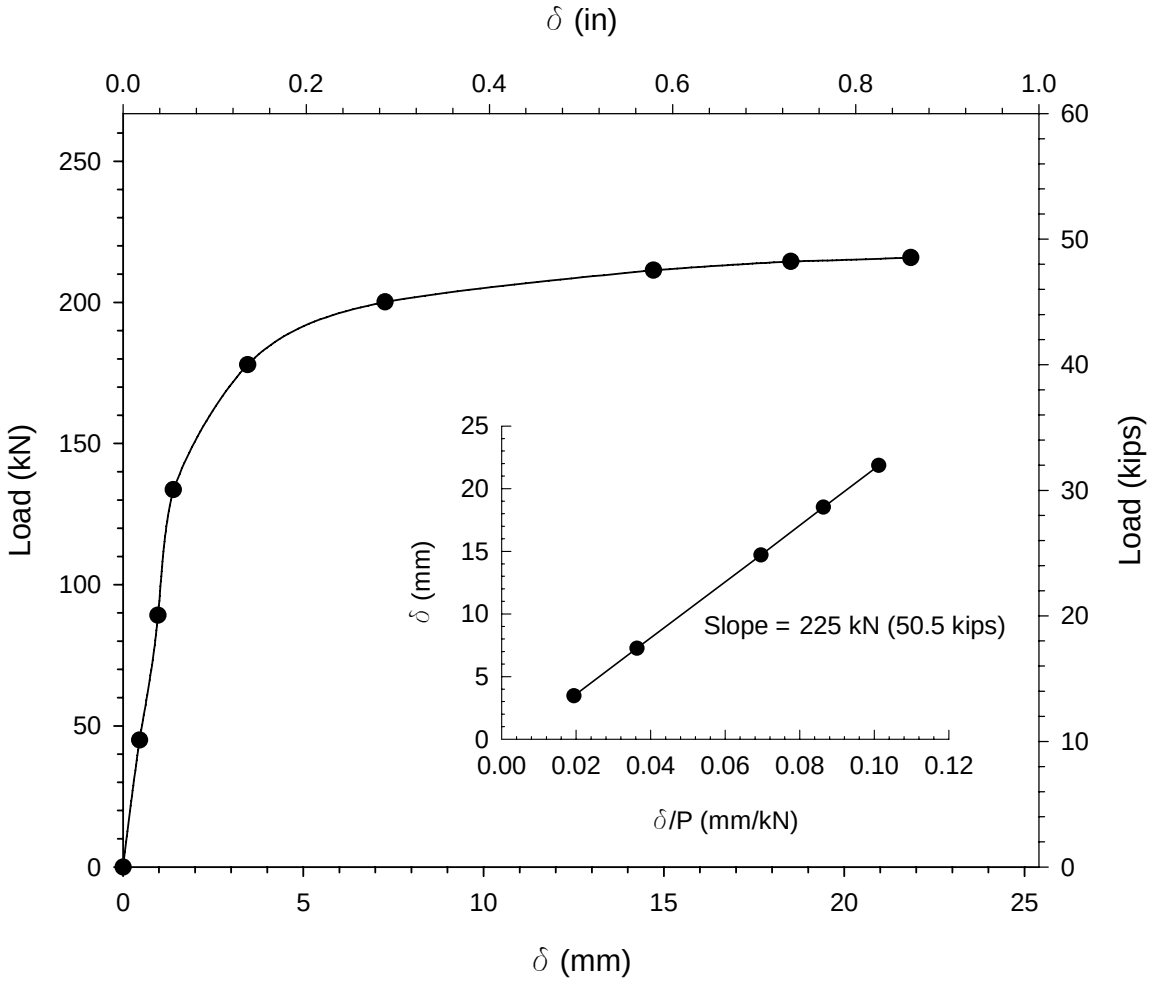

Figure 3.8: Load vs. Deflection and Southwell Plot from Buckling Test

Figure 3.9: Buckled Column from Short-Term Buckling Test

$$P_E = \frac{\pi^2 E_L^C I}{L_{eff}^2} \tag{3.1}$$

in which $E_L{}^C$ is the longitudinal elastic modulus in compression, I is the moment of inertia of the section about one of its axes of symmetry, and L_{eff} is the distance between knife-edge supports. The modified form used was:

$$P_e = \frac{P_E}{1+\left(n_s P_E / A_g G_{LT}\right)} \tag{3.2}$$

where P_E is the load calculated in Equation 3.1, n_s is a form factor for shear equal to 2 for a square tube section, A_g is the gross area of the section, and G_{LT} is the shear modulus. Table 3.6 presents the results of the various means of approximating the critical buckling load.

Based on the results, a slightly conservative value for the critical buckling load was taken at 200 kN (45 kips). This conservatism minimized the possibility of failure of the specimens before creep testing could be performed.

Table 3.6: Critical Buckling Load Approximations

	Approximation			
	Current Study (Experimental)	Butz (Experimental)	Euler (Equation 3.1)	Modified Euler (Equation 3.2)
P_{cr} kN (kips)	225 (50.5)	207 (46.6)	238 (53.5)	222 (49.9)
Values used in Equations 3.1 and 3.2: $E_L{}^C$ = 23.83 GPa (3456 ksi); I = 3.67x10^6 mm^4 (8.82 in^4); L_{eff} = 190.5 cm (75 in); n_s= 2 (Square Tube); A_g = 2412.9 mm^2 (3.74 in^2); G_{LT} = 2.73 GPa (396 ksi)				

CHAPTER IV

SUSTAINED LOAD EXPERIMENTS

4.1 TEST SPECIMENS

A total of six specimens having square tube cross-sections were tested under sustained concentric axial loads. The effective length L_{eff} of the specimens consisted of the overall length of the member L_0 = 182.9 cm (72 in) and an additional 7.6 cm (3 in) from the knife-edge supports, for a total effective length of L_{eff} = 190.5 cm (75 in). The slenderness ratio was L_{eff}/r = 49. A schematic of the cross-section is provided in Figure 4.1 with typical dimensions and properties in Table 4.1.

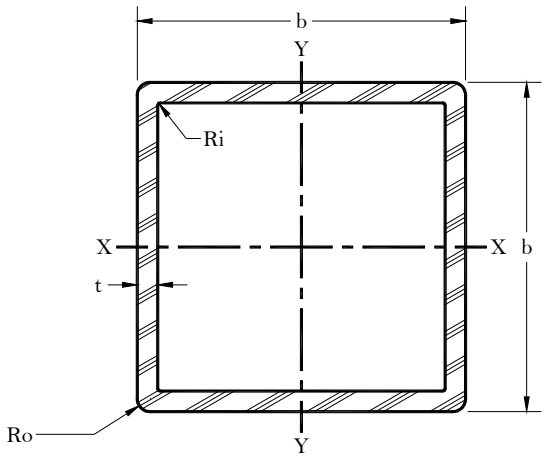

Figure 4.1: Cross-Section of Typical Test Specimen

Table 4.1: Typical Dimensions and Section Properties of Test Specimens

Section Dimension				Section Properties					
b mm (in)	T mm (in)	R_o mm (in)	R_i mm (in)	A mm^2 (in^2)	I mm^4 (in^4)	r mm (in)	$\frac{b}{t}$	L_0 cm (in)	L_{eff} cm (in)
101.6 (4)	6.35 (1/4)	3.97 (5/32)	0.79 (1/32)	2412.9 (3.74)	$3.67x10^6$ 8.82	38.86 1.53	16	182.9 (72)	190.5 (75)

The identification system chosen for the test specimens designates the composite type, the ratio of the applied load to the short-term critical load, and whether the test was conducted at room temperature or at the elevated temperature of 65.5°C (150°F). As an example, specimen PG-33-E represents a polyester/glass specimen tested at 33% of its critical load at the elevated temperature.

4.2 OUT-OF-STRAIGHTNESS

The maximum out-of-straightness δ_i of each specimen was measured prior to testing in the same fashion as in the short-term buckling test. The values are presented in Table 4.2. As shown in the table, the measured values for all specimens were well below the specified maximum value.

Table 4.2: Maximum Out-of-Straightness of Test Specimens

Specimen	δ_i mm (in)	$\frac{\delta_i}{L_0}$
PG-33-R	0.30 (0.012)	0.00016
PG-33-E	0.38 (0.015)	0.00020
PG-67-R	0.30 (0.012)	0.00016
PG-67-E	0.15 (0.006)	0.00008
PG-90-R	0.10 (0.004)	0.00005
PG-90-E	0.23 (0.009)	0.00012
ASTM Max. Allowable	7.62 (0.300)	0.00417

4.3 TESTING APPARATUS

Creep tests and buckling tests were performed in four frames consisting of four threaded steel rods and four steel plates, held in place by hexagonal nuts. A typical test frame schematic is shown in Figure 4.2. Knife-edge supports were used at both ends of each specimen in order to simulate pinned boundary conditions and to ensure the plane of bending of the section. The specimens were held in adjustable clamps made up of two sliding angle sections with threaded rods for tightening, and a bottom plate welded to a 38.1 mm (1.5 in) thick rectangular steel bar. The rectangular steel bar was notched in a v-shape for seating on the knife-edge supports, enabling free rotation about one axis. A close-up view of a typical end support and clamp is shown in Figure 4.3.

The axial load was applied using a manual hydraulic jack. A load cell was placed between the top of the hydraulic jack and the bottom of the bottom plate to measure the

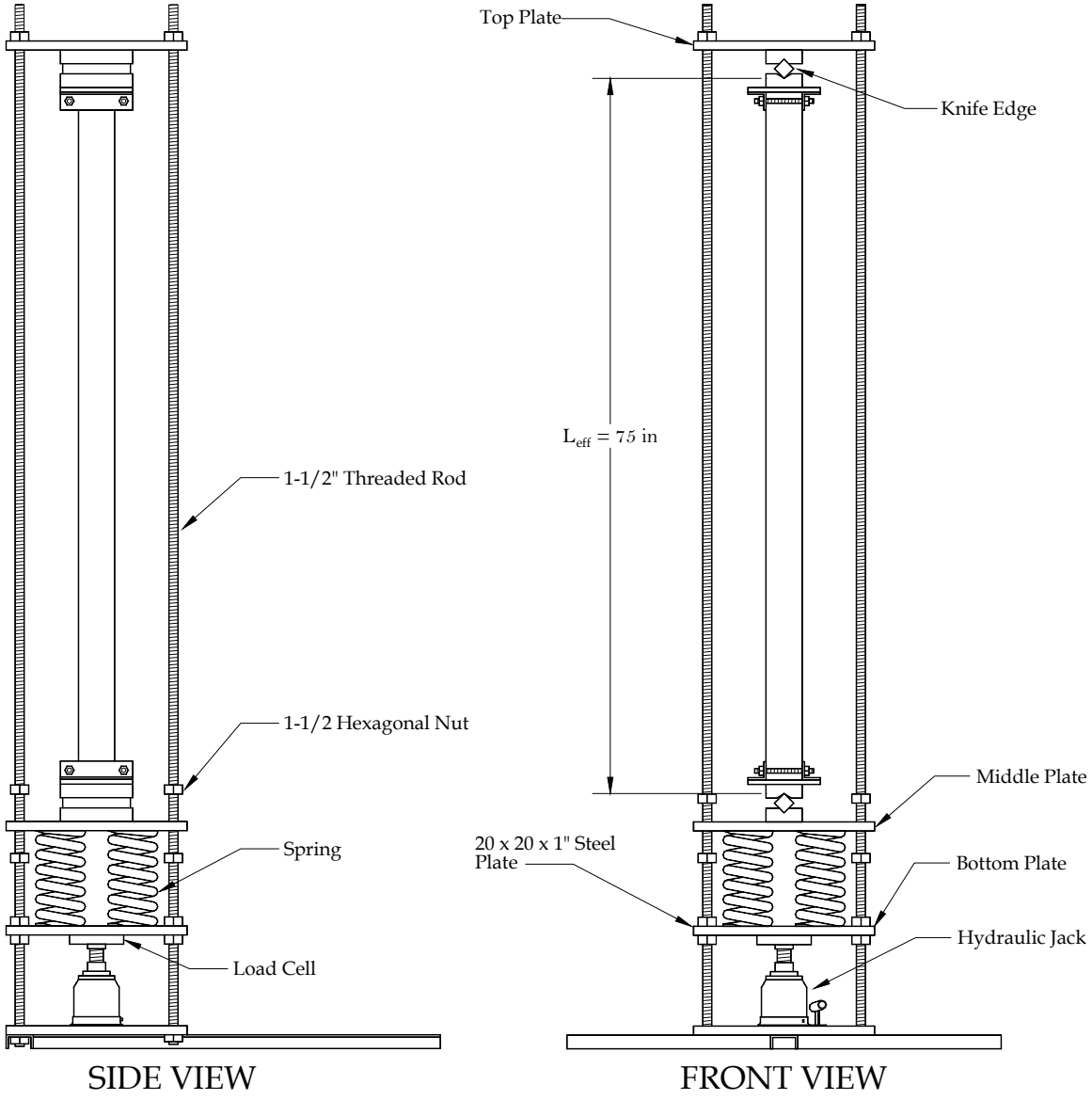

Figure 4.2: Creep Reaction Frame

Figure 4.3: Typical Knife-Edge Support and Clamp

applied load. In order to ensure verticality of the specimen, a plummet was affixed to the top knife-edge support and any needed adjustments were made. Large capacity coil springs were placed between the bottom and middle plates in a symmetric arrangement so that the load would be transferred from the jack to the specimen. A close-up of the hydraulic jack, load cell, and springs is presented in Figure 4.4. For the creep tests, after applying the desired amount of axial load, the bottom plate was locked in place using the hexagonal nuts. The pressure in the hydraulic jack was slowly removed, while the springs remained compressed; this arrangement was used to sustain the load for the duration of the test. Prior to testing, the stiffness *K* of each spring was

Figure 4.4: Hydraulic Jack, Load Cell, and Springs

determined using a servo-hydraulic testing machine. The resulting average value for *K* was found to be 520 N/mm (2970 lb/in). The summation of the spring constants of all springs in a given frame provided an estimate of *K* for that frame. The spring arrangement for each frame was chosen such that a minimal difference in spring constants existed; this helped provide a more uniform distribution of the load. Based on the total spring constant and the measured axial displacement, the approximate amount of load lost due to relaxation of the specimen throughout the test could be monitored. The maximum amount of load lost throughout the tests was only 3.8% of the applied load. It was therefore unnecessary to re-apply the load to any of the specimens.

Dial gages with a precision of 0.025 mm (0.001 in) were placed at midheight to measure lateral deflection, on the middle plate to measure axial displacement, and on both sides of the end support to estimate end rotation. The positions of the dial gages are illustrated in Figure 4.5.

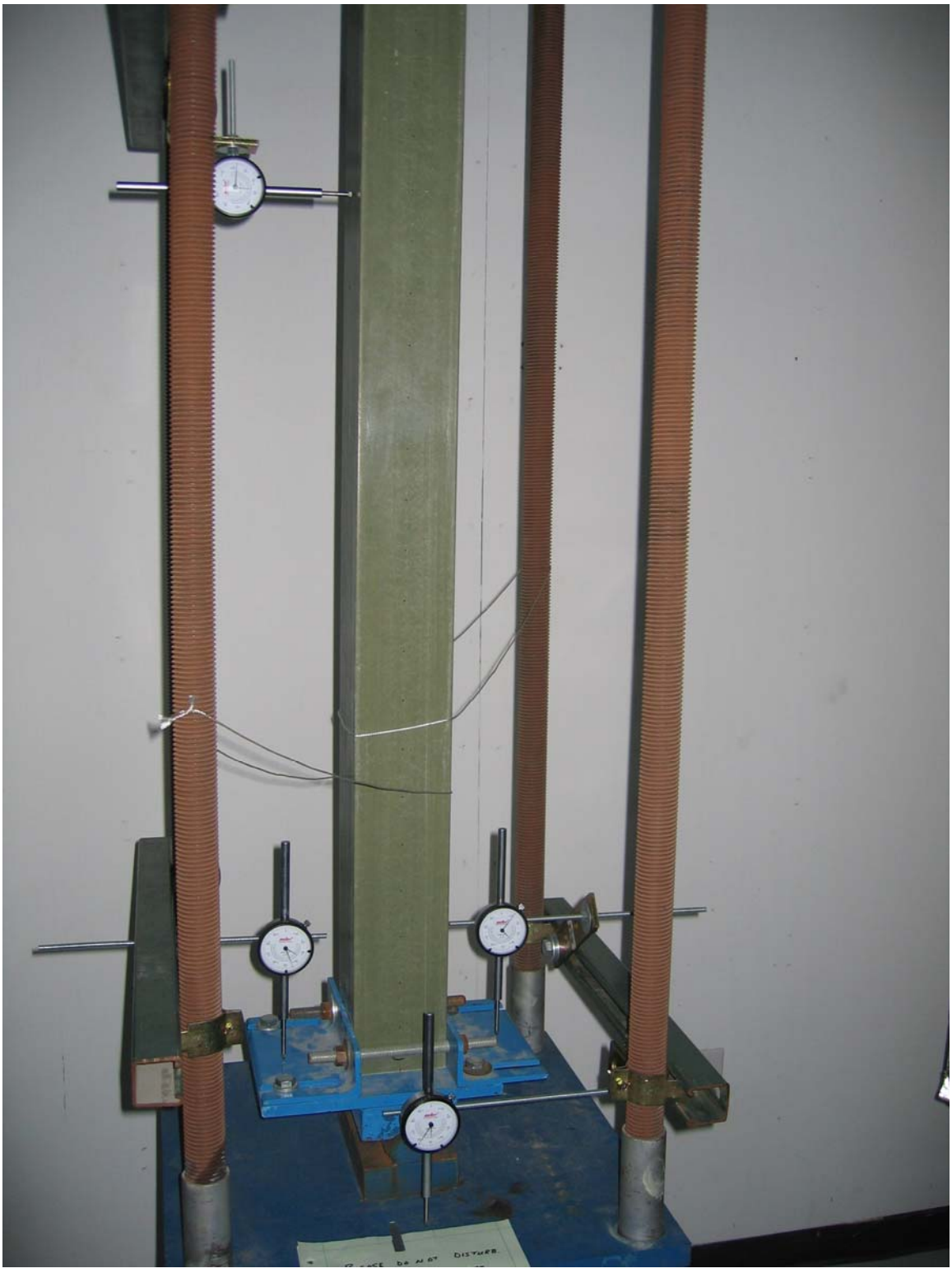

Figure 4.5: Location of Dial Gages

4.4 ELEVATED TEMPERATURE CREEP FIXTURES

Two of the creep frames were outfitted with 38.1 mm (1.5 in) thick fiberglass insulation in order to create a heating chamber for the specimens. An electrical finned strip heater was used to heat the air inside the chamber, and the air was circulated using a blower and insulated flexible duct. The temperature inside the chamber was monitored using a panel thermometer and regulated with a remote bulb thermostat. A fiberglass heat shield was placed between the strip heater and the specimen in an effort to minimize thermal concentrations on the specimen. Figure 4.6 shows a non-insulated creep fixture beside an insulated creep fixture with a blower and flexible duct, and Figure 4.7 shows a finned strip heater mounted inside a creep fixture.

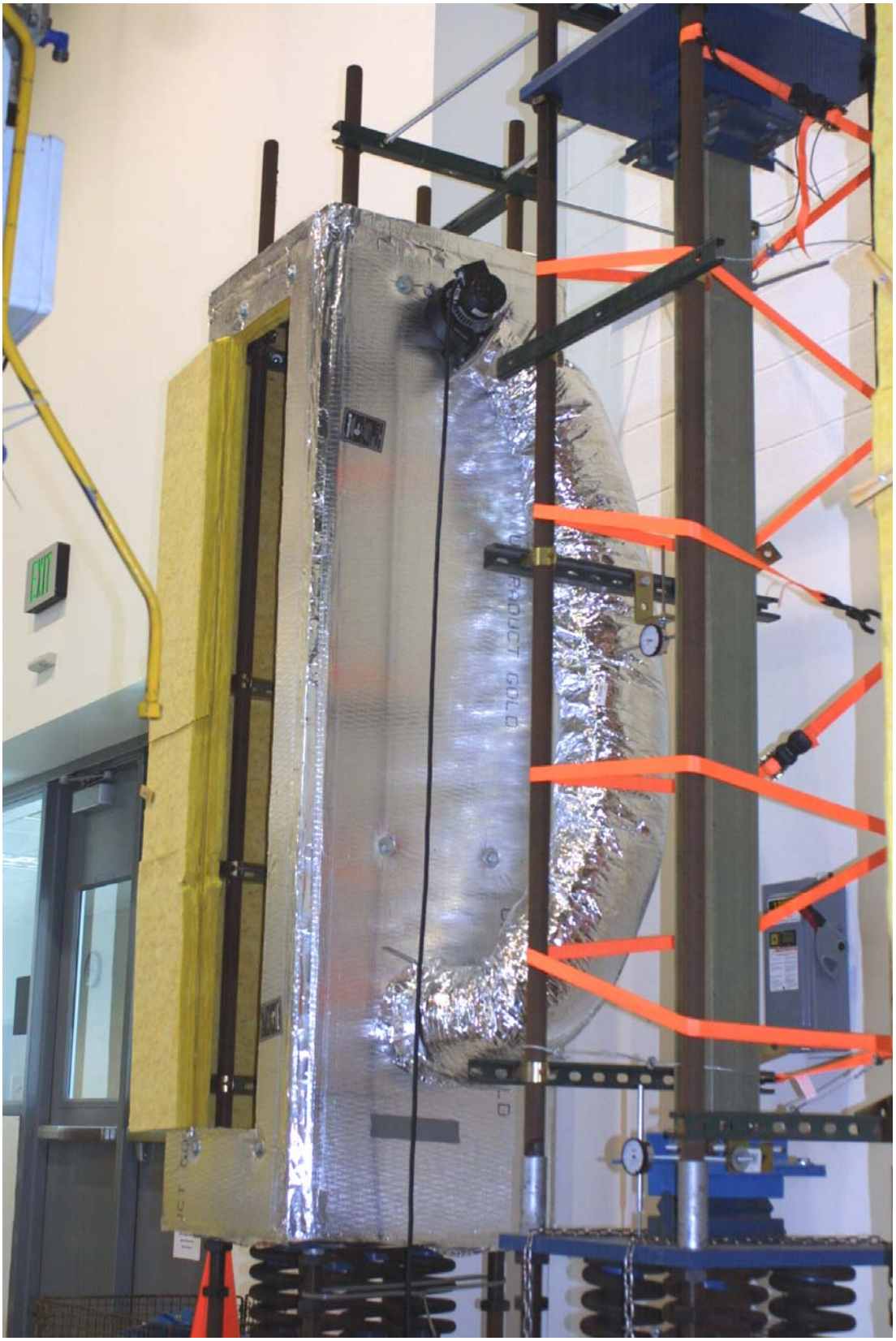

Figure 4.6: Insulated and Non-insulated Creep Fixtures

Figure 4.7: Finned Strip Heater Inside Insulated Creep Fixture

4.5 EXPERIMENTAL PROGRAM

4.5.1 Creep Tests

Most manufacturers of pultruded structural shapes provide design manuals with their product lines. Design manuals published by three different manufacturers were reviewed (Strongwell Corporation (2002), Bedford Reinforced Plastics Inc. (2004), Creative Pultrustions Inc. (2004)), and each provides the same basic guidelines for the design of the specimens in the current study. In all cases, it is recommended that members made with polyester resin not be exposed to service temperatures in excess of 65.5ºC (150ºF). Also, for compression members a safety factor of 3 is used in all design equations. The Eurocomp Design Code for Structural Design of Polymer Composites (1996) requires that when creep testing polymer composites, a temperature no greater than 20ºC (36ºF) less than the material's glass transition temperature T_g, otherwise known as heat distortional temperature, be used. The glass transition temperature for the material in this study is 78.9ºC (174ºF), making the maximum test temperature specified by the Eurocomp Design Code 58.9ºC (138ºF). However, this is a general requirement that was meant to encompass all polymeric composites. It is very realistic to expect service temperatures up to 65.5ºC (150ºF) in attics and crawlspaces, and in many industrial environments.

The service temperature and load levels used in this study were chosen based on these guidelines. Three sets of creep tests at different axial loads were carried out, each set consisting of one test at room temperature, 23ºC (73ºF), and one at 65.5ºC (150ºF). The ratios, λ, of applied axial load to the short-term critical buckling load determined in Chapter 3 were 0.33, 0.67, and 0.89. The lowest load represents a safety factor of 3.

These ratios correspond to loads of 66.7 kN (15 kips), 133.4 kN (30 kips), and 177.9 kN (40 kips), respectively. Based on the short-term coupon testing, the resulting stress levels were 7, 15, and 22% of the ultimate strength of the material.

Typically, the creep behavior of viscoelastic materials can be represented in three stages. The primary stage is characterized by an initially high rate of creep, decreasing over time until it becomes constant. Once the rate becomes constant the material is considered to be in the secondary stage, typically the longest stage of creep behavior. The tertiary stage is characterized by an increasing rate of creep over time until failure. Based on the staged creep behavior of the material, it was necessary to take frequent readings at the onset of the tests when the creep rate was at its highest, and at a decreasing rate as the tests progressed. Throughout the initial loading process, the axial displacement of the specimen was monitored so that an initial elastic response of the material could be established. The commencement of each creep test was taken as the point at which the load was released from the hydraulic jack. At that time, initial dial gage readings were taken. Some of the load on the specimen was lost in the transition of support from the jack to the hexagonal nuts, so the reading at the end of the loading process was not the same as the reading after the release of the jack. This loss was accounted for based on the spring constants calculated prior to the test. At the start of the test, readings were taken at 15 minute intervals for the first hour, 30 minute intervals up to 4 hours in, 1 hour intervals up to 8 hours in, 2 hour intervals up to 16 hours in, 4 hour intervals up to 36 hours in, 12 hour intervals up to 72 hours in, 24 hour intervals up to 14 days in, and finally 1 week intervals until termination of the test. Each test was terminated after 1,000 hours.

4.5.2 Post-Creep Short-Term Buckling Tests

After each specimen had been tested for 1,000 hours, the load was removed and the specimen was allowed to recover. The buckling load of each tested specimen was subsequently determined in the same fashion as that discussed in Chapter 3. It was assumed that the majority of the creep deformations were almost immediately recovered once the loads were removed. McClure and Muhammadi (1995) observed that more than half of the creep strain in their samples was recovered within 250 hours of releasing the stress. The channel sections in that investigation were tested at a stress equal to 45% of ultimate for 2500 hours; the specimens in the current study were tested at a maximum stress of 22% of ultimate for only 1000 hours. With substantially smaller stress levels and shorter test durations, it follows that the time to full recovery of creep deformation in the square tube sections in question would be much shorter. Also due to the lower stress levels, it was far less likely that any nonlinear plastic deformation due to creep developed, enabling a higher percentage of the creep deformation to be recovered. Based on this, each specimen was given a minimum of one week (168 hours) of recovery time before a short-term buckling test was performed.

CHAPTER V

RESULTS AND EVALUATION

5.1 RESULTS

5.1.1 Creep Tests

A typical load vs. axial displacement diagram from the initial application of load is shown in Figure 5.1. It can be seen that the material behaved in a reasonably linear fashion. Table 5.1 presents the experimentally measured midheight lateral deflection of the specimens due to creep, $\delta(t)-\delta_0$, at time intervals of 10, 100, and 1,000 hours; the values of initial midheight lateral deflection δ_0 are also provided in the table. The entire data set for all specimens is shown graphically in Figure 5.2. An illustration of the midheight lateral deflection at various time intervals is given in Figures 5.3 through 5.5 for each specimen.

Specimen PG-90-E, with a creep deflection of 3.10 mm (0.122 in), exhibited the most lateral creep deflection among the specimens tested. As expected, the lowest magnitude of creep deflection, 0.05 mm (0.002 in), was seen in specimen PG-33-R.

As with lateral creep deflection, the most axial creep displacement was observed in specimen PG-90-E, and the least was seen in specimen PG-33-R, having creep displacements of 0.86 mm (0.034 in) and 0.10 mm (0.004 in), respectively. However, many of the measured axial displacements did not follow the same trend as the lateral deflections. The inconsistency of the measured values of axial displacement meant that

any meaningful analysis of the data would be limited. The discrepancies will be discussed in Chapter 6. Table 5.2 presents the axial creep displacement, $\Delta(t) - \Delta_0$. The axial creep displacement for all specimens is plotted in Figure 5.6.

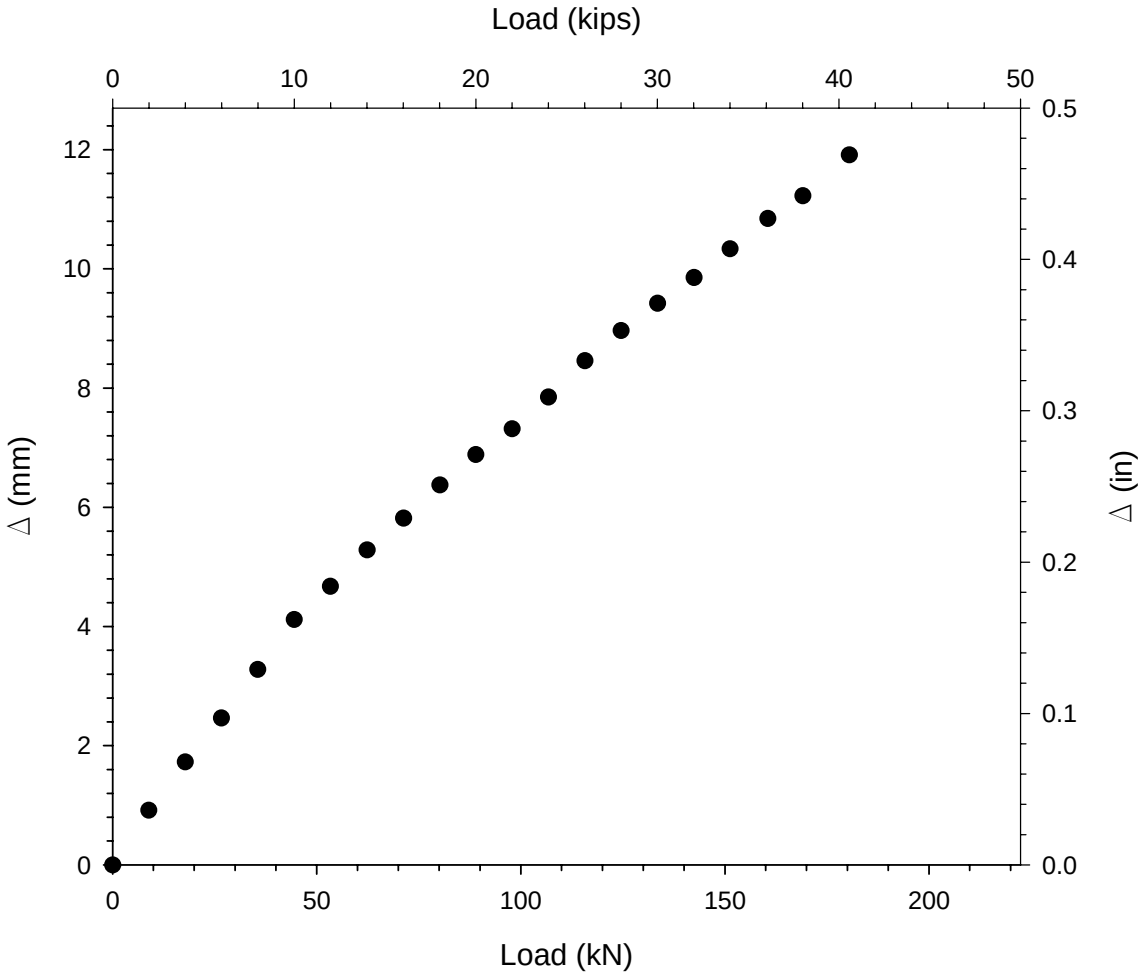

Figure 5.1: Typical Load vs. Axial Displacement from Initial Loading Process

Table 5.1: Midheight Lateral Creep Deflection

Specimen	PG-33-R	PG-33-E	PG-67-R	PG-67-E	PG-90-R	PG-90-E
δ_0	0.74 mm (0.029 in)	1.32 mm (0.052 in)	2.49 mm (0.098 in)	2.51 mm (0.099 in)	2.97 mm (0.117 in)	2.13 mm (0.084 in)
Time Hours	$\delta(t)-\delta_0$ mm (in)	$\delta(t)-\delta_0$ mm (in)	$\delta(t)-\delta_0$ mm (in)	$\delta(t)-\delta_0$ mm (in)	$\delta(t)-\delta_0$ mm (in)	$\delta(t)-\delta_0$ mm (in)
10	0.03 (0.001)	0.05 (0.002)	0.10 (0.004)	0.18 (0.007)	0.20 (0.008)	0.43 (0.017)
100	0.03 (0.001)	0.10 (0.004)	0.15 (0.006)	0.41 (0.016)	0.30 (0.012)	1.55 (0.061)
1000	0.05 (0.002)	0.30 (0.012)	0.28 (0.011)	0.69 (0.027)	0.53 (0.021)	3.10 (0.122)

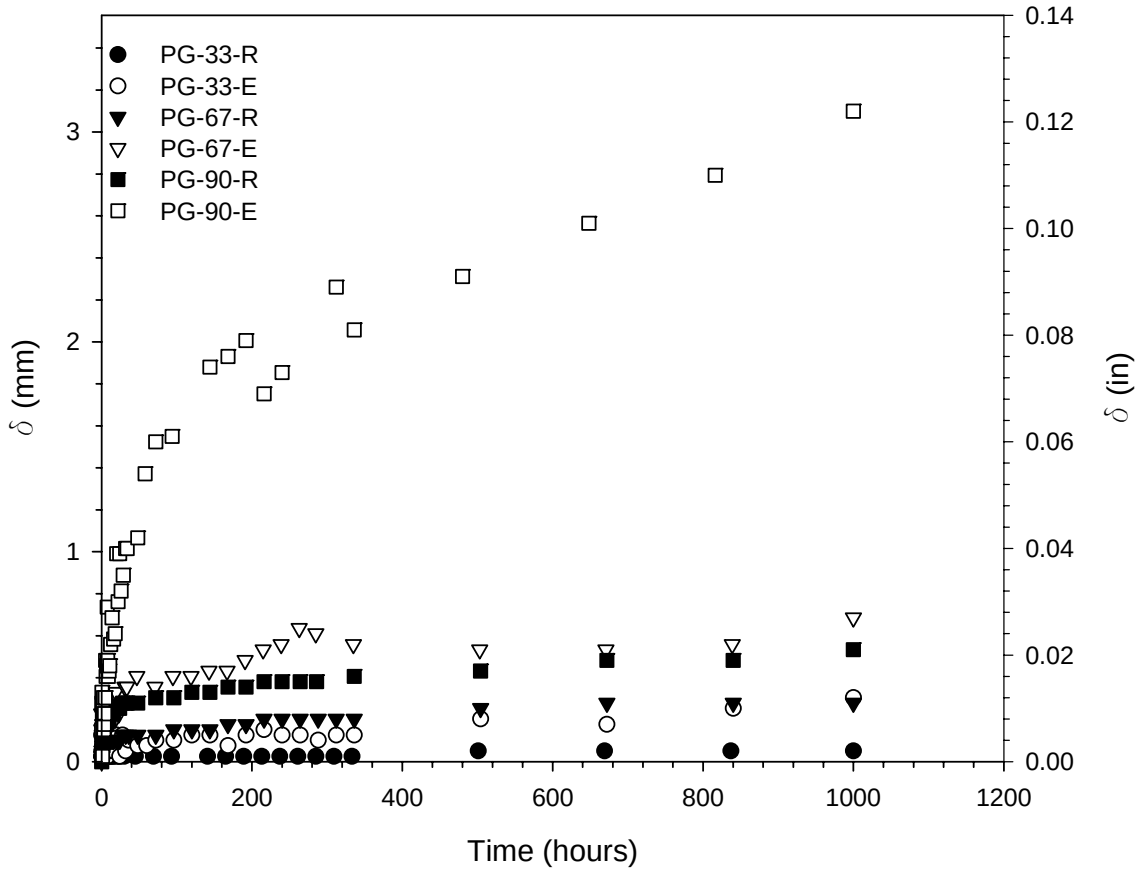

Figure 5.2: Midheight Lateral Creep Deflection of All Specimens

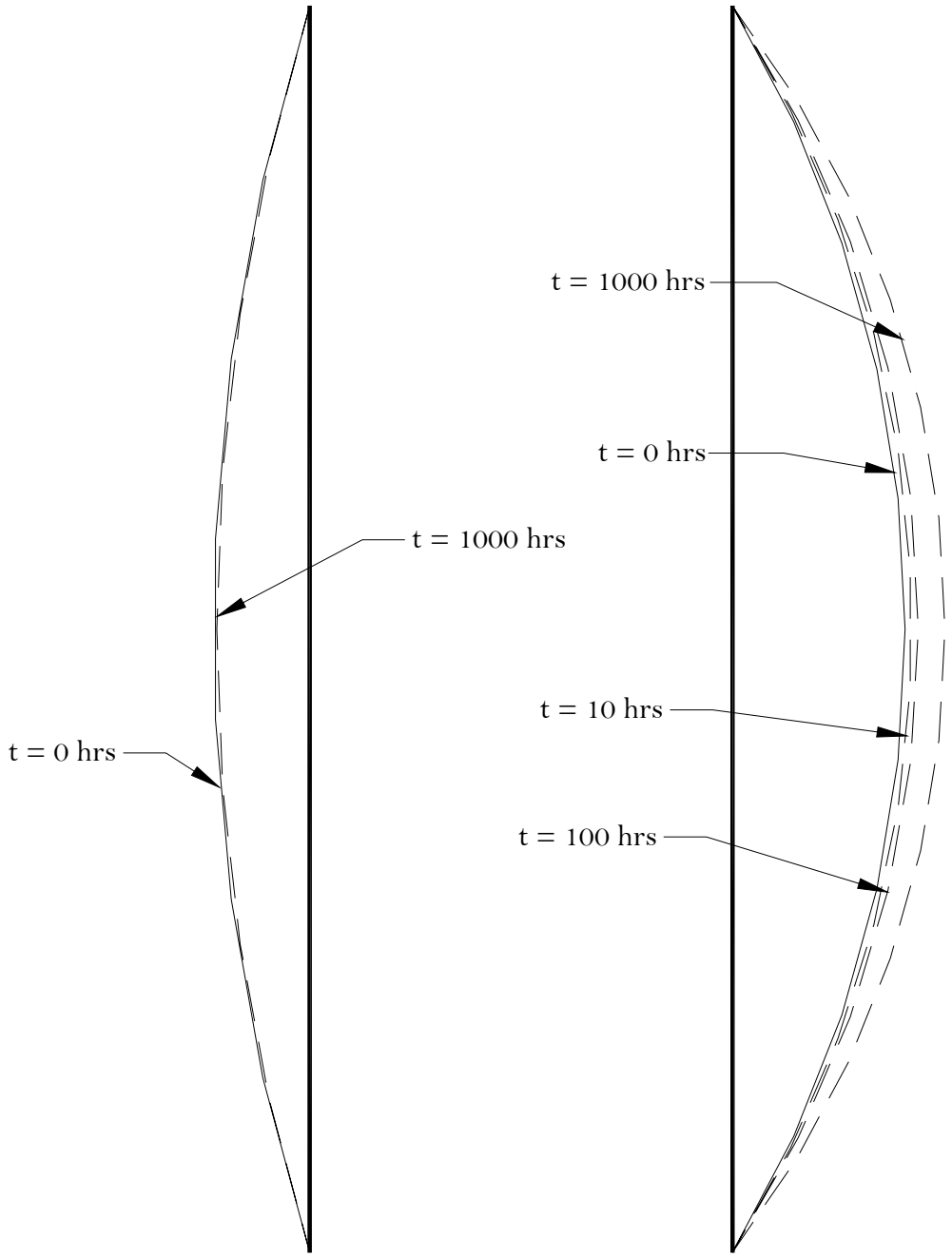

Figure 5.3: Deflection of Specimens at Various Time Intervals (λ = 0.33)

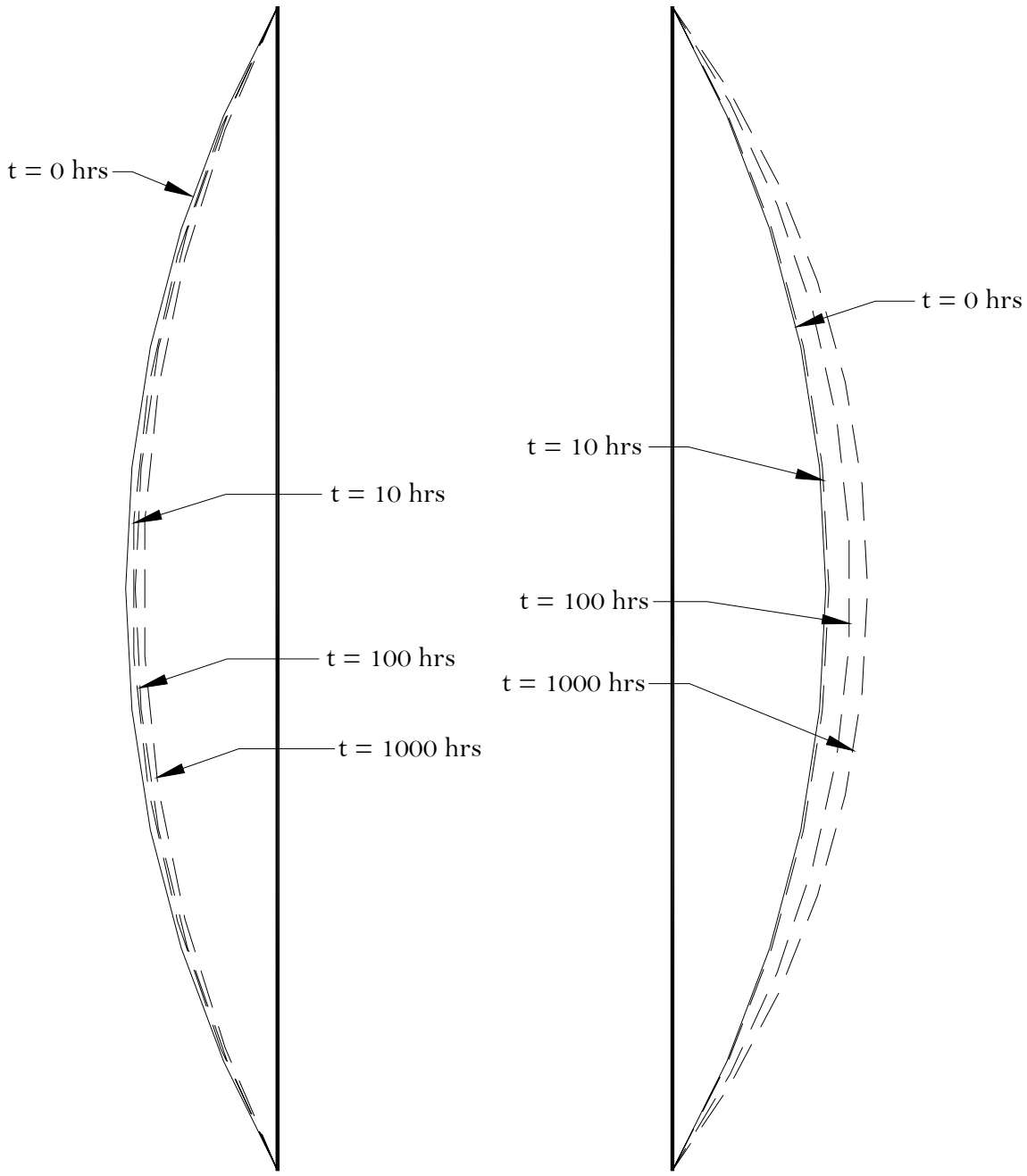

Figure 5.4: Deflection of Specimens at Various Time Intervals (λ = 0.67)

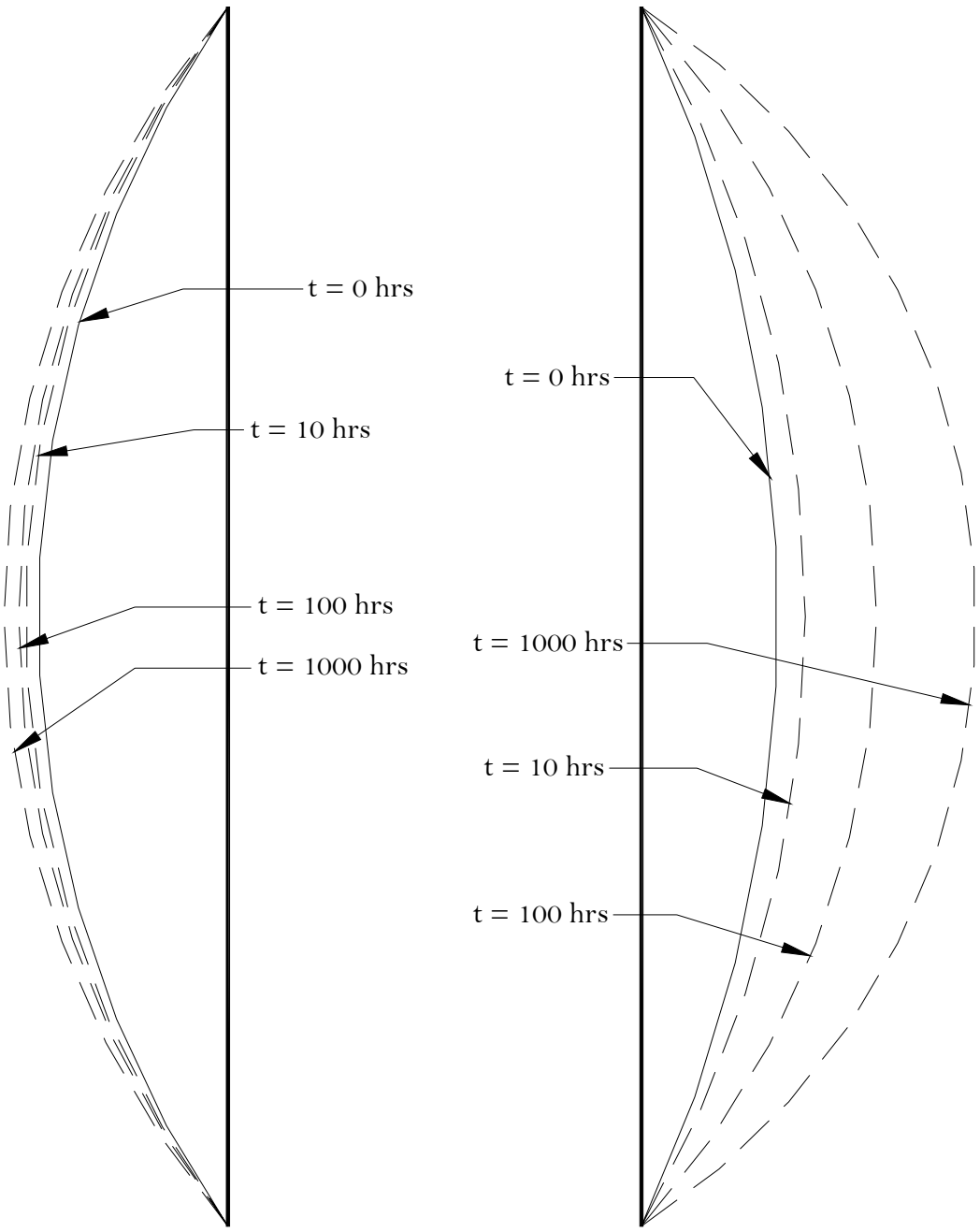

Figure 5.5: Deflection of Specimens at Various Time Intervals (λ = 0.90)

Table 5.2: Axial Creep Displacement

Specimen	PG-33-R	PG-33-E	PG-67-R	PG-67-E	PG-90-R	PG-90-E
Δ_0	3.76 mm (0.148 in)	6.60 mm (0.260 in)	11.38 mm (0.448 in)	9.73 mm (0.383 in)	14.73 mm (0.580 in)	11.43 mm (0.450 in)
Time Hours	$\Delta(t)-\Delta_0$ mm (in)	$\Delta(t)-\Delta_0$ mm (in)	$\Delta(t)-\Delta_0$ mm (in)	$\Delta(t)-\Delta_0$ mm (in)	$\Delta(t)-\Delta_0$ mm (in)	$\Delta(t)-\Delta_0$ mm (in)
10	0.03 (0.001)	0.18 (0.007)	0.20 (0.008)	0.20 (0.008)	0.10 (0.004)	0.69 (0.027)
100	0.05 (0.002)	0.23 (0.009)	0.25 (0.010)	0.30 (0.012)	0.10 (0.004)	0.71 (0.028)
1000	0.10 (0.004)	0.41 (0.016)	0.38 (0.015)	0.58 (0.023)	0.13 (0.05)	0.86 (0.034)

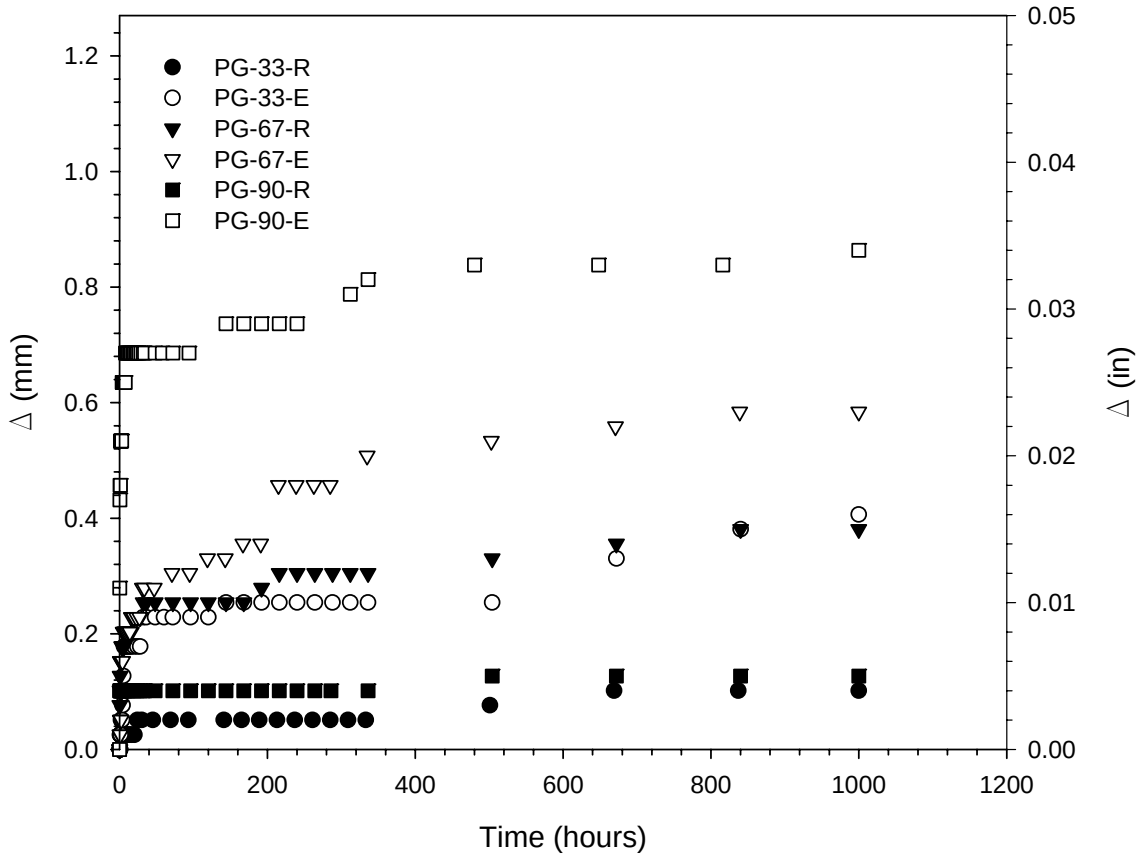

Figure 5.6: Axial Creep Displacement of All Specimens

5.1.2 Post-Creep Short-Term Buckling Tests

A summary of the results from the buckling tests performed after the termination of creep testing is given in Table 5.3. The maximum applied load, P_{max}, and the Southwell approximation of the critical buckling load, P_{exp}, are provided along with the difference between the experimentally obtained values and the predicted critical buckling load, P_E, based on Euler's equation. The difference between each of the experimental buckling loads and the short-term buckling load determined in Chapter 3, P_{ST}, is also given. Load vs. midheight lateral deflection, P vs. δ, plots are given in Appendix C.

Table 5.3: Buckling Loads from Post-Creep Buckling Tests

Specimen	P_{max} kN (kips)	P_{exp} kN (kips)	P_{exp}/ P_E %	P_{exp}/ P_{ST} %
PG-33-R	220 (49.5)	225 (50.5)	94.4	99.9
PG-33-E	220 (49.6)	227 (50.9)	95.3	100.8
PG-67-R	220 (49.5)	225 (50.5)	94.4	99.9
PG-67-E	138 (31.0)	152 (34.1)	63.7	67.5
PG-90-R	254 (57.0)	263 (59.2)	110.7	117.2
PG-90-E	141 (31.7)	145 (32.5)	60.7	64.4
	P_E kN (kips)	238 (53.5)	P_{ST} kN (kips)	225 (50.5)

5.2 EVALUATION OF RESULTS

5.2.1 Creep Tests

Two semi-empirical approaches were used to accurately predict the creep behavior of the specimens tested in this study. Each approach assumes a linear viscoelastic response of the material to sustained loads. Given the relatively low stress levels (relative to ultimate) used in this study, this assumption appears reasonable. The first approach was based on Schapery's quasielastic method, and the second was based on Findley's power law.

Many of the analytical approaches used to model the viscoelastic behavior of slender specimens under axial compression refer to the ultimate limit state as "creep buckling" (for example, Vinogradov (1987)). However, experimental studies have revealed that failure of axially loaded specimens under sustained loads generally occurs as a result of excessive deflections; a specific point at which specimens become "unstable" prior to failure is extremely difficult to determine. Therefore, it would appear more reasonable to define the failure mechanism more generally as "creep collapse."

Quasielastic Method

This method was chosen based on the results of the study by Kang (2001), which examined creep buckling of eccentrically loaded columns of the same type. Vinogradov (1987) applied Schapery's quasielastic method (1965) to the problem of creep buckling of viscoelastic beam-columns and proposed an equation for time-dependent midheight lateral deflection.

Based on the governing differential equation for lateral deflection $w(x)$ of a simply supported column under axial load, the initial shape of a column can be modeled as

$$w(x) = A_i \sin\left(\frac{n\pi x}{L}\right) \tag{5.1}$$

where A_i is the amplitude of the initial imperfection. For $n = 1$, this amplitude is equal to the out-of-straightness of the specimen. From elastic buckling theory, the lateral deflection at midheight of a concentrically loaded column $w(l/2)$ with initial imperfection can be written as

$$\delta = A_i \frac{\lambda}{1-\lambda} \tag{5.2}$$

in which λ is the ratio of the applied load to the critical buckling load, P/P_{cr}. A comparison of measured initial lateral deflections to those predicted by Equation 5.2 is provided in Table 5.4.

Table 5.4: Measured and Predicted Initial Midheight Lateral Deflection

Specimen	Temperature °C (°F)	Temperature °C (°F)	Measured δ_0 mm (in)	Predicted δ_0 mm (in)
PG-33-R	22.8 (73)	33	0.74 (0.029)	0.15 (0.006)
PG-33-E	65.5 (150)	33	1.32 (0.052)	0.19 (0.008)
PG-67-R	22.8 (73)	67	2.49 (0.098)	0.61 (0.024)
PG-67-E	65.5 (150)	67	2.51 (0.099)	0.31 (0.012)
PG-90-R	22.8 (73)	90	2.97 (0.117)	0.91 (0.036)
PG-90-E	65.5 (150)	90	2.13 (0.084)	2.06 (0.081)

The defection at midheight of an eccentrically loaded column as determined by Timoshinko and Gere (1961) can be written as

$$\delta = \sec\left(\frac{kL}{2} - 1\right)e \tag{5.3}$$

where k^2 is the curvature of the member and e is the eccentricity of the applied load. Therefore, the total midheight deflection of a column with initial imperfection loaded eccentrically is equal to the sum of the equations 5.2 and 5.3:

$$\delta = \sec\left(\frac{kL}{2} - 1\right)e + A_i\frac{\lambda}{1-\lambda} \tag{5.4}$$

Neglecting the contribution of shear to the curvature, k can be written as

$$k = \frac{\pi}{L}\sqrt{\lambda} \tag{5.5}$$

Then equation 5.4 becomes

$$\delta = \sec\left(\frac{\pi}{2}\sqrt{\lambda} - 1\right)e + A_i\frac{\lambda}{1-\lambda} \tag{5.6}$$

The addition of a creep function $\psi(t)$ is necessary to account for the time-dependent behavior of the column. The function $\psi(t)$ can be assumed to have the form

$$\psi(t) = \frac{t^n}{\beta} \tag{5.7}$$

Including the creep function to model the time-dependent midheight lateral deflection $\delta(t)$ of a column yields

$$\delta(t) = \sec\left\{\frac{\pi}{2}\sqrt{\lambda[1+\psi(t)]} - 1\right\}e + A_i\frac{\lambda[1+\psi(t)]}{1-\lambda[1+\psi(t)]} \tag{5.8}$$

The first component of the right side of Equation 5.8 represents the midheight lateral deflection of an eccentrically loaded column with no imperfection, and the second component represents the midheight lateral deflection of a concentrically loaded column with initial imperfection. Thus, for the concentrically loaded columns in this study, a value of $e = 0$ can be substituted, giving

$$\delta(t) = A_1 \frac{\lambda[1+\psi(t)]}{1-\lambda[1+\psi(t)]} \tag{5.9}$$

This solution is based on the assumption of small deformations and is valid as long as

$$\lambda < \frac{1}{1+\psi(t)} \tag{5.10}$$

The creep parameters β and n from Equation 5.7 were determined through a nonlinear regression of the midheight lateral deflections of each specimen. The resulting values can be found in Table 5.5. Kang (2001) obtained values of β and n for eccentrically loaded E-glass/polyester columns in a similar fashion using Equations 5.7 and 5.8, resulting in a range of β from 62 to 75 and a range of n from 0.195 to 0.239. As can be seen in Table 5.5, specimen PG-90-E was the only specimen to possess values within these ranges.

The midheight lateral creep deflection of each specimen was predicted using its respective values of β and n. The predictions are shown in Figure 5.7. It can be seen that Equation 5.9 adequately predicted the deflections using individually determined creep parameters; however, there was no consistency in the parameters determined from experimental data. Additionally, due to the small magnitudes of deflections exhibited by

the specimens, the predictive model was extremely sensitive to β and *n*. Therefore, no effective normalization could be made for the parameters.

Table 5.5: Creep Parameters from Analysis

Specimen	Temperature °C (°F)	λ %	Quasielastic Method		Power Law Model	
			β	n	m	n
PG-33-R	22.8 (73)	33	0.88	0.002	0.0008	0.090
PG-33-E	65.5 (150)	33	0.75	0.007	0.0009	0.338
PG-67-R	22.8 (73)	67	2.95	0.004	0.0022	0.236
PG-67-E	65.5 (150)	67	2.40	0.005	0.0053	0.236
PG-90-R	22.8 (73)	90	13.25	0.007	0.0051	0.120
PG-90-E	65.5 (150)	90	70.92	0.229	0.0100	0.368

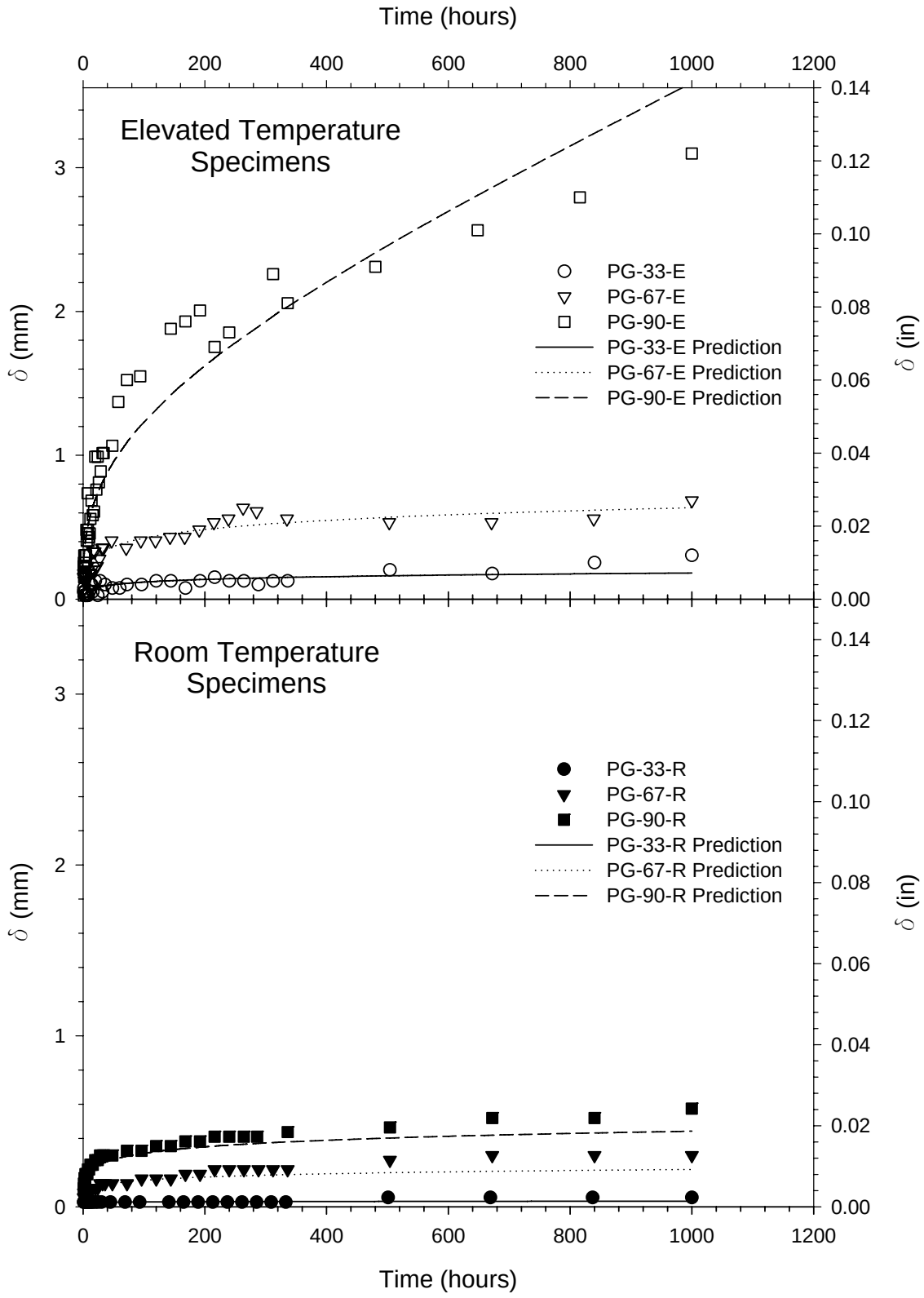

Figure 5.7: Quasielastic Predictions of Midheight Lateral Creep Deflection

Findley's Power Law Model

This method was chosen based on its wide acceptance for the modeling of creep behavior of viscoelastic materials. The original power law equation proposed by Findley (1944) is typically given in terms of strain, i.e.

$$\varepsilon(t) = \varepsilon_0 + mt^n \tag{5.13}$$

If the power law is applied to lateral displacements, the resulting equation will have the form

$$\delta(t) = \delta_0 + mt^n \tag{5.14}$$

In logarithmic form,

$$\log[\delta(t) - \delta_0] = \log(m) + n\log(t) \tag{5.15}$$

in which $\delta(t)$-δ_0 represents midheight lateral creep deflection, *n* is assumed independent of stress and temperature, and *m* is assumed dependent on stress and temperature. When plotted on a log-log scale, Equation 5.15 forms a straight line with *m* equal to the intercept at the unit time (1 hour) and *n* equal to the slope of the line. Plotting the equation with the creep data in this study produced values of *m* and *n* for each specimen, which are given in Table 5.5. Figure 5.8 demonstrates how Equation 5.15 was applied to the data from sample PG-90-R. Similar plots for the remainder of the specimens can be found in Appendix B.

Findley et al. (1956) expanded the power law in the form

$$\varepsilon(t) = \varepsilon'_0 \sinh\left(\frac{\sigma}{\sigma_\varepsilon}\right) + m't^n \sinh\left(\frac{\sigma}{\sigma_m}\right) \tag{5.16}$$

where ε'$_0$, σ_e, *m*', and σ_m are empirically determined constants dependent on material and environmental effects. Since lateral deflection of columns is more dependent on

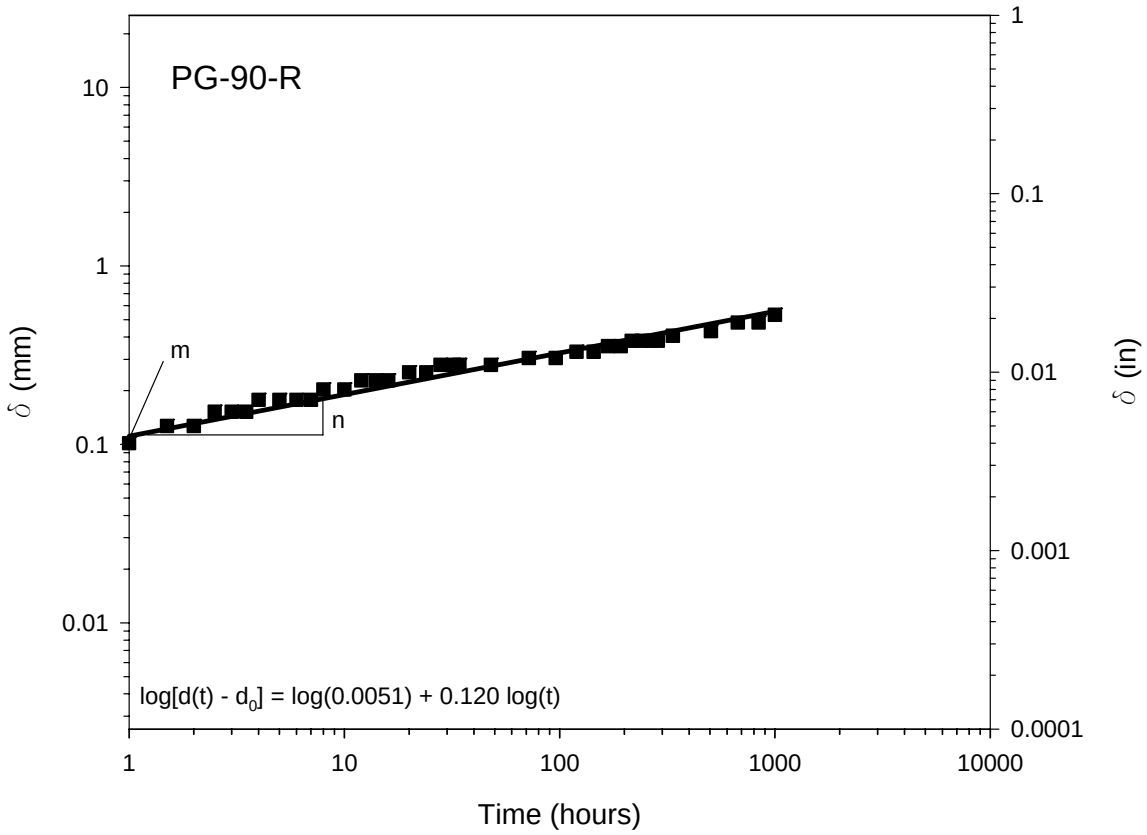

Figure 5.8: Determination of Creep Parameters *m* and *n* in Equation (5.15) (PG-90-R)

geometric effects and the magnitude of applied load than stress, Equation 5.16 was rewritten as

$$\delta(t) - \delta_0 = m' t^n \sinh\left(\frac{\lambda}{\lambda_m}\right) \tag{5.17}$$

where λ is the ratio of applied load to critical buckling load and λ_m is an empirical constant. A value of $\lambda_m = 0.32$ was chosen such that a plot of m vs. $\sinh(\lambda/\lambda_m)$ for the room temperature specimens produced a straight line intersecting the origin. Figure 5.9 shows this linearization. The value of m' was then taken as the slope of the line (0.0006).

Assuming n to be wholly material dependent, an average value was used in the predictive equation. Averaging the values obtained from the application of Equation 5.14 to the data from each specimen produced a quantity of $n = 0.244$, which appears reasonable given that Kang (2001) obtained an average value of 0.21 for the same material. Predictions of midheight lateral creep deflection based on Equation 5.17 are shown graphically for the room temperature and elevated temperature specimens in Figure 5.10.

It can be seen from the figure that the power law predictions for the specimens tested at elevated temperatures underestimate the measured amount of creep deflection. Thus, it was necessary to incorporate a parameter for temperature into Equation 5.17. It was observed that when λ_m as determined previously was plotted against the values of m obtained from the power law equations for the elevated temperature specimens, another straight line was generated. Figure 5.9 shows the linearized plot. It followed that the slope of this line was greater than that of the previously obtained line by a factor of τ, which was equal to

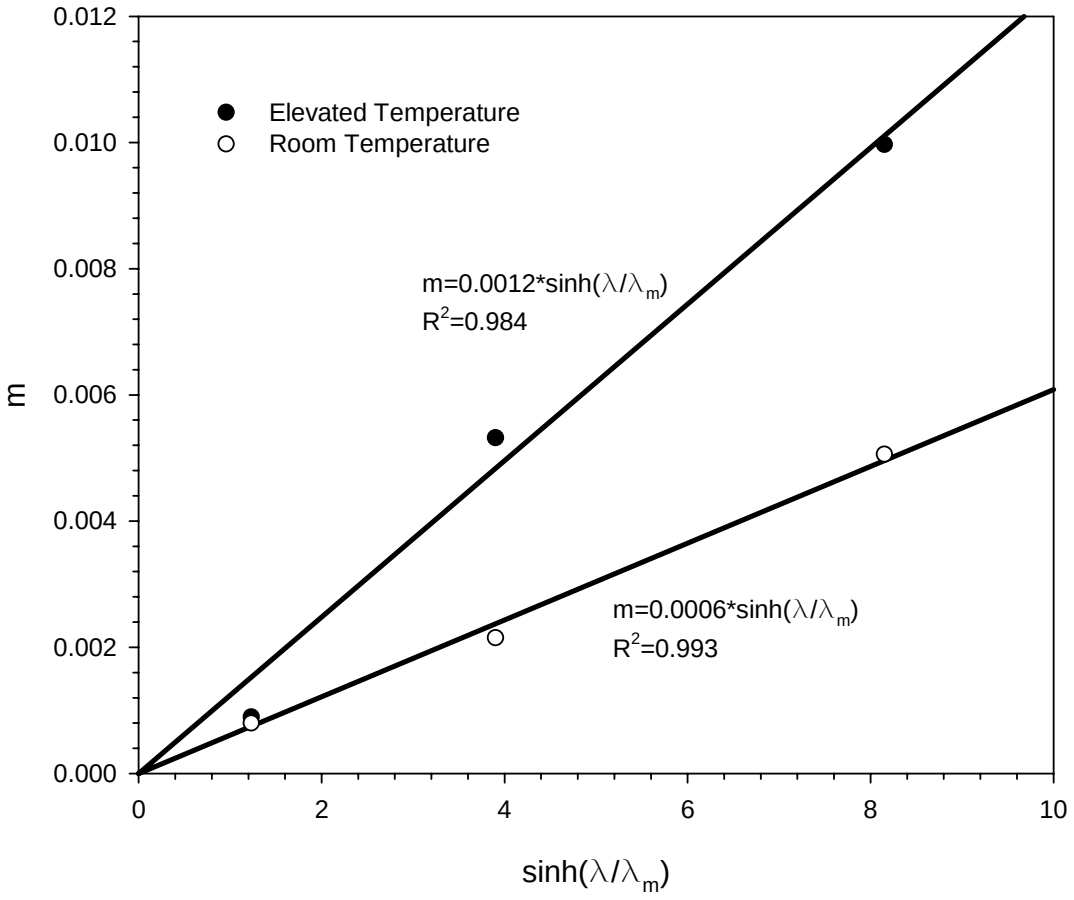

Figure 5.9: Linearized Plots for Determining *m*' in Power Law Model

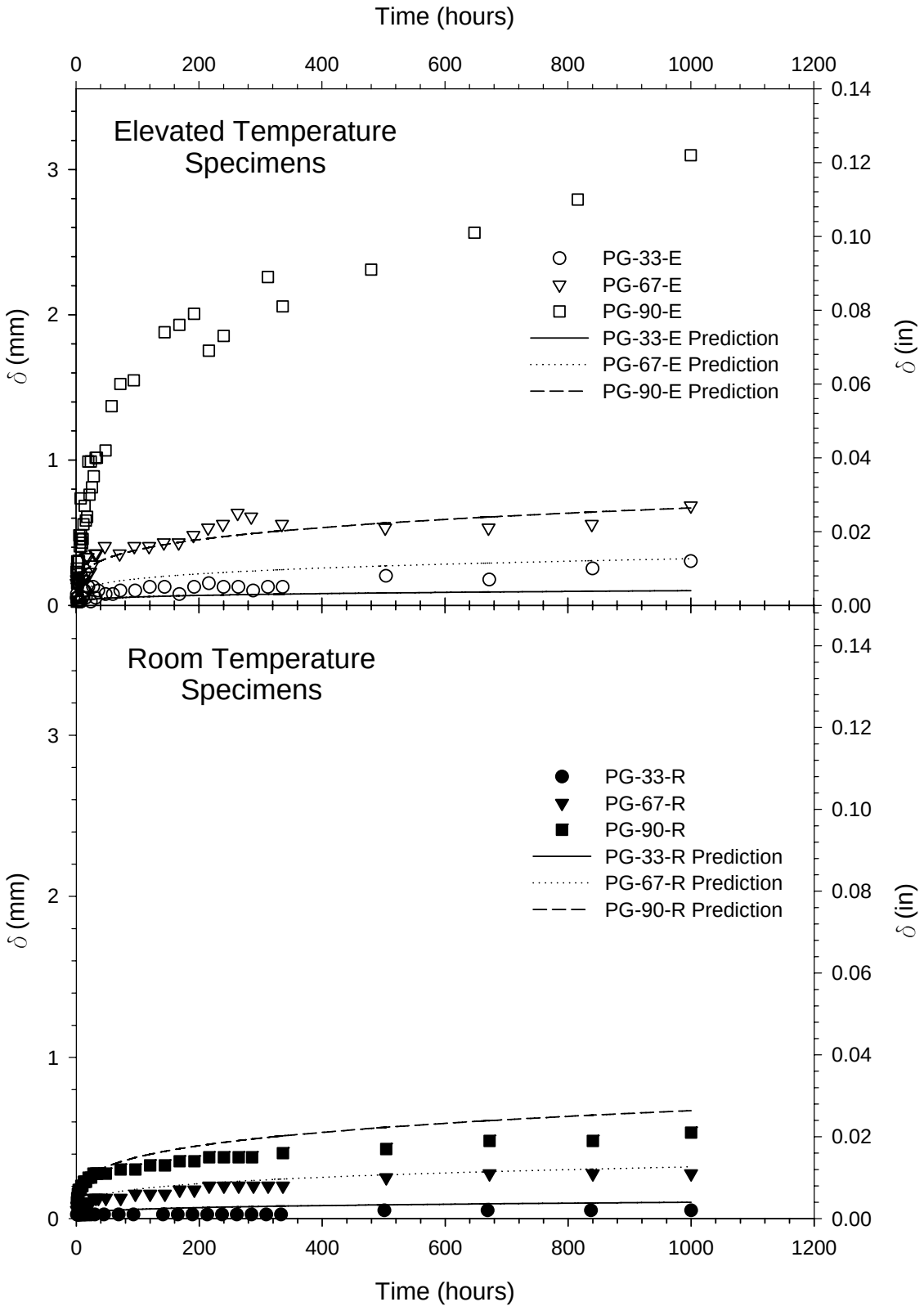

Figure 5.10: Power Law Predictions of Midheight Lateral Creep Deflection

$$\tau = \frac{T}{T_R} \tag{5.18}$$

applicable only for $T<T_R$, where T is the test temperature and T_R is room temperature in ^{o}F. The addition of this heat parameter to Equation 5.17 yields

$$\delta(t,\tau) - \delta_0 = \tau m' t^n \sinh\left(\frac{\lambda}{\lambda_m}\right) \tag{5.19}$$

Predictions using Equation 5.19 for the room temperature specimens and for the elevated temperature specimens are shown in Figure 5.11. It was observed that this model underestimated the creep deflection of specimen PG-90-E, which will be discussed in Chapter 6. Using the average value of n in the predictive equation resulted in some conservatism. The total measured and predicted lateral creep deflections at 1000 hours are compared in Table 5.6.

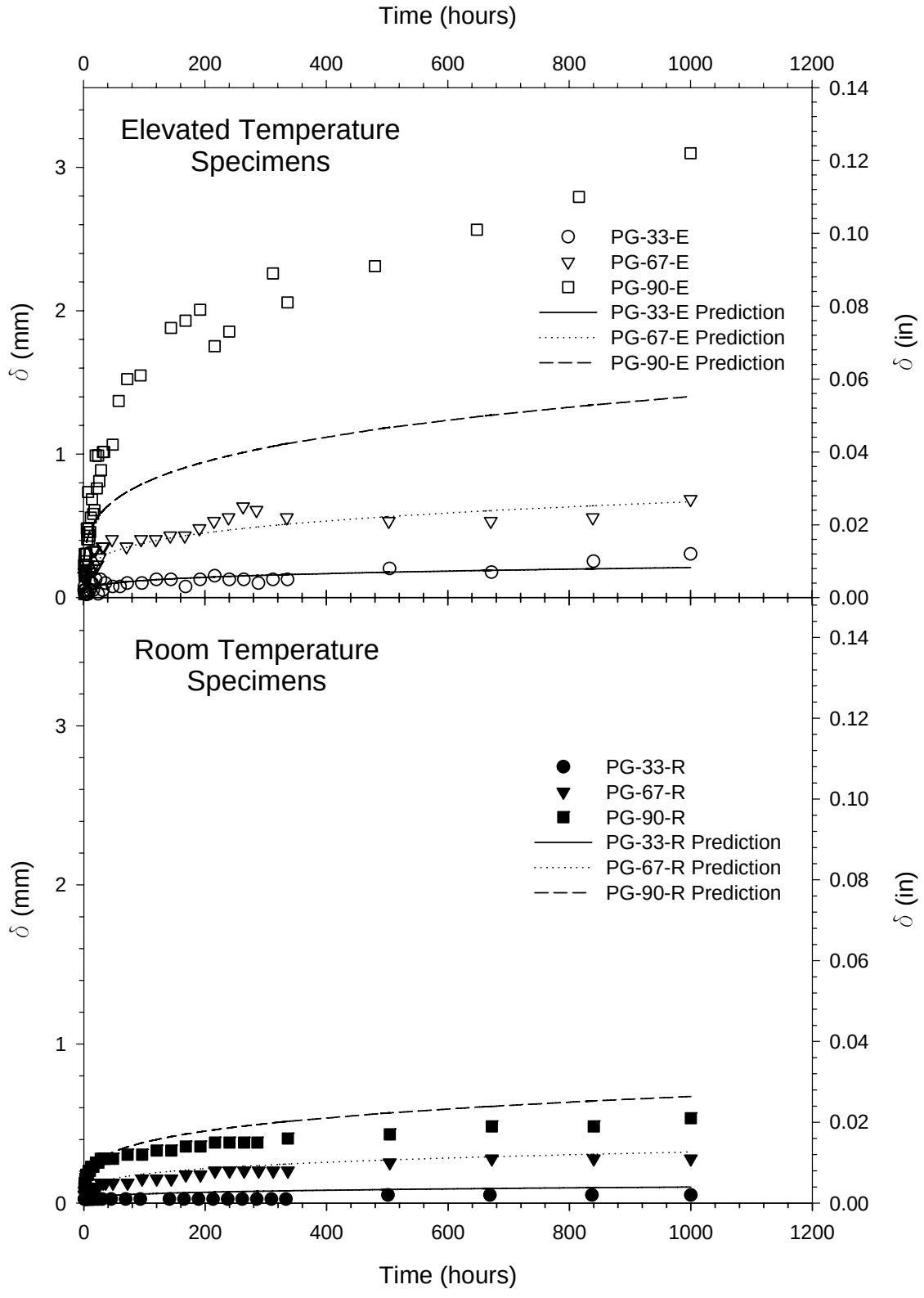

Figure 5.11: Power Law Predictions Including Temperature Parameter

Table 5.6: Total Measured and Predicted Creep Deflections at 1000 Hours

Specimen	Temperature °C (°F)	λ %	Measured mm (in)	Quasielastic Method mm (in)	Power Law Model mm (in)
PG-33-R	22.7 (73)	33	0.05 (0.002)	0.03 (0.001)	0.10 (0.004)
PG-33-E	65.5 (150)	33	0.30 (0.012)	.18 (0.007)	.20 (0.008)
PG-67-R	22.7 (73)	67	0.28 (0.011)	0.23 (0.009)	0.31 (0.012)
PG-67-E	65.5 (150)	67	0.69 (0.027)	0.64 (0.025)	0.64 (0.025)
PG-90-R	22.7 (73)	90	0.53 (0.021)	0.48 (0.019)	0.65 (0.026)
PG-90-E	65.5 (150)	90	3.10 (0.122)	3.58 (0.141)	1.40 (0.055)

5.2.2 Post-Creep Short-Term Buckling Tests

In many of the previous studies of creep behavior of FRP components, there have been attempts to develop predictive models for the time-dependent elastic modulus. A comparison of buckling strengths of columns that have been creep tested to their initial buckling strength provides a means of analyzing any reduction in modulus that has occurred. Based on Euler's equation, the buckling strength of a column is directly proportional to its modulus of elasticity. Thus, the percent reduction in buckling strength could be used to estimate the percent reduction in modulus.

No substantial reduction was seen in the specimens tested at room temperature. In fact, specimen PG-90-R possessed a critical buckling load higher than its Euler estimation. However, in two of the specimens tested at 65.5ºC (150ºF) a reduction of more than 35% from the short-term critical buckling load determined in Chapter 3 was observed. The apparent modulus values based on the reduced buckling loads were E_L = 15.07 GPa (2186 ksi) for specimen PG-67-E and E_L = 14.37 GPa (2084 ksi) for specimen PG-90-E. Figure 5.12 is a normalized plot relating the experimental buckling load P_{exp} of the specimens to their test temperatures and load levels. The normalization takes the form of

$$\lambda\left(\frac{T - T_R}{T_R}\right) \tag{5.20}$$

where T is the test temperature and T_R is room temperature.

Rearranging Euler's buckling equation and combining with the linear trend shown in Figure 5.12 yields an expression for reduced modulus in the form of

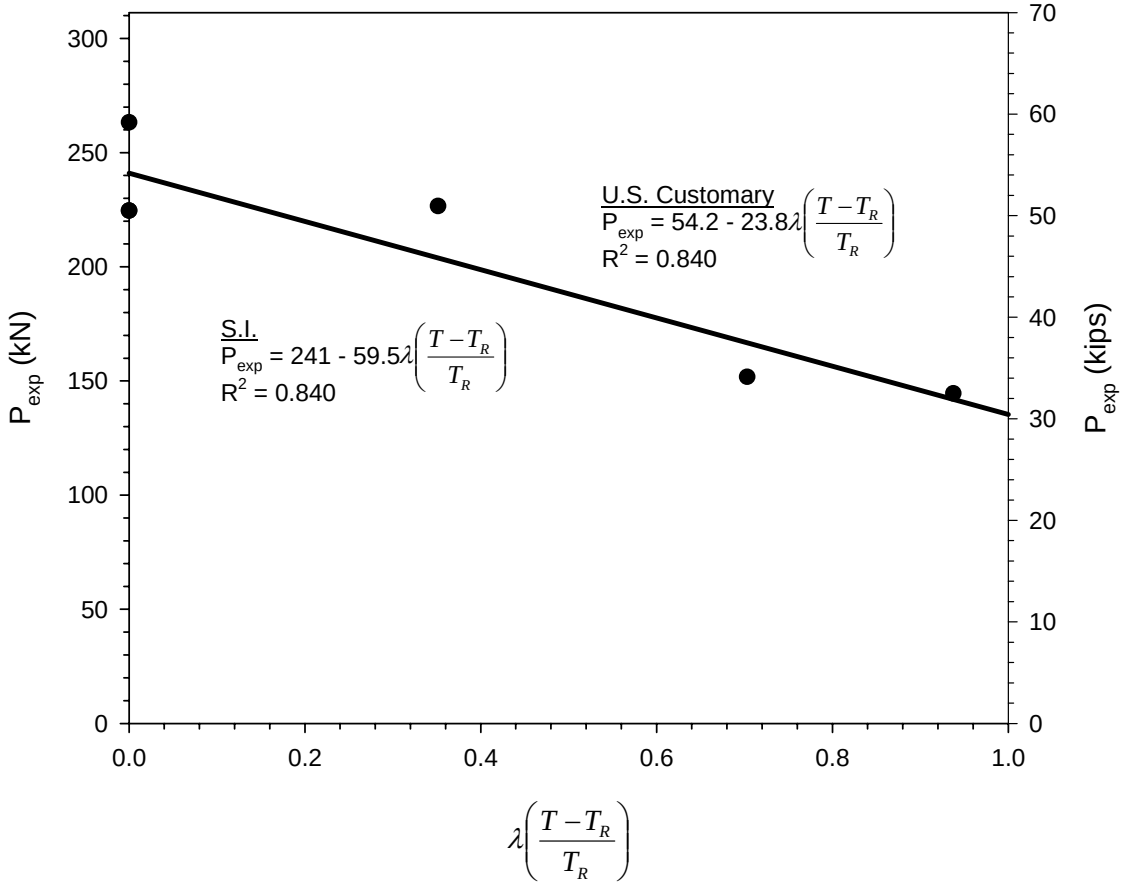

Figure 5.12: Critical Buckling Load Normalization

$$E_{1000} = \frac{L^2\left[P_{cr} - 59.5\lambda\left(\frac{T - T_R}{T_R}\right)\right]}{\pi^2 I}, \text{ S.I.} \qquad (5.21)$$

$$E_{1000} = \frac{L^2\left[P_{cr} - 23.8\lambda\left(\frac{T - T_R}{T_R}\right)\right]}{\pi^2 I}, \text{ U.S. Customary} \qquad (5.22)$$

applicable only for $T>T_R$, where P_{cr} is the initial critical load, L is the effective length of the column, and I is the moment of inertia of the section. The fact that modulus measurements could not be taken throughout the testing period limits the applicability of Equations 5.21 and 5.22 to a duration of exposure to axial loads and elevated temperatures of 1000 hours. Also, it is necessary to note that these equations are based on one elevated temperature, and further research would be needed on a range of temperatures and load durations to make this approach generally applicable.

CHAPTER VI

DISCUSSION AND CONCLUSIONS

6.1 DISCUSSION

As stated previously, there were some discrepancies in the measurements of axial creep displacement. In the buckling of a column, axial shortening is proportional to lateral deflection. However, this was not always the case among the measurements taken throughout the experiments. A possible explanation for this is a slight rotation of the base plate as the column changed shape. As load was lost due to relaxation of the column, the springs were able to expand somewhat. Despite the effort to minimize the differences in stiffness among the springs in each machine, there was some variation. Therefore, the stiffest spring would have been the first to expand, which could have led to a very small rotation of the plate above. Given the relatively small deflections (δ < 3 mm) being measured, the rotation of this plate could have a disproportionate impact.

Further discrepancy existed between the measured and predicted initial midheight lateral deflections. In most cases, the measured value greatly exceeded the predicted value. This is likely a problem of geometry. Firstly, the predictive equation assumes a sinusoidal shape for the initial imperfection in the column, which is very unlikely. Also, buckling of a column is a bifurcation problem. For a perfectly straight column loaded concentrically, no lateral displacement takes place until the point of buckling. At this point there is a transition of equilibrium from a stable position to one in which the

column must deflect to maintain its equilibrium. There are no reliable expressions for the deflection of an imperfect column prior to the bifurcation point if there is no significant bending in the column. The predictive equation that was employed for the initial deflected shape is based on the theory used in Southwell's method of buckling analysis, which is also unreliable at small magnitudes of deflection.

Kang (2001) was successful in utilizing both the quasielastic method and Findley's power law to predict the lateral creep deflection of eccentrically loaded columns. However, without eccentricity the axial loads applied to the specimens in the current investigation were not sufficient to impose significant bending, with the exception of specimen PG-90-E. The behavior of this specimen is likely the result of unbounded nonlinear creep deformation that could have eventually led to failure of the column. The short-term buckling tests revealed that the bifurcation point of the all of the columns occurred at a lateral deflection of approximately 2.54 mm (0.1 in). The total deflection of specimen PG-90-E after creep testing was 5.23 mm (0.206 in), which suggests that the column was in the process of buckling. This issue was addressed in the creep buckling analysis of viscoelastic beam columns by Vinogradov (1987). Vinogradov asserted that a safe load exists for columns above which the deformation becomes unbounded and nonlinear. The addition of elevated temperature to the specimen likely caused a sufficient reduction in elastic modulus to lower the safe load and initiate unbounded deformation.

Based on the similarity of the creep parameters determined by Kang (2001) to those found for specimen PG-90-E, the quasielastic approach appears to be an effective method for predicting lateral deflection when significant bending occurs. The power law

approach proved to be more appropriate for the prediction of the lateral creep deflections of the specimens without significant bending. However, a consistent power law model could not be used for specimen PG-90-E due to the nonlinear nature of its deflection.

As an illustration of how the proposed methods could be effective, midheight lateral creep deflections were predicted for each specimen tested for the extended durations of 1 year, 5 years, 10, years, and 25 years. Table 6.1 presents the resulting values. The quasielastic method was used in the predictions for specimen PG-90-E, and the remainder of the predictions were made using the power law model.

Consider as an example of the application of the predictive model an E-glass/polyester composite I-shaped column, shown in Figure 6.1, with an effective length L_{eff} = 3.05 m (10 ft). The moment of inertia and radius of gyration of the section are I_x = 16.72x10^6 mm^4 (40.17 in^4), I_y = 5.63x10^6 mm^4 (13.52 in^4), r_x = 63.5 mm (2.50 in), and r_y = 36.8 mm (1.45 in). The configuration shown in the figure gives the column a slenderness ratio of L/ r_y = 83. The load level is equal to 1/2 of the critical buckling load (λ = 0.5), and the section will be exposed to service temperatures of 22.8ºC (73ºF) and 65.5ºC (150ºF). The specimen is referred to as PG-50-R/E in the table.

The quasielastic method could not be applied because this model predicts the total time-dependent deflection, which includes initial deflection. In the power law model, the creep and instantaneous deflections can be separated. In the experimental data, nonlinear behavior was observed only in the heated specimen loaded to more than 67% of its critical buckling load. Since λ in this case is less than 0.67, it will be assumed that nonlinear deformation does not occur in the column, so a value of n = 0.244 may be used. The resulting power law predictions using Equation (5.17) are included in Table 6.1. It

must be noted that much more work is required to assess the general applicability of the predictive models developed in this study.

Table 6.1: Extended Predictions of Midheight Lateral Creep Deflection

Specimen	Predicted Lateral Creep Deflection δ(t)-δ_0 mm (in)				
	1000 hours	1 year	5 years	10 years	25 years
PG-33-R	0.10 (0.004)	0.17 (0.007)	0.26 (0.010)	0.30 (0.012)	0.38 (0.015)
PG-33-E	0.21 (0.008)	0.36 (0.014)	0.53 (0.021)	0.62 (0.025)	0.78 (0.031)
PG-67-R	0.33 (0.013)	0.55 (0.022)	0.82 (0.032)	0.97 (0.038)	1.21 (0.048)
PG-67-E	0.67 (0.026)	1.13 (0.045)	1.68 (0.066)	1.99 (0.078)	2.49 (0.098)
PG-90-R	0.68 (0.027)	1.16 (0.046)	1.72 (0.068)	2.03 (0.080)	2.54 (0.100)
PG-90-E	3.59 (0.127)	-195.42 (-7.694)	-7.31 (-0.288)	-5.57 (-0.219)	-4.42 (-0.174)
PG-50-R	0.19 (0.007)	0.32 (0.013)	0.47 (0.019)	0.56 (0.022)	0.70 (0.027)
PG-50-E	0.39 (0.015)	0.65 (0.026)	0.97 (0.038)	1.15 (0.045)	1.44 (0.056)

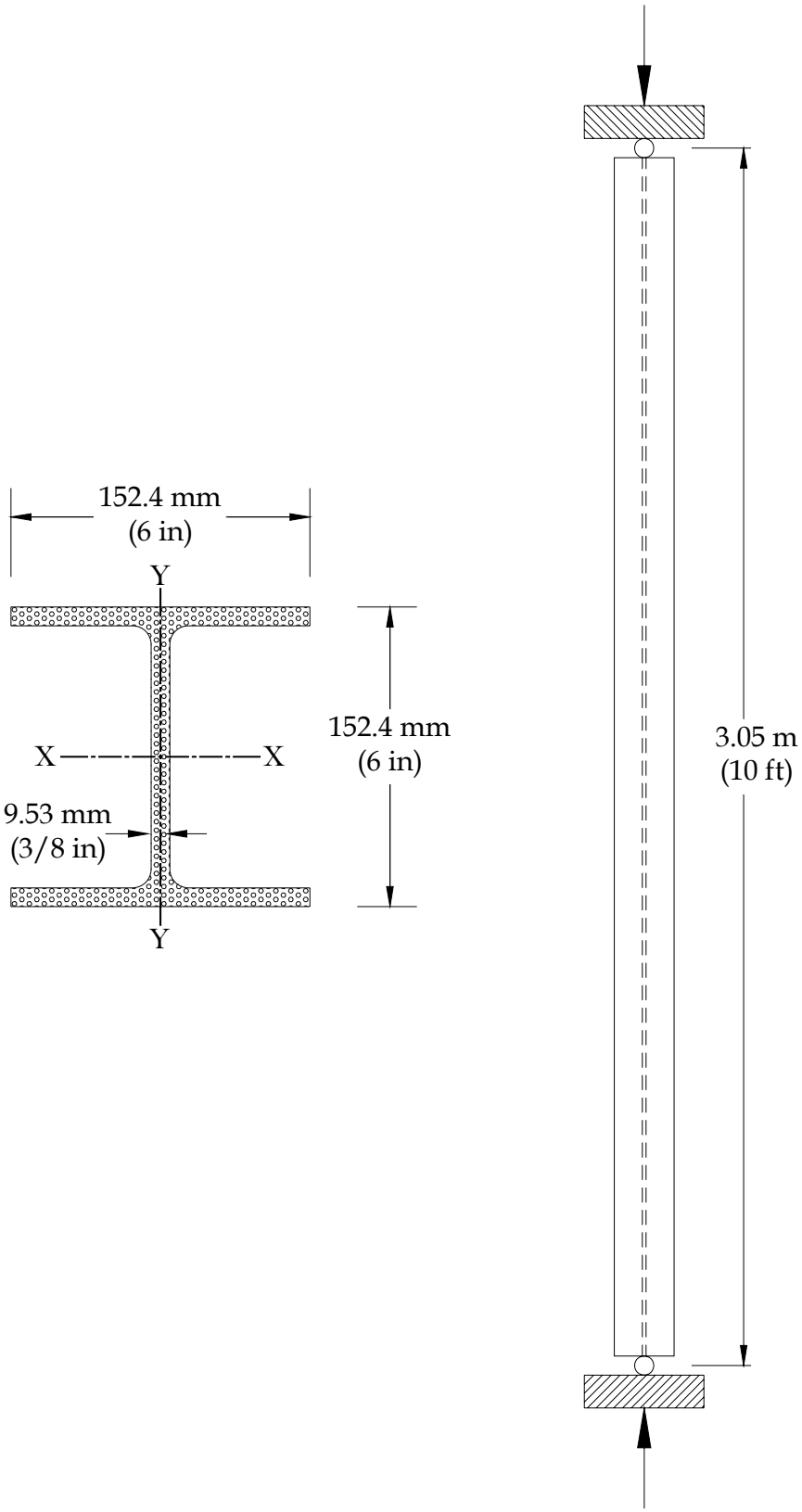

Figure 6.1: Additional Specimen for Analysis

Negative predicted values of lateral deflection appear in Table 6.1 for specimen PG-90-E at some point between 1000 hours and 1 year. This is due to the limitation that $\lambda < \frac{1}{1+\psi(t)}$. After a duration of slightly less than 6500 hours, the predicted total midheight lateral deflection was more than the maximum deflection measured in the short-term buckling tests. This suggests that creep collapse of the specimen would have occurred if the test had been allowed to continue for that amount of time.

Despite the lack of a reliable model for the reduction of modulus over time, the post creep short-term buckling tests revealed some very useful information. It was shown that a considerable permanent reduction in the modulus occurred after 1000 hours of exposure to a compressive force at the elevated temperature, even after allowing sufficient recovery time. It was also shown that specimens tested with identical load levels at room temperature did not exhibit this reduction. It is interesting to note that the final lateral creep deflections of specimens PG-90-R and PG-67-E were approximately equal. Yet the modulus of the former had not reduced after creep testing, while the modulus of the latter had reduced. This suggests: (1) that creep deflection is more detrimental to the structural integrity of columns of this type when they are exposed to elevated service temperatures; and (2) that an elevated service temperature of 65.5ºC (150ºF) has a more complicated effect on the columns than simply accelerating creep deflection.

6.2 CONCLUSIONS

Based on the results and observations of this investigation, the following conclusions can be made:

1) For E-glass/polyester composite columns loaded concentrically, midheight lateral creep deflection increases with both axial load and temperature.
2) The Quasielastic Method of predicting midheight lateral creep deflection is effective when the specimen exhibits sufficient bending.
3) A modified form of Findley's power law model can be used to predict the midheight lateral creep deflection of specimens tested at room temperature. The addition of a heat parameter to the model allowed reasonable predictions for specimens tested at 65.5ºC (150ºF) which did not exhibit significant bending.
4) A transition point exists somewhere between a sustained load level of λ = 0.67 and λ = 0.90 for a service temperature of 65.5°C (150°F) at which a column of this type begins to exhibit nonlinear elastic lateral deflection. This type of behavior could lead to eventual buckling failure of the column.
5) Based on the limited number of tests performed, it appears that sustained axial loads at elevated service temperatures can permanently reduce the longitudinal elastic modulus of this type of column by a significant amount.
6) Based on the performance of specimens PG-33-R and PG-33-E, the manufacturers' recommendation to use a safety factor of 3 regarding buckling as part of design considerations appears reasonable.

6.3 RECOMMENDATIONS FOR FUTURE STUDY

The specimens in this study were tested at only one elevated temperature, and for only 1000 hours. The power law approach when applied to the specimens tested at the elevated temperature requires further verification, as only one elevated temperature was examined. This also applies to the modulus reduction model derived from the post creep short-term buckling tests. An extension of the study is recommended to verify the predictive models developed in the current work involving more specimens and temperatures and longer test durations. A study of this nature could also establish the point at which FRP columns under these conditions begin to exhibit nonlinear elastic lateral deflection. Also, buckling tests could be performed without allowing any recovery in the columns. This could supply a more practical depiction of the time dependent reduction of modulus of FRP columns exposed to moderate elevated temperatures over the service life of a structure.

APPENDIX A: MATERIAL PROPERTIES

Table A.1: Tension Test Results

Sample		F_L^t (psi)	ε_L^t (in/in)	E_L^t (10^3ksi)
A	PG-T1-A2	55750	0.0181	3.089
	PG-T1-A3	52386	0.0164	3.192
	PG-T1-A4	60580	0.0178	3.407
	PG-T2-A1	50853	0.0142	3.582
	PG-T2-A2	59960	0.0172	3.482
	PG-T2-A3	53062	0.0149	3.550
	PG-T2-A4	56959	0.0168	3.382
A Average		55650	0.0165	3.383
C	PG-T-C1	46508	0.0147	3.172
	PG-T-C2	48252	0.0160	3.022
	PG-T-C3	51924	0.0167	3.109
	PG-T-C4	57466	0.0169	3.410
C Average		51038	0.0160	3.178
D	PG-T-D1	49755	0.0170	2.932
	PG-T-D2	65028	0.0170	3.817
	PG-T-D3	55691	0.0176	3.164
	PG-T-D4	55547	0.0174	3.186
D Average		56505	0.0173	3.275
Overall Average		54648	0.0166	3.300
STD		4817	0.0011	0.235
COV (%)		8.82	6.74	7.11

Table A.2: Compression Test Results

Sample		F_L^c (psi)	ε_L^c (in/in)	E_L^c (10^6psi)
A	PG-C1-A1	55763	-	-
	PG-C1-A4	62963	-	-
	PG-C2-A1	45972	-	-
	PG-C2-A3	55832	-	-
	PG-C2-A4	57477	-	-
A Average		55601	-	-
C	PG-C1-C1	51534	-	-
	PG-C1-C2	55951	-	-
	PG-C1-C4	52202	-	-
	PG-C2-C1	47079	0.0157	3.004
	PG-C2-C2	52914	0.0137	3.867
	PG-C2-C3	48519	0.0136	3.558
C Average		51367	0.0143	3.476
D	PG-C-D1	47824	-	-
	PG-C-D2	59857	-	-
	PG-C-D3	51983	-	-
	PG-C-D4	53309	-	-
D Average		53243	-	-
Overall Average		53279	0.0143	3.476
STD		4653	0.0010	0.357
COV (%)		8.73	6.75	10.27

APPENDIX B: POWER LAW LOG PLOTS

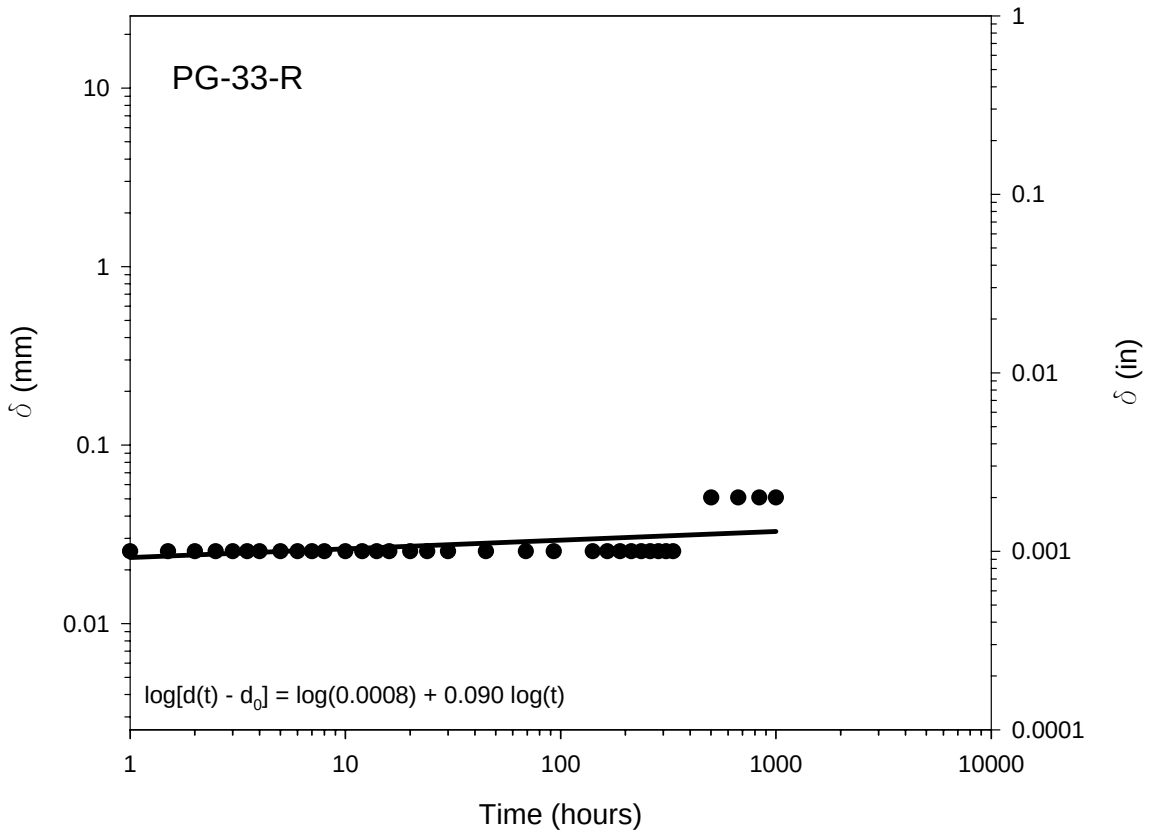

Figure A.1: Determination of Creep Parameters *m* and *n* in Equation (5.15) (PG-33-R)

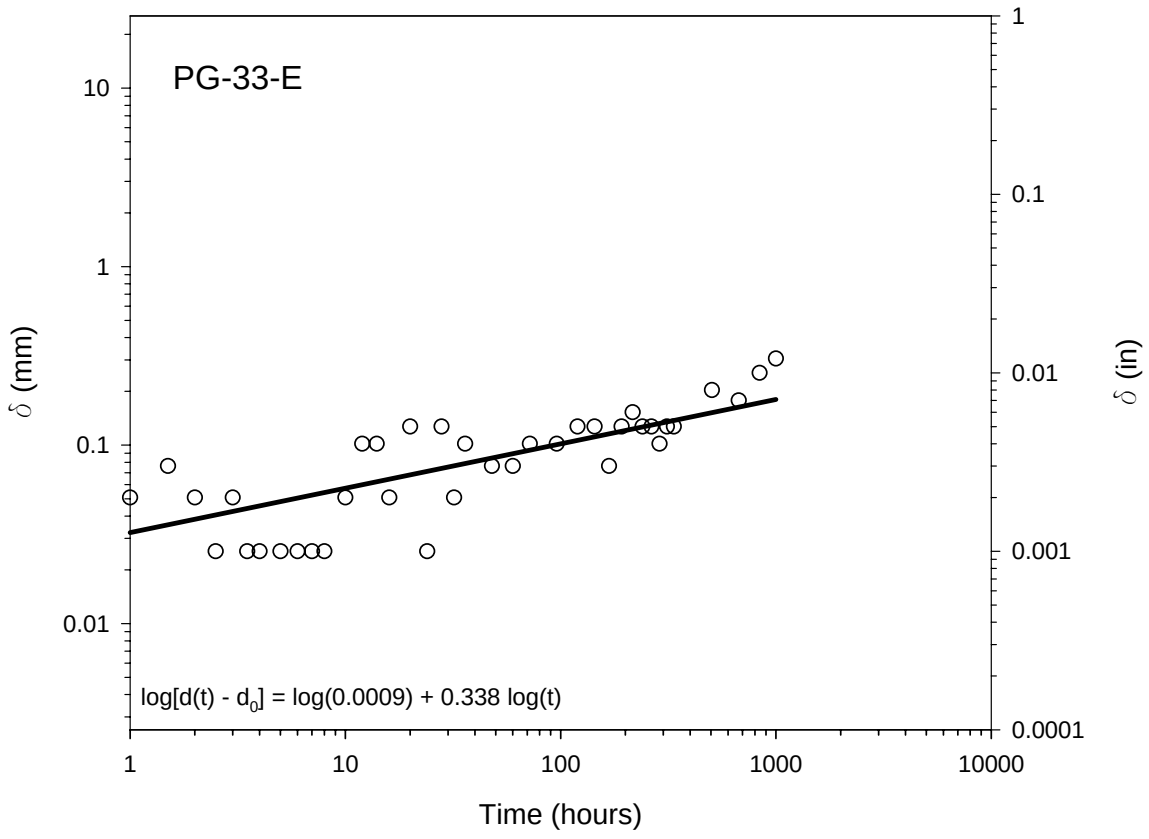

Figure A.2: Determination of Creep Parameters *m* and *n* in Equation (5.15) (PG-33-E)

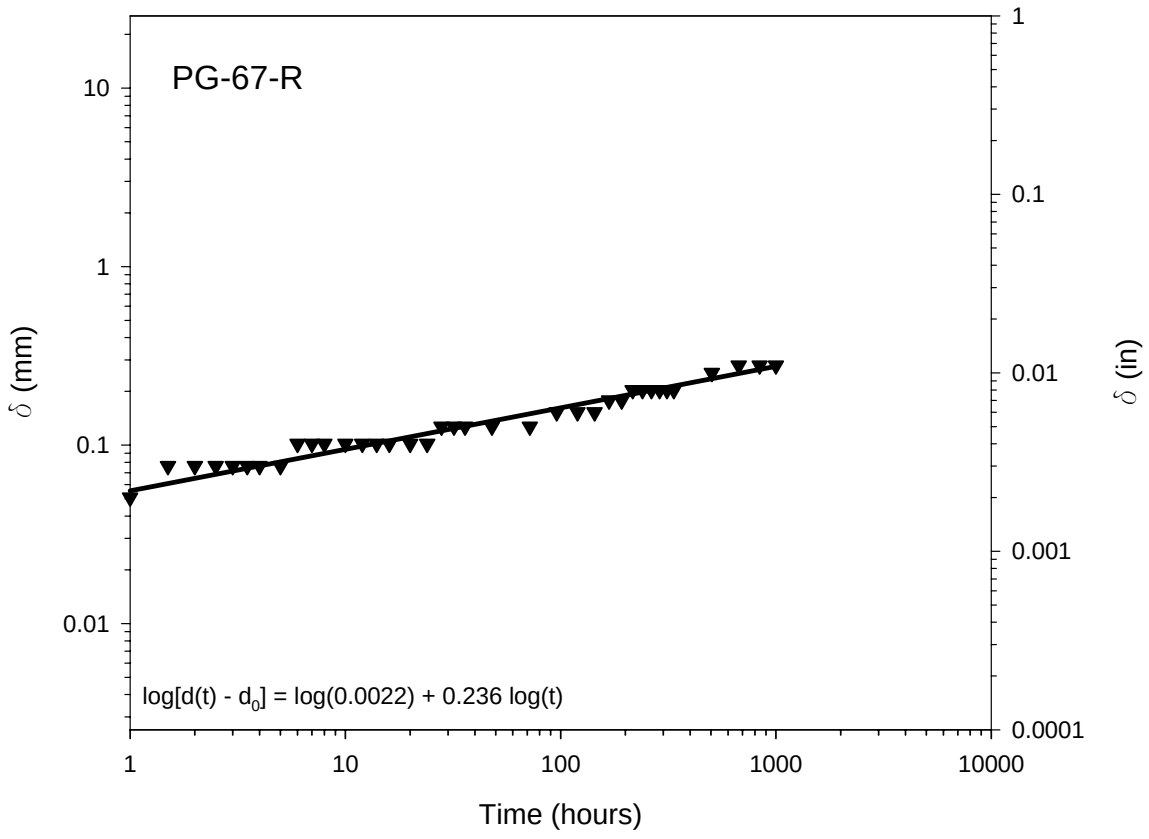

Figure A.3: Determination of Creep Parameters *m* and *n* in Equation (5.15) (PG-67-R)

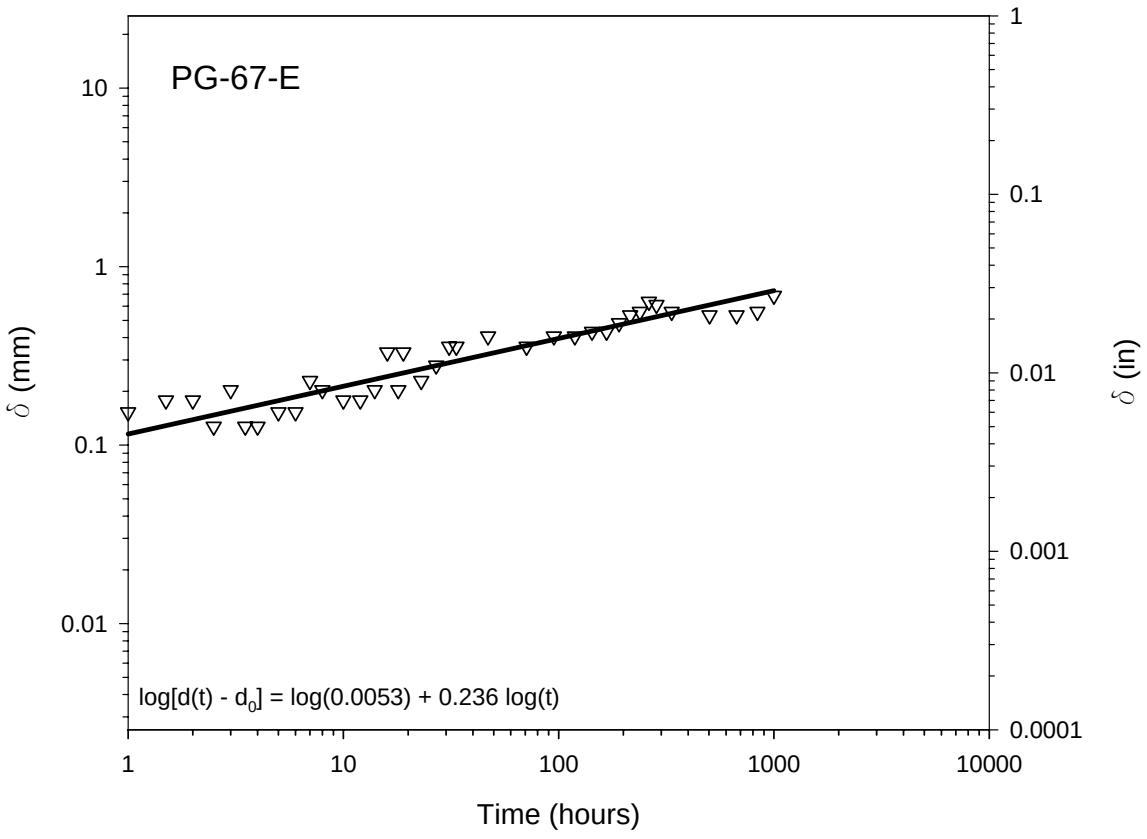

Figure A.4: Determination of Creep Parameters *m* and *n* in Equation (5.15) (PG-67-E)

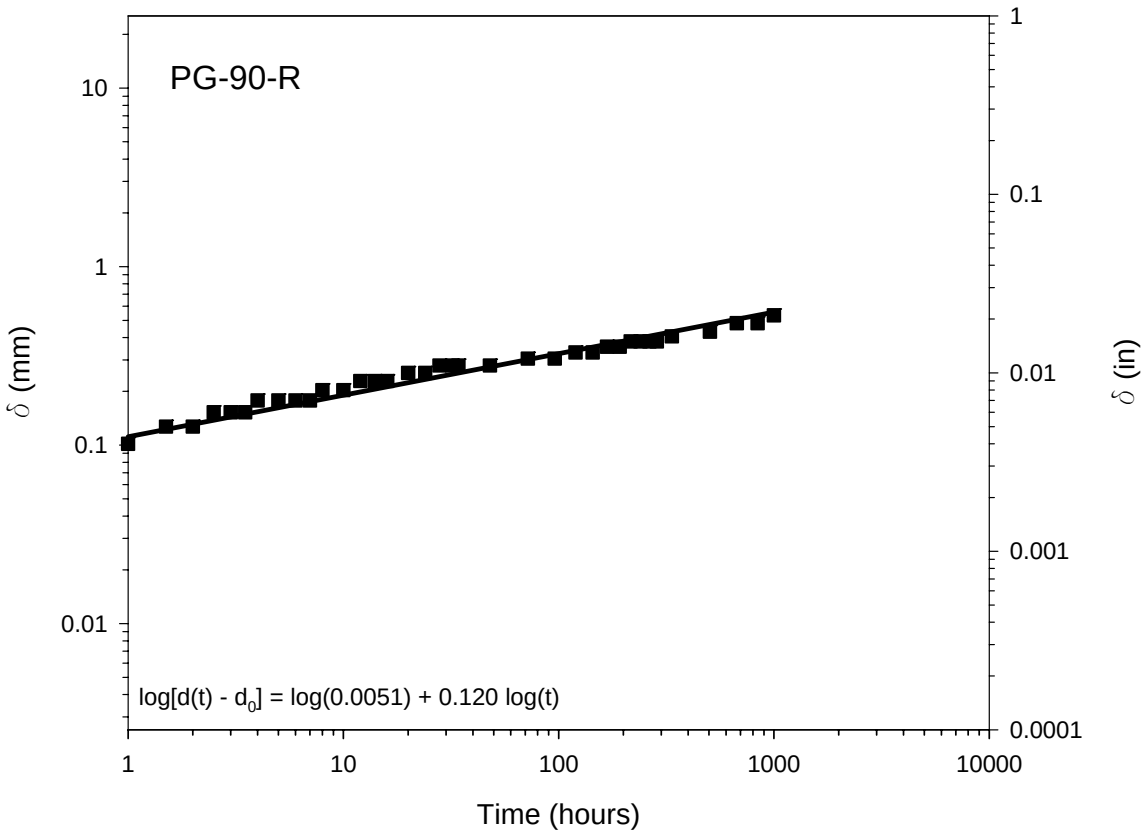

Figure A.5: Determination of Creep Parameters *m* and *n* in Equation (5.15) (PG-90-R)

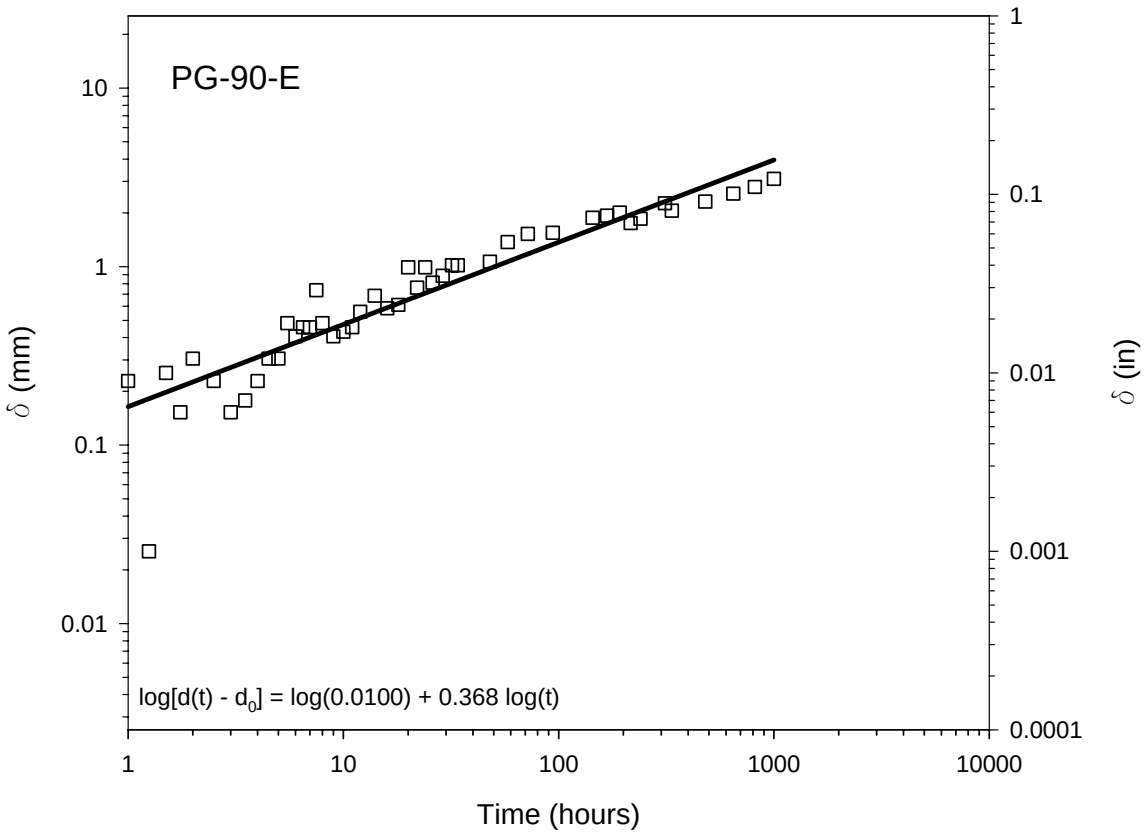

Figure A.6: Determination of Creep Parameters *m* and *n* in Equation (5.15) (PG-90-E)

APPENDIX C: POST-CREEP BUCKLING TESTS

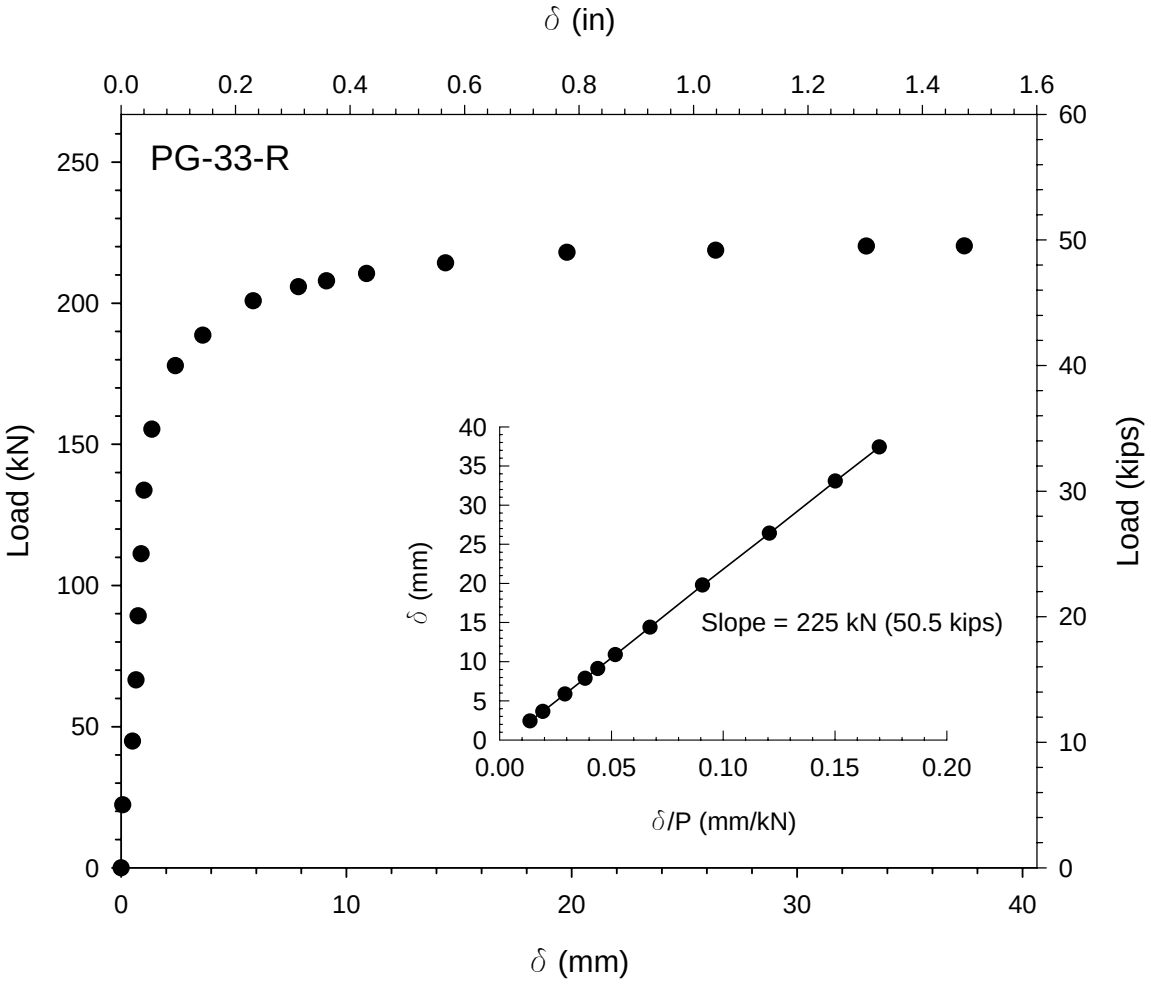

Figure A.7: Load vs. Deflection and Southwell Plot from Post-Creep Buckling Test (PG-33-R)

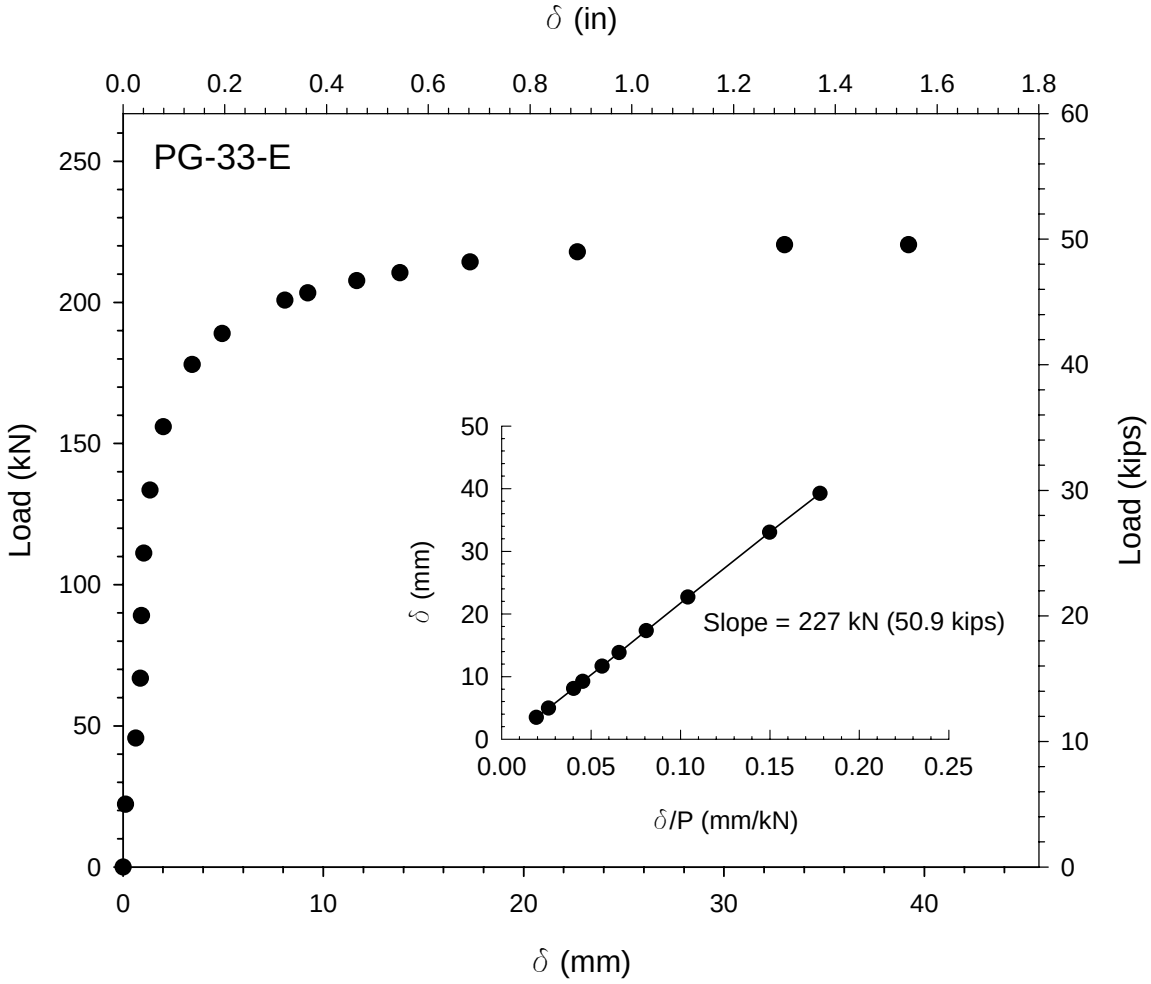

Figure A.8: Load vs. Deflection and Southwell Plot from Post-Creep Buckling Test (PG-33-E)

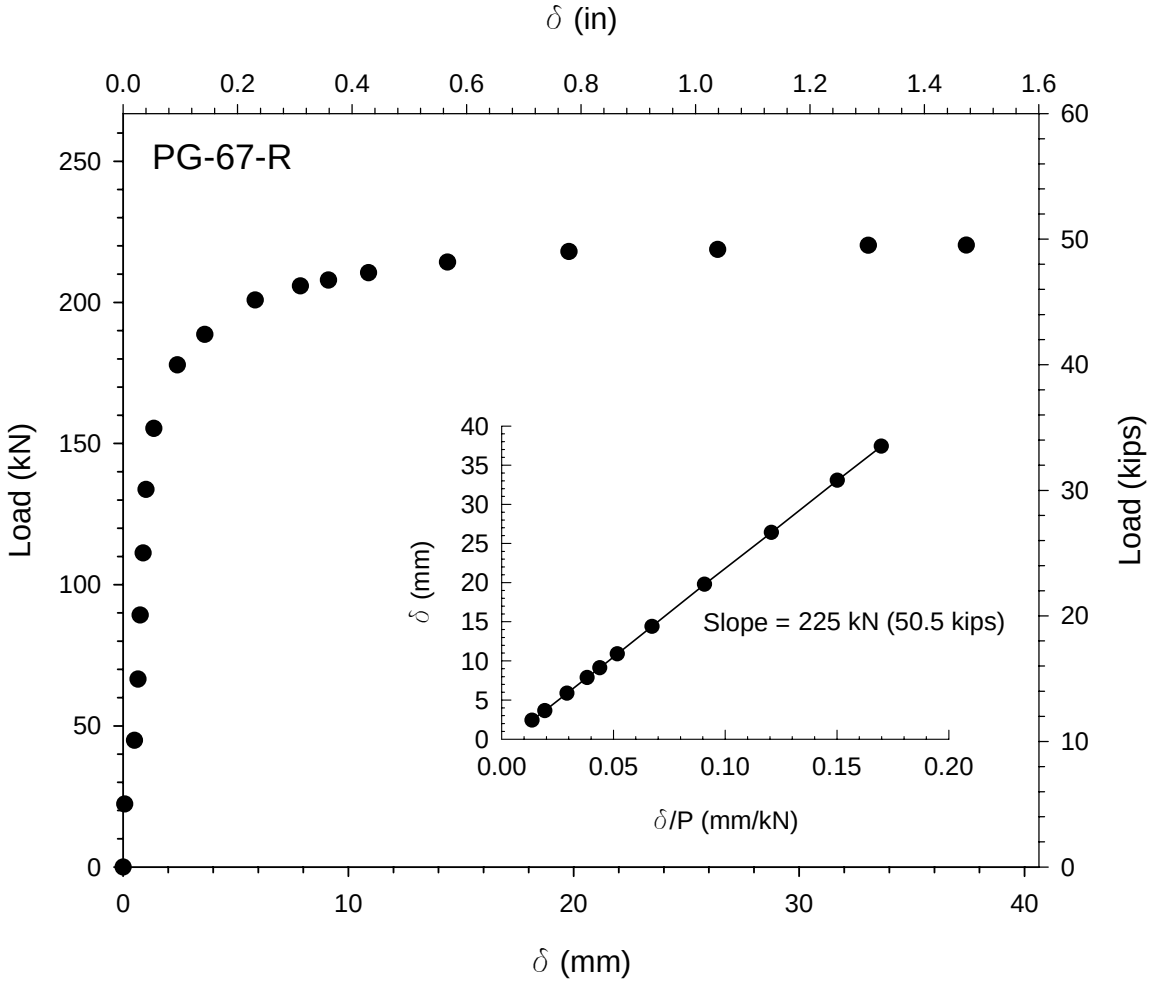

Figure A.9: Load vs. Deflection and Southwell Plot from Post-Creep Buckling Test (PG-67-R)

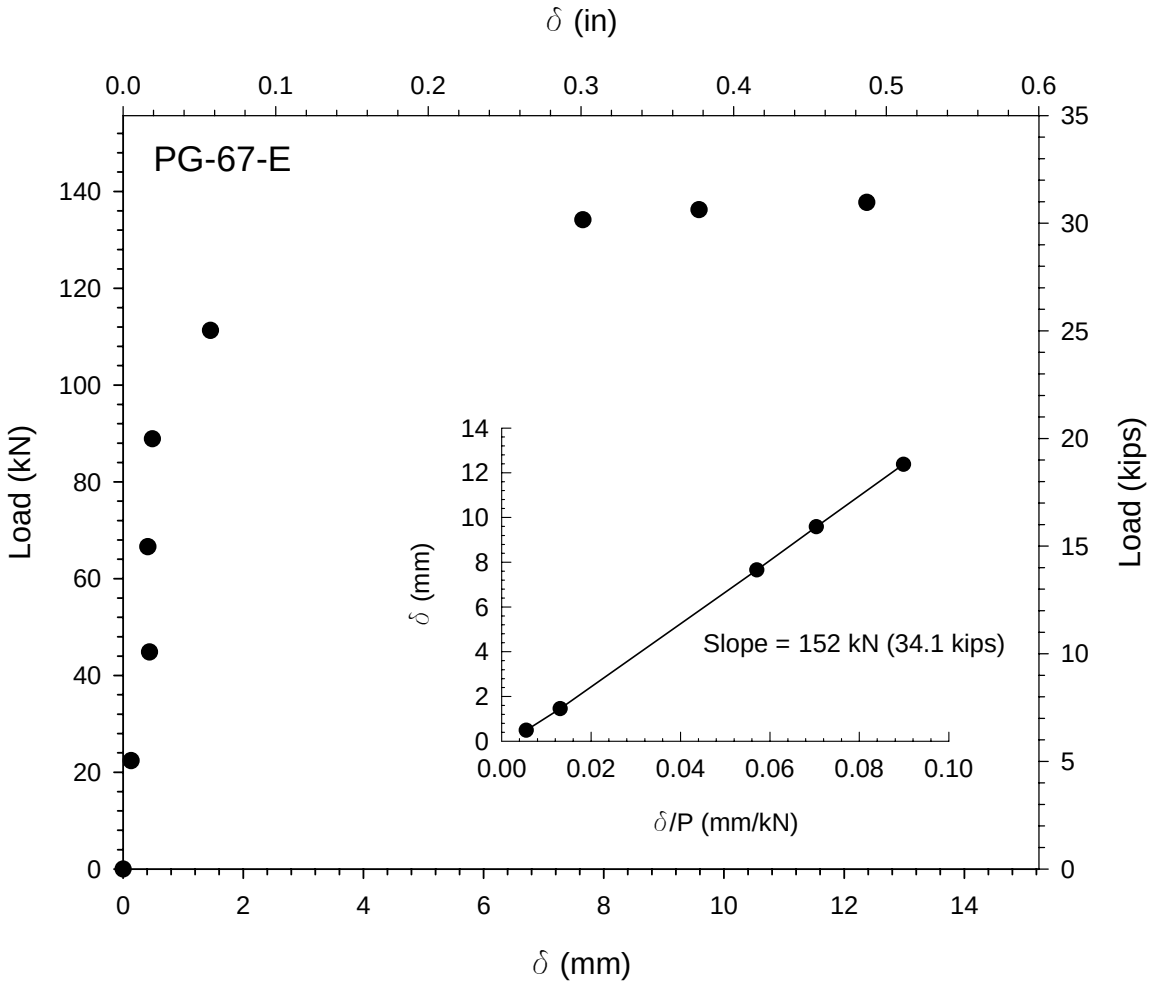

Figure A.10: Load vs. Deflection and Southwell Plot from Post-Creep Buckling Test (PG-67-E)

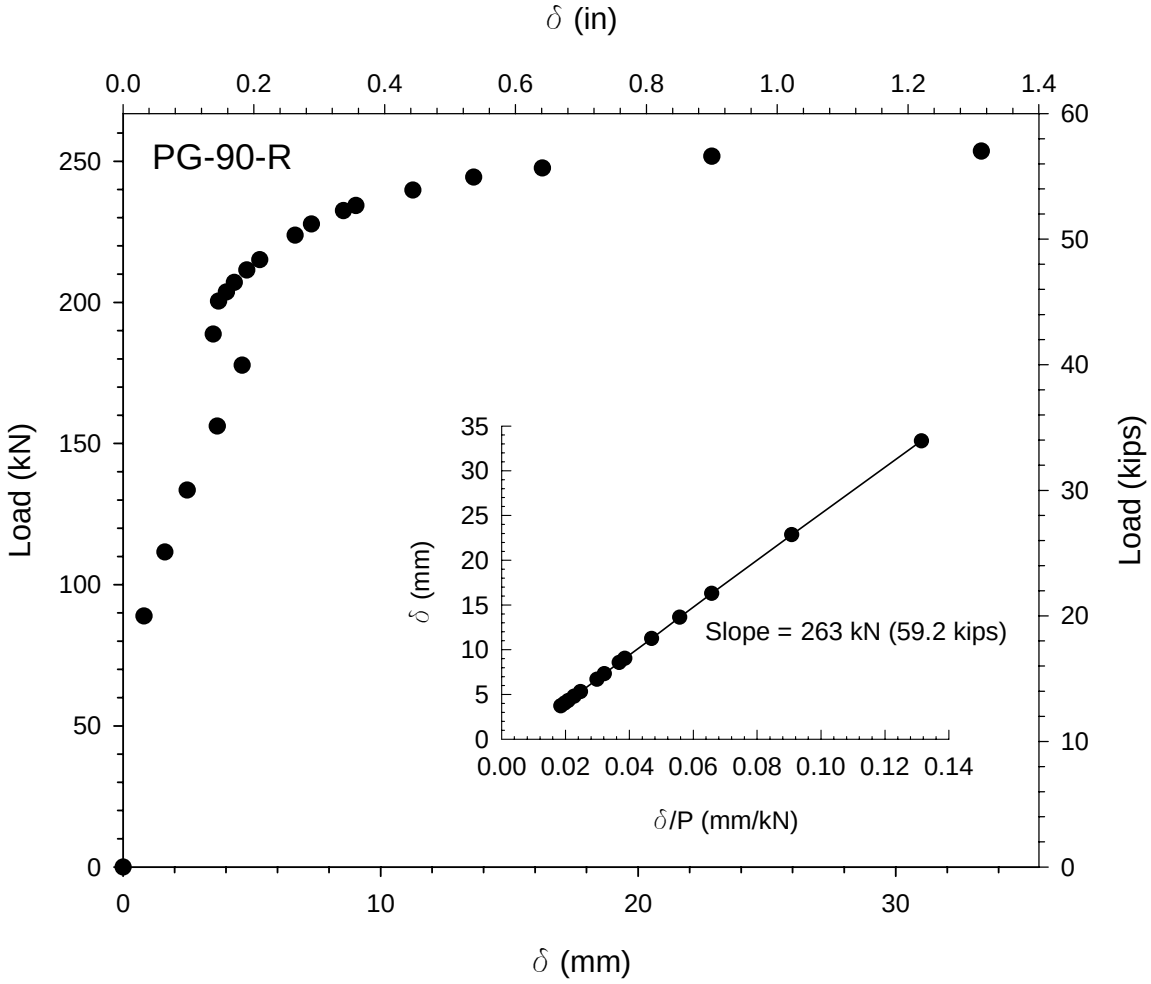

Figure A.11: Load vs. Deflection and Southwell Plot from Post-Creep Buckling Test (PG-90-R)

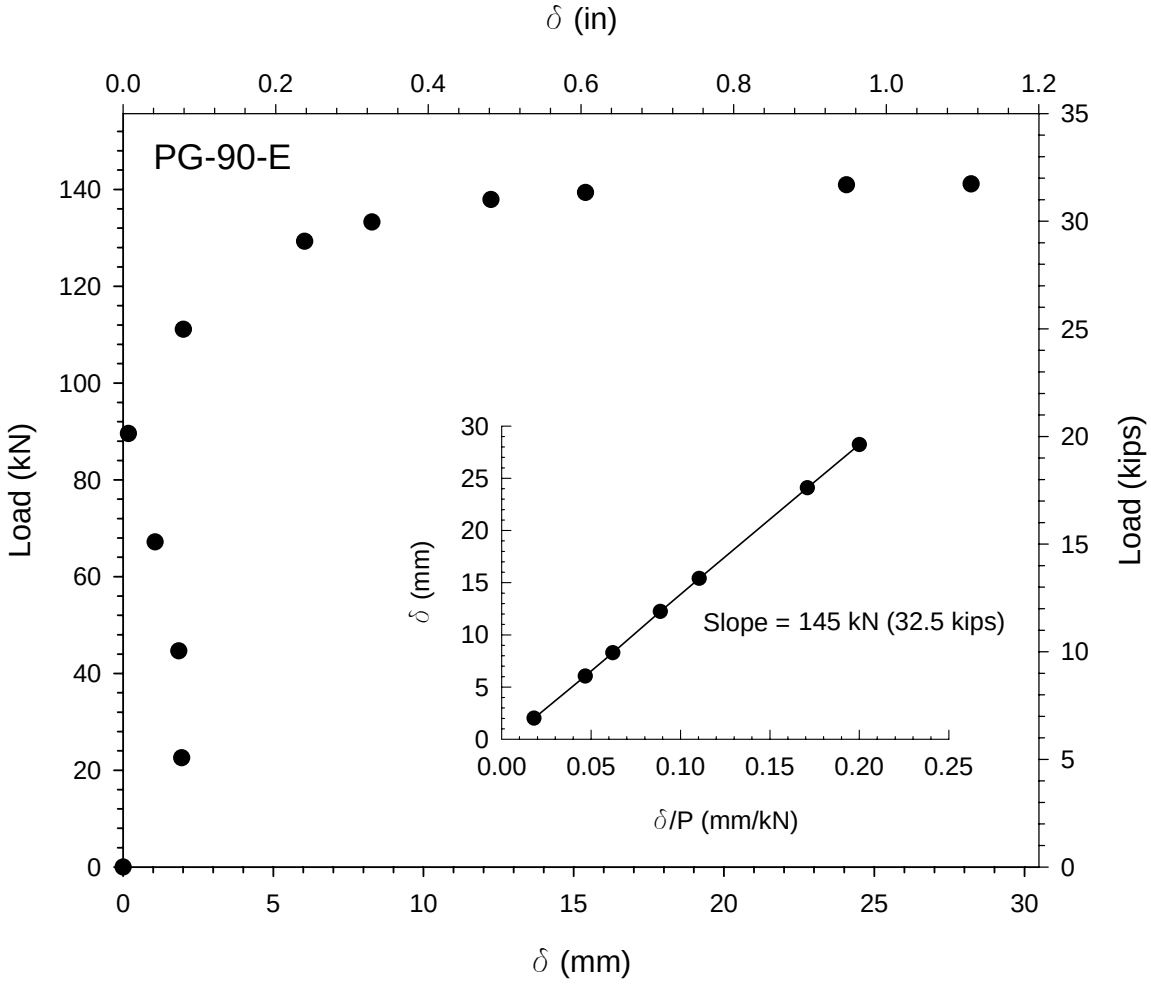

Figure A.12: Load vs. Deflection and Southwell Plot from Post-Creep Buckling Test (PG-90-E)

REFERENCES

ACI 440R-96 (1996), "State-of-the-Art Report on Fiber Reinforced Plastic (FRP) Reinforcement for Concrete Structures," American Concrete Institute, Farmington Hills, MI, 68 pp.

American Society of Civil Engineers (1984), *Structural Plastic Design Manual*, ASCE Manuals and Reports on Engineering Practice, No. 63, New York, NY.

ASTM D792-96a, Standard Test Methods for Density and Specific Gravity (Relative Density) of Plastics by Displacement, American Society for Testing and Materials.

ASTM D3039/D3039M-93, Standard Test Methods for Tensile Properties of Polymer Matrix Composite Materials, American Society for Testing and Materials.

ASTM D3410/D3410M-95, Standard Test Method for Compressive Properties of Polymer Matrix Composite Materials with Unsupported Gage Section by Shear Loading, American Society for Testing and Materials.

ASTM D3917-94, Standard Specification for Dimensional Tolerance of Thermosetting Glass-Reinforced Plastic Pultruded Shapes, American Society for Testing and Materials.

ASTM D5379/D5379M-93, Standard Test Method for Shear Properties of Composite Materials by the V-notched Beam Method, American Society for Testing and Materials.

Bank, L.C. and Mosallam, A.S. (1990), "Creep and Failure of a Full-Size Fiber Reinforced Plastic Pultruded Frame," American Society of Mechanical Engineers, Petroleum Division (Publications) PD, Vol. 32, pp. 49-56.

Barbero, E.J. and Raftoyiannis, I.G. (1993), "Euler Buckling of Pultruded Composite Columns," Composite Structures, Vol. 24, pp. 139-147.

Barbero, E.J. and Tomblin, J. (1992), "Buckling Testing of Composite Columns," AIAA Journal, Vol. 30, No. 11, pp. 2798-2800.

Bedford Reinforced Plastics Inc. (2004), *Bedford Reinforced Plastics' Design Guide*, Bedford PA.

Boltzmann, L. (1876), “Zur Theorie der Elastischen Nachwirkung,” Annals of Physical Chemistry, Vol. 7, pp. 624-654.

Booker, J.R., Frankham, B.S., and Trahair, N.S. (1974), “Stability of Visco-elastic Structural Members,” Institution of Engineers, Australia, Civil Engineering Transactions, pp. 45-51.

Bradley, S.W., Puckett, P.M., Bradley, W.L., and Sue, H.J. (1998), “Viscoelastic Creep Characteristics of Neat Thermosets and Thermosets Reinforced with E-glass,” Journal of Composites, Technology, and Research, Vol. 20, No. 1, pp. 51-58.

Butz, T.M. (1997), *Tests on Pultruded Square Tubes under Eccentric Axial Load*, M.S. Dissertation, Georgia Institute of Technology.

Chen, S. and Lottman, R.P. (1991), “Buckling Loads of Columns Made of Viscoelastic Materials,” *Mechanics Computing in 1990’s and Beyond*, pp. 691-695.

Creative Pultrusions Inc. (2004), *The New and Improved Pultex Pultrusion Design Manual of Standard and Custom Fiber Reinforced Polymer Structural Profiles*, Vol. 4, Alum Bank, PA.

Daniali, S. (1990), “Time-Dependent Behavior of FRP Lintels,” Serviceability and Durability of Construction Materials – Proceedings of the First Engineering Materials Congress, Part 2, pp. 814-823.

Distefano, J.N. (1965), “Creep Buckling of Slender Columns,” American Society of Civil Engineers Proceedings, Journal of the Structural Division, Vol. 91, No. ST3, Part 1, pp. 127-150.

Dutta, P.K. and Hui, D. (2000), “Creep Rupture of a GFRP Composite at Elevated Temperatures,” Computers and Structures, Vol. 76, No. 1-3, pp. 153-161.

Engesser, F. (1889), “Die Knickfestigkeit gerader Stabe,” *Zeitschrift fürArchitekter und Ingenieur Vereins zu Hannover*, Weisbaden, Germany, 35, 455.

European Structural Polymeric Composites Group (EUROCOMP) (1996), *Structural Design of Polymer Composites – EUROCOMP Design Code and Handbook*, Chapman and Hall, London, U.K.

Findley, W.N. (1944), “Creep Characteristics of Plastics,” Symposium on Plastics, American Society for Testing Materials, pp. 118-134.

Findley, W.N. and Khosla, G. (1956), “An Equation for Tension Creep of Three Unfilled Thermoplastics,” Society of Plastics Engineers – Journal, Vol. 12, No. 12, pp. 20-25.

Galli, J.R. and Pollock, M.R., Boeing Co. (1965), "Engineering Exploitation of Reinforced Plastics for Aircraft Structures," AIAA, Royal Aeronautical Society, and Japan Society for Aeronautical and Space Sciences, Aircraft Design and Technology Meeting, Los Angeles, CA, Paper 65-762, 16 pp.

Goodman, J.W. and Gilksman, J.A. (1969), "Structural Evaluation of Long Boron Composite Column," *Composite Materials: Testing and Design, ASTM STP 460*, West Conshohocken, PA, pp. 460-469.

Hashem, Z.A. and Yuan, R.L. (2001), "Short vs. Long Column Behavior of Pultruded Glass-Fiber Reinforced Polymer Composites," Construction and Building Materials, Vol. 15, No. 8, pp. 369-378.

Hewson, P. (1978), "Buckling of Pultruded Glass Fibre-Reinforced Channel Sections," Composites, Vol. 9, No. 1, pp. 56-60.

Holmes, M. and Rahman, T.A. (1980), "Creep Behavior of Glass Reinforced Plastic Beams," Composites, Vol. 11, No. 2, pp. 79-85.

Jackson, L.R., Schwope, A.D., and Shober, F.R. (1949), "Information on the Plastic Properties of Aircraft Materials and Plastic Stability of Aircraft Structures at High Temperatures," RM-333, Project RAND, Battelle Memorial Institute.

Kang, J.O. (2001), *Fiber Reinforced Polymeric Pultruded Members Subjected to Sustained Loads*, Ph.D. Dissertation, Georgia Institute of Technology.

Kempner, J. (1954), "Creep Bending and Buckling of Linearly Viscoelastic Columns," National Advisory Committee for Aeronautics – Technical Notes, No. 3137, 27 p.

Liskey, K.A. (1989), "Pultrusion on a Fast Track," Advanced Materials and Processes, Vol. 135, No. 2, pp. 31-35.

McClure, G. and Mohammadi, Y. (1995), "Compression Creep of Pultruded E-glass Reinforced Plastic Angles," Journal of Materials in Civil Engineering, Vol. 7, No. 4, pp. 269-276.

Minahen, T.M. and Knauss, W.G. (1993), "Creep Buckling of Viscoelastic Structures," International Journal of Solids and Structures, Vol. 30, No. 8, pp. 1075-1092.

Petrie, G.L., Sorathia, U., and Warren, L.W. (1999), "Testing and Analysis of Marine Composite Structures in Elevated Temperature Conditions," International SAMPE Symposium and Exhibition (Proceedings), Vol. 44, Part 1, pp. 1165-1178.

Rosenthal, D. and Baer, H.W. (1952), "An Elementary Theory of Creep Buckling of Columns," ASME, Proceedings of the First U.S. National Congress of Applied Mechanics, pp. 603-611.

Schapery, R.A. (1965), “A Method of Viscoelastic Stress Analysis Using Elastic Solutions,” Journal of Franklin Institute, Vol. 279, No. 4, pp. 268-289.

Schapery, R.A. (1967), “Stress Analysis of Viscoelastic Composite Materials,” Journal of Composite Materials, Vol. 1, No. 3, pp. 228-267.

Scott, D.W., Lai, J.S., and Zureick, A. (1995), “Creep Behavior of Fiber-Reinforced Polymeric Composites: A Review of the Technical Literature,” Journal of Reinforced Plastics and Composites, Vol. 14, pp. 588-617.

Scott, D.W., Yoon, S.J., and Zureick, A. (1992), “Full Scale Tests on Concentrically Loaded Fiber-Reinforced Pultruded Columns,” Materials: Performance and Prevention of Deficiencies and Failures, pp. 572-576.

Scott, D.W., Zureick, A. (1998), “Compression Creep of a Pultruded E-glass/Vinylester Composite”, Composites Science and Technology, Vol. 58, No. 8, pp. 1361-1369.

Southwell, R.V. (1932), “On the Analysis of Experimental Observations in Problems of Elastic Stability,” Proceedings of the Royal Society, London, Series, Vol. 135, pp. 601-616.

STRONGWELL (2002), Extren Design Manual, Strongwell Corporation, Vristol, VA.

Timoshenko, S.P. and Gere, J.M. (1961), *Theory of Elastic Stability*, McGraw-Hill Book Co., New York, NY.

Tomblin, J.T. (1991), *A Universal Design Equation for Pultruded Composite Columns*, M.S. Thesis, Mechanical and Aerospace Engineering, West Virginia University, Morgantown, WV.

Vinogradov, A.M. (1987), “Buckling of Viscoelastic Beam Columns,” AIAA Journal, Vol. 25, No. 3, pp. 479-483.

Vinogradov, A.M. (1992), “Some Aspects of Nonlinear Creep Buckling,” American Society of Mechanical Engineers, Pressure Vessels and Piping Division (Publication) PVP, Vol. 248, pp. 57-62.

Vinogradov, A.M. (1993), “Nonlinear Buckling Analysis of Some Composite Structural Members,” American Society of Mechanical Engineers, Pressure Vessels and Piping Division (Publication) PVP, Vol. 269, pp. 47-55.

Vinogradov, A.M. and Wijeweera, H. (1985), “Theoretical and Experimental Studies on Creep Buckling,” Collection of Technical Papers – AIAA/ASME/ASCE/AHS Structures, Structural Dynamics and Materials Co, Part 1, pp. 160-164.

Violette, M.G. and Schapery, R.A. (2002), “Time-Dependent Compressive Strength of Unidirectional Viscoelastic Composite Materials,” Mechanics of Time-Dependent Materials, Vol. 6, No. 2, pp. 133-145.

Volterra, V. (1913), “Lecon sur les Fonctions des Lignes,” Gauthier-Villars, Paris, France.

Wong, P.M.H., Davies, J.M., and Wang, Y.C. (2003), “An Experimental and Numerical Study of the Behavior of Glass Fibre Reinforced Plastics (GRP) Short Columns at Elevated Temperatures,” Composite Structures, Vol. 63, No. 1, pp. 33-43.

Ye, B.S., Svenson, A.L., and Bank, L.C. (1995), “Mass and Volume Fraction Properties of Pultruded Glass Fiber Reinforced Composites,” Composites, Vol. 26, pp. 479-483.

Yeow, Y.T., Morris, D.H., and Brinson, H.F. (1979), “Time-Temperature Behavior of a Unidirectional Graphite/Epoxy Composite,” ASTM Special Technical Publication, n 674, pp. 263-281.

Zureick, A., Kahn, L.F., and Bandy, B.J. (1995), *The In-Plane Shear Properties of Pultruded Materials*, FHWA-Report, Georgia Institute of Technology, Atlanta, Georgia.

Zureick, A., Scott, D.W. (1997), “Short-term Behavior and Design of Fiber-Reinforced Polymeric Slender Members under Axial Compression,” Journal of Composites for Construction, Vol. 1, No. 4, pp. 140-149.